University of Nevada, Reno

Structural Controls of the MacFarlane Geothermal System, Humboldt County, Nevada: New Insights Based on Detailed Geologic Mapping, Shallow Temperature Surveys, and Magnetic Data

A thesis submitted in partial fulfillment of the

requirements for the degree of Master of Science in

Geology

By Sabina M. Kraushaar

Dr. Patricia H. Cashman/Thesis Advisor

May, 2014

University of Nevada, Reno
Statewide • Worldwide

THE GRADUATE SCHOOL

We recommend that the thesis
prepared under our supervision by

SABINA M. KRAUSHAAR

entitled

Structural Controls of the MacFarlane Geothermal System, Humboldt County, Nevada: New Insights Based on Detailed Geologic Mapping, Shallow Temperature Surveys, and Magnetic Data

be accepted in partial fulfillment of the
requirements for the degree of

MASTER OF SCIENCE

Patricia H. Cashman, Ph. D., Advisor

James E. Faulds, Ph. D., Committee Member

Robert S. Sheridan, Ph. D., Graduate School Representative

Marsha H. Read, Ph. D., Dean, Graduate School

May, 2014

ABSTRACT

Detailed geologic mapping, structural analysis, magnetic and two-meter temperature data, integrated with previous datasets, constrain the structural controls of the MacFarlane geothermal system. MacFarlane hot springs and the travertine fissure ridges lie within a relay ramp. The relay ramp is formed between two overlapping, north-northeast-striking, west-dipping Holocene normal faults exposed in Lake Lahontan sediments. Other mapped faults near the hot spring include a north-striking, west-dipping Tertiary fault east of MacFarlane hot springs. The highest temperature gradient is found at the projected intersection between the Tertiary and north-northeast-striking Quaternary fault, ~2.5 km northeast of the hot spring (Sibbett et al., 1982; Swanberg and Bowers, 1982). Our new data suggest other controls involving the relay ramp geometry of the Holocene faults.

The anomalous orientation of the travertine fissure ridge motivated this study of the structural controls of the geothermal system. MacFarlane hot spring is located on the eastern margin of the Black Rock Desert, ~85 km west of Winnemucca, in Humboldt County, Nevada. The active hot spring emerges from the west end of an east-trending travertine fissure ridge, which is ~180 m long. The travertine fissure ridge is up to ~2 m tall and ~5 m wide, and has a central fissure along its long axis. The orientation of the travertine fissure ridge indicates local north-south extension, which is inconsistent with the regional west-northwest extension of the northwestern Basin and Range province. The anomalous travertine orientation is due to fractures that occurred during formation of a relay ramp between two overlapping fault segments.

ACKNOWLEDGMENTS

This work was generously supported by grant 10EE0003997, awarded to the Great Basin Center for Geothermal Energy by the Department of Energy. Partial support for this project was provided from grant DE-EE0002748, awarded to Jim Faulds. I would especially like to thank my advisor, Patricia Cashman, for her thoughtful feedback and guidance throughout this project. I am a better structural geologist and writer because of her. I am also grateful to John Bell for his Quaternary expertise and willingness to help me with my mapping. I would like to thank Chris Sladek for his help and enthusiasm with two-meter temperature surveys, and for accompanying me to the field to do the actual survey. I am very grateful to Jim Faulds for suggesting this project and for his help with structural interpretations throughout the project. I would like to thank John Louie for encouraging me to do a magnetic survey and for his willingness and enthusiasm in teaching me about geophysics. Wendy Calvin and the Great Basin Center for Geothermal Energy at UNR have been especially helpful in facilitating this work. I would like to thank Jim Trexler for his expertise dealing with surficial deposits and willingness to accompany me to the field. I'd like to thank Katie Ryan for her field assistance and positive attitude dealing with flat tires, rattlesnakes, and long field days. I would also like to thank Ryan Anderson and Greg Dering for sharing their ArcGIS knowledge and assisting me with cartography. I am grateful to Lyndsay Hazelwood for being a great camping companion and field assistant, and for helping me complete my magnetic surveys. I would like to thank Kyle Gray and Paul Schwering for helping me model my magnetic data in Oasis, Kyle Reeder and Dustin Naphan for their help with my

magnetic survey, and others who volunteered to help in the field: Corina Forson, Tyler Kent, Paul Garvin and the Kona dog. I would also like to thank my family and Mike Schmidt for their unwavering support and love throughout this process.

TABLE OF CONTENTS

LIST OF TABLES

LIST OF FIGURES

INTRODUCTION

Although the structural settings of many geothermal systems in the Basin and Range province are well understood, the controlling factors for specific systems are commonly unclear. In the Basin and Range, geothermal systems are generally found in north-northeast-trending belts (e.g., Faulds et al., 2004), near ranges bounded by normal faults; however, it is the smaller faults and fractures that commonly control the permeability in these systems. Therefore, it is imperative to completely understand the structural setting of a system in order to determine the fluid pathways. The most efficient geothermal production wells are commonly located near faults that control the upwelling of a geothermal system.

MacFarlane hot springs, located in Humboldt County, Nevada, about 85 km west of Winnemucca (Figure 1), emerges from a prominent east-trending travertine fissure ridge; this suggests local north-south extension, which is anomalous within the Basin and Range province. Travertine fissure ridges are structurally controlled (Altunel and Handcock, 1993; Handcock et al., 1999; Brogi and Capezzuoli, 2009). However, the immediate structural control of the travertine fissure ridges at MacFarlane hot springs is not apparent. The largest travertine fissure ridge is ~180 m long, up to 5 m wide, and 2 m tall (Figure 2). Water flows out of its western end at temperatures between 75°- 85° C, and at a rate of several gallons/minute. There are additional smaller travertine features in the area, all of which exhibit central fissure ridges, indicating local extension

perpendicular to their current long dimension. Although there are other hot springs in the region, most do not have travertine fissure ridges or east-striking structures.

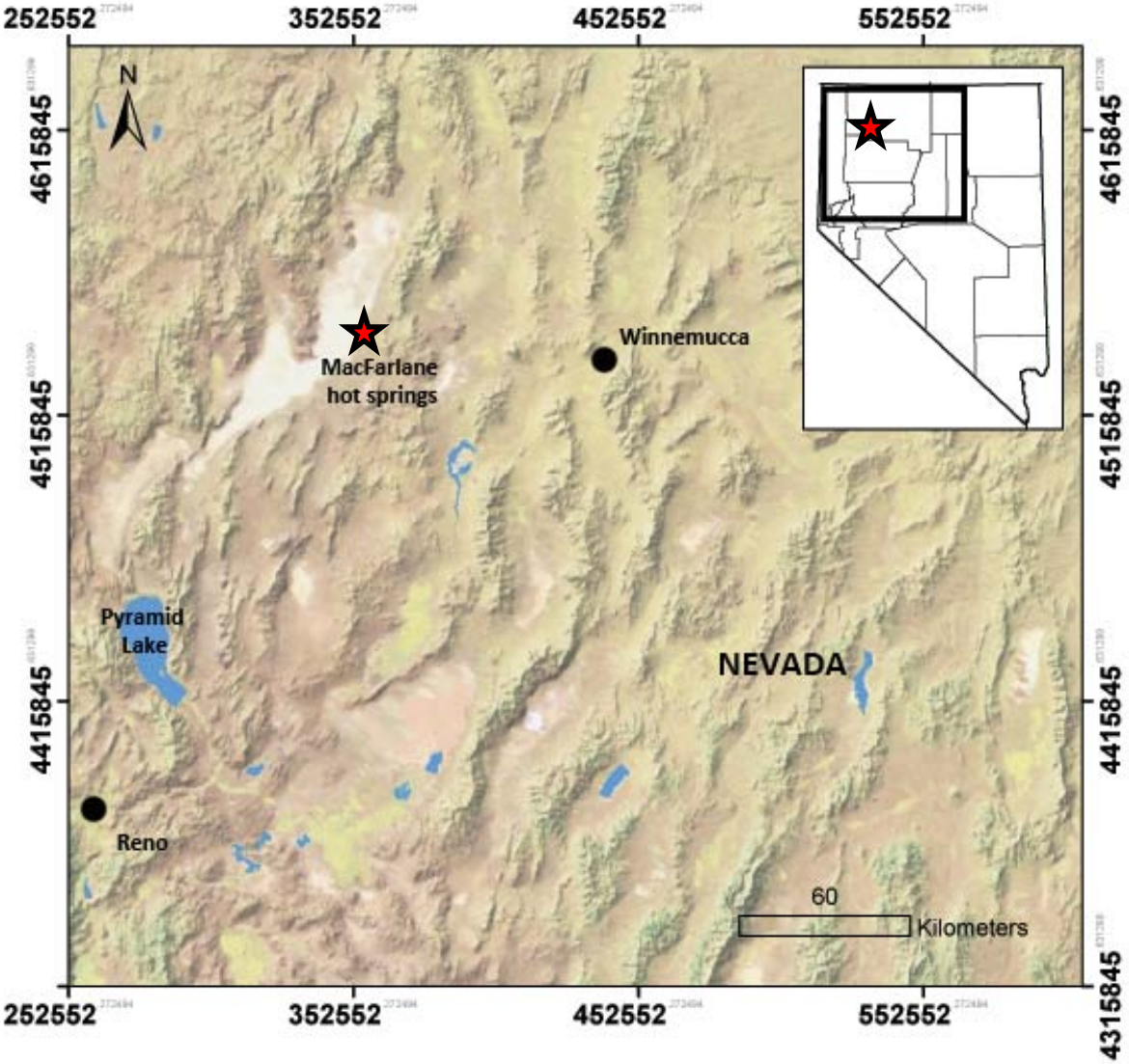

Figure 1. Location of MacFarlane hot springs (shown as a star) in Humboldt County, Nevada. MacFarlane hot springs is located about 85 km west of Winnemucca.

Figure 2. Main travertine mound at MacFarlane hot springs, looking east. Photo is taken from location of the actual hot springs surface expression, at the west end of the travertine mound.

This thesis presents an analysis of the structural controls of the MacFarlane geothermal system. The introduction includes a brief review of the necessary criteria for the formation of a geothermal system, the distinction between upwelling and outflow of geothermal water, and a summary of the common structural controls on geothermal systems in the Great Basin. Next, I present the regional structural setting and the previous geological and geothermal studies of MacFarlane hot springs and the surrounding area. I then present my new results; these include geologic mapping, shallow temperature data, and magnetic data. The new data are discussed in the context of the regional setting and integrated with previous work. The results have significant

implications for the specific controls of the travertine fissure ridges and the overall geothermal system at MacFarlane hot springs.

GEOTHERMAL BACKGROUND

The main factors required for a geothermal resource are a heat source, a fluid to transport heat, and permeability. Heat sources for geothermal systems are generally magmatic and related to tectonic plate boundaries. However, amagmatic geothermal systems can reside in actively extending continental crust, such as in the Basin and Range province in Nevada, due to high heat flow and thinning of the lithosphere. Permeability in these systems permits circulation of fluids. Permeability is commonly controlled by the subsurface geology and structures, including permeable and impermeable geologic units, as well as structures such as discrete joints, fractures and faults. Young faults are especially important in controlling permeability because they typically have not sealed due to precipitation of minerals (e.g., Hose and Taylor, 1974; Faulds et al., 2004; 2006; 2011).

A typical geothermal system in the Basin and Range province has upwelling and outflow zones (Figure 3). An upwelling zone is where hot geothermal fluids travel upwards through structurally or lithologically controlled permeable areas, reaching the surface or near-surface (e.g., Richards and Blackwell, 2002). After rising in an upwelling zone, the fluid commonly travels laterally, influenced by topography, groundwater, and the hydrological gradient; this is referred to as the outflow zone (e.g., Richards and

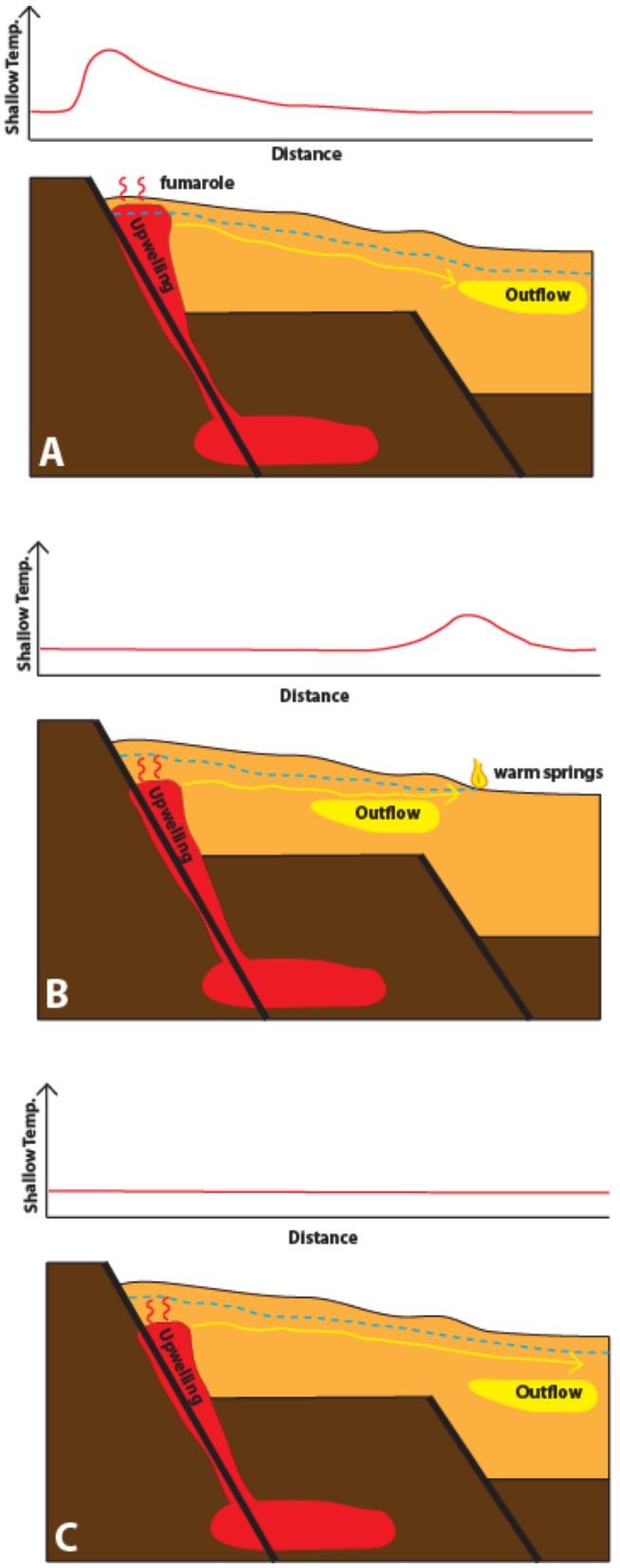

Blackwell, 2002). Outflow zones typically form a broad, umbrella shape that changes over time. Both upwelling and outflow can produce surface manifestations. Fumaroles with boiling water can indicate upwelling, whereas warm or hot springs are typically related to outflow interacting with topography and groundwater (Figure 3; Richards and Blackwell, 2002).

Commonly, surface expressions of geothermal water or shallow high temperatures can be misleading, because they are related to outflow, not upwelling. Examples of shallow temperature signatures of upwelling and outflow zones are shown in Figure 3, A-C. In Figure 3A,

Figure 3. Three scenarios of geothermal upwelling and outflow and their two-meter temperature signature. Upwelling is red; ouflow is yellow; the water table is a blue dashed line; shallow temperatures are shown above each scenario. In A, upwelling reaches the ground surface and produces an elevated two-meter temperature. In B, the upwelling boils without reaching the surface, then mixes with groundwater and travels laterally until it reaches the ground surface, where it is expressed as a warm spring. The two-meter temperature data show elevated temperatures at the location of outflow, but not upwelling. In C, neither the upwelling nor outflow is shown in shallow temperature data. This occurs when the hot water does not get close enough to the ground surface.

the upwelling zone is expressed at the surface as a fumarole with a corresponding elevated shallow temperature. The hot water flows down topography, mixes with groundwater and becomes cooler, as shown in the shallow temperature data. In Figure 2B, the hot water in the upwelling zone boils below the water table and is not expressed on the surface or at a shallow temperature. The hot water again flows down topography and mixes with groundwater. In this example, the outflow reaches the surface as a warm spring. The shallow temperatures in this example would be elevated at the location of the outflow, but not at the actual location of upwelling. In Figure 3C, both the upwelling and outflow zones are too deep to be detected by a shallow temperature survey. In this case, there is an underground resource without any elevated shallow temperatures.

A reliable indicator of upwelling is a linear increase in deep temperature gradient (i.e., change in temperature/depth), (e.g. Richards and Blackwell, 2002, Figure 4). In areas of upwelling, the temperature gradient will be linear and gradually increase, as shown in Figure 4A. Areas of outflow will not show a linear increase in temperature gradient (Figure 4B). However, the temperature gradient in shallow wells can increase in the shallow subsurface before cooling off with depth (Figure 4B).

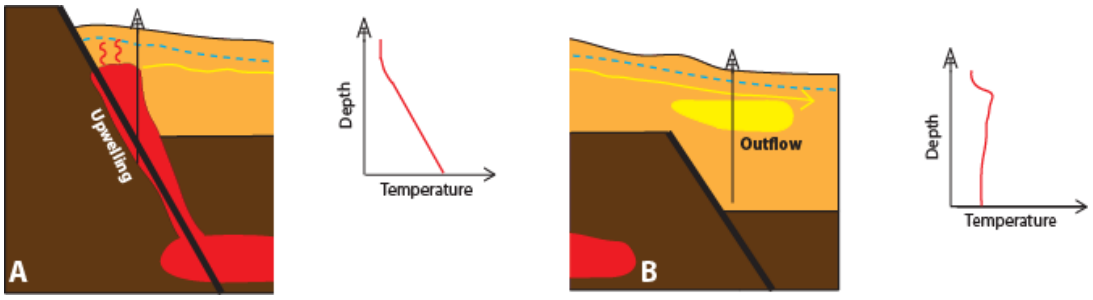

Figure 4. Temperature gradient signatures in areas of upwelling (A) and areas of outflow (B). The triangle above a vertical black line represents a temperature gradient well. Areas of upwelling will show a linear increase in temperature gradient, while temperature gradient in areas of outflow will not increase with depth.

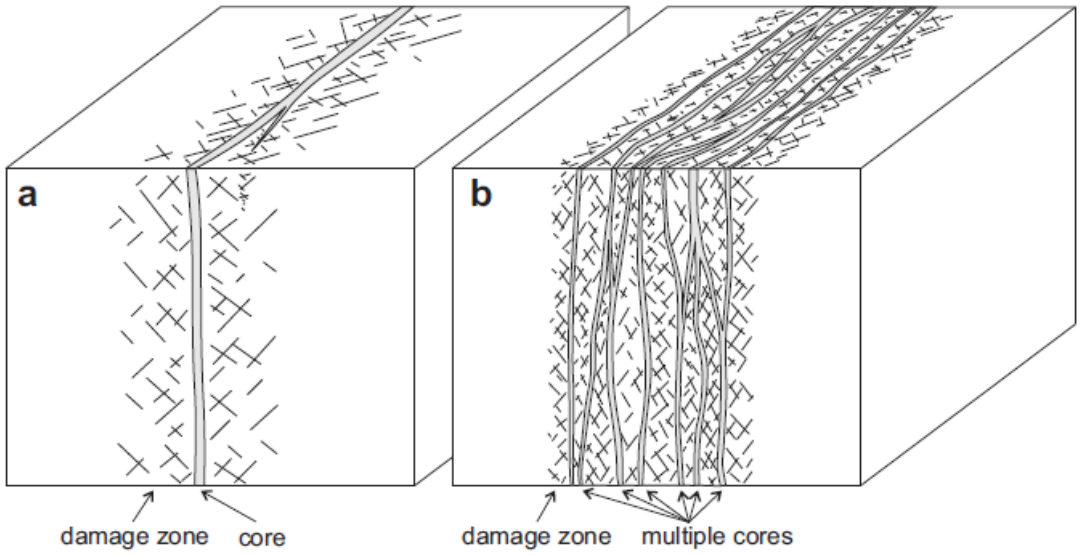

Figure 5. Typical fault zone structure (from Faulkner et al., 2010; Faulkner et al., 2003; Chester and Logan, 1986). (a) a single fault core surrounded by a fractured damage zone and (b) multiple fault cores enclosing lenses of fractured rock.

Favorable Structural Settings for Geothermal Systems:

Within the Basin and Range province, the main factors that affect the permeability of a geothermal system are structural. The faults controlling the geothermal systems are typically not in the middle segments of major range-bounding faults with considerable offset. Rather, they correspond to the more complex pervasive fractures and damage zones related to fault step-overs (relay ramps), intersections, terminations, and accommodation zones (Faulds et al., 2006). Generally, the greater the structural complexity of a system, the greater the likelihood of the geothermal system being hot enough to generate electricity (Faulds et al., 2013). In addition, the specific faults

associated with geothermal systems are generally Holocene in age (Bell and Ramelli, 2007).

Fault damage zones have been shown to increase permeability and control fluid flow in the crust (e.g., Faulkner et al., 2010). The fault damage zone surrounds the fault plane, or high-strain core (Figure 5). The high-strain fault core can decrease permeability and act as a seal, although this depends on the rock type and the geometric architecture of the fault in three dimensions (Faulkner et al., 2010). As the number and complexity of faults increase, the associated pervasive fractures in the damage zones and the permeability of a system will also typically increase. Compartmentalization of permeable areas can also occur where damage zones surround multiple sealing faults (Faulkner et al., 2010, Figure 5). Damage zones can be classified into wall-, tip-, and linking-damage zones based on position within and around the fault zone (Kim et al., 2004). These faults and fractures occur at many scales, ranging from km to mm.

The wall-damage zones directly surround the fault core, and might be related to fault tip-damage zones that are abandoned as the fault propagates through the rock (Figure 6). Wall-damage zone can also be formed as a result of slip on the major fault

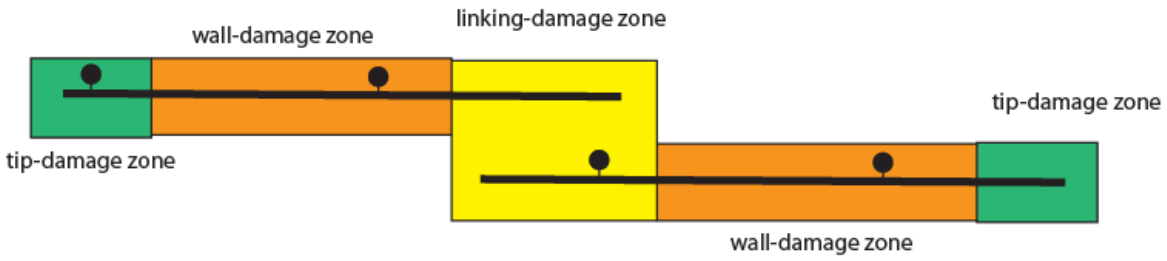

Figure 6. Locations of damage zones along a normal fault. The tip-damage zones are shown in green, the wall-damage zones are shown in orange, and the linking-damage zones are shown in yellow. Figure modified from Kim et al., 2004.

(Kim et al., 2004). The fracture density typically is highest directly adjacent to the fault core and decreases exponentially as distance from the core increases (Figure 5, Faulkner et al., 2010). Fractures that increase permeability in wall-damage zones typically include en echelon extensional fractures, antithetic faults, synthetic faults, and rotated blocks (Kim et al., 2004). Pre-existing joints and fractures in bedrock also have a direct influence on fault propagation (e.g., Crider and Peacock, 2004). Faults are typically initiated in the brittle crust by the linkage of pre-existing joints and fractures (Crider and Peacock, 2004).

The fault tip-damage zone develops as a result of stress concentration at the fault tip (Figure 6, e.g., Cowie and Scholz, 1992; Kim et al., 2004). The surrounding rock experiences the highest stresses in the vicinity of the fault tip, and the resulting fractures are greater in density than fractures resulting from slip on the fault plane (e.g., Cowie and Scholz, 1992; Kim et al., 2004). Steep displacement gradients at fault tips cause perturbations in the stress field, allowing for fractures to form with varying orientations (Ferrill and Morris, 2001). This in turn increases the permeability in the area of the fault tip. Fracture patterns common in tip-damage zones include wing cracks, horsetail fractures, antithetic faults and synthetic faults (Kim et al., 2004).

Linking-damage zones are formed when the tips of two adjacent faults interact (Figure 6, Kim et al., 2004). Linking-damage zones are generally very complex compared to other damage zone types. The geometry of the pervasive fractures in a linking-damage zone is strongly controlled by whether the faults are strike-slip or oblique-slip, and whether they form an extensional or contractional step. Connecting faults typically develop in contractional steps, whereas pull-aparts and extensional

fractures typically form in extensional steps. Isolated lenses, rotated blocks, and strike-slip duplexes can occur in both types of fault steps (Kim et al., 2004).

Within fault zones, fault segments that are critically stressed are most likely to increase permeability (e.g., Barton et al., 1995: Sibson, 1994: Ferrill et al., 1999; Siler and Faulds, 2013). This includes fault segments with higher tendencies to slip or dilate. The slip tendency (T_s) of a fault is defined as the ratio of shear stress (τ) to normal stress ($\sigma_{n)}$ acting on the fault plane surface:

$$T_s = \tau/\sigma_n \qquad \text{(Morris et al., 1996)}$$

The dilational tendency (T_d) is the total stress perpendicular to fault surface:

$$T_d = (\sigma_1-\sigma_n) / (\sigma_1-\sigma_3) \qquad \text{(Ferrill et al., 1999)}$$

The most active geothermal systems in the Basin and Range are generally found in association with faults and fault zones oriented north-northeast, perpendicular to the least principal stress direction and therefore ideal for dilation (e.g., Faulds et al., 2004). Faults that are subvertical are also more likely to have increased dilation tendencies (e.g., Ferrill et al., 1999; Faulds et al., 2006).

Specific structural settings have fault damage zones or a combination of damage zones that increase permeability and are favorable for geothermal systems in the Basin and Range province (Figure 7). Based on an inventory taken from > 400 systems in the Great Basin, relay ramps and step-overs in normal fault systems (fault linking-damage zones) are the most favorable structural setting, hosting ~33% of the geothermal systems (Figure 7C and 7D, Faulds et al., 2013; 2011). Other common favorable structural settings for geothermal systems include: A) intersections between normal faults and

strike-slip or oblique-slip faults (~22%, Figure 7B) and B) normal fault terminations or tip-lines (~22%, Figure 7A).

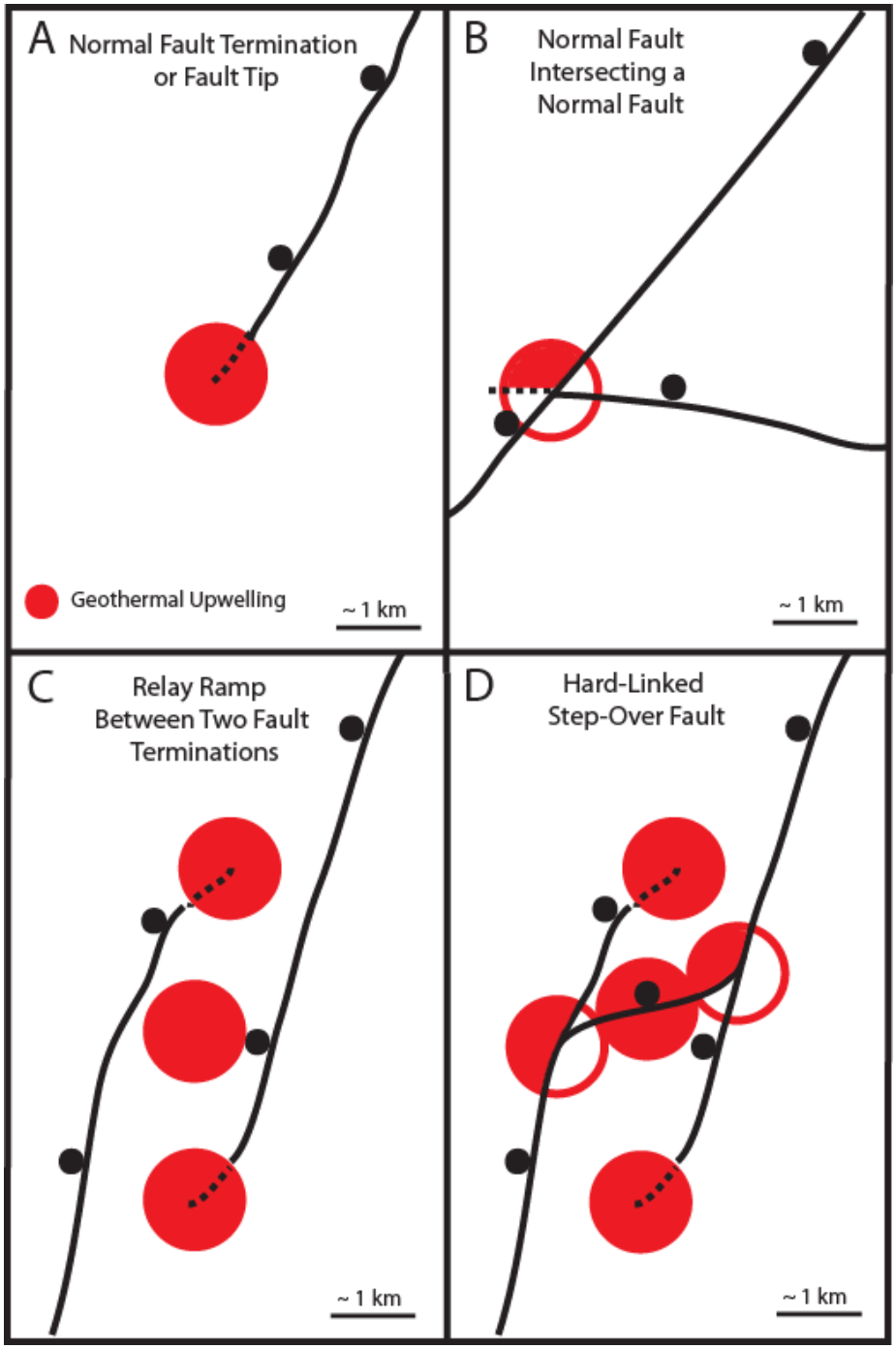

Figure 7. Favorable structural settings for geothermal systems in the Basin and Range. Areas of increased permeability and geothermal upwelling are shown as the red circles. Solid red within open circles indicate locations with increased dilational tendencies. The structural scenarios are as follows: A – Normal fault termination or fault tip, B – Normal fault intersecting another normal fault, C – a relay ramp formed between two fault terminations, D – Hard-linked step-over fault that has dissected the relay ramp. Figure modified from Faulds et al, 2006; 2011.

Normal fault terminations or tip-lines can increase permeability and provide conduits for fluid flow (Figure 7A, e.g., Gartell et al., 2004). The permeability in these systems is increased due to the tip-damage zones associated with fault terminations (Figure 6). This is the simplest structural setting that can increase permeability.

Intersections between normal faults and strike-slip or oblique-slip faults are also favorable for geothermal systems (Figure 7B, Curewitz and Karson, 1997; Faulds, 2011; 2013). In the example shown in Figure 7B, pervasive fracturing is caused by wall-damage zones associated with two intersecting normal faults, as well as a tip-line damage zone (area shown outlined in red). The fault intersection in Figure 7B also creates a dilational quadrant that is more likely to have increased permeability due to the fault geometries (shown in solid red).

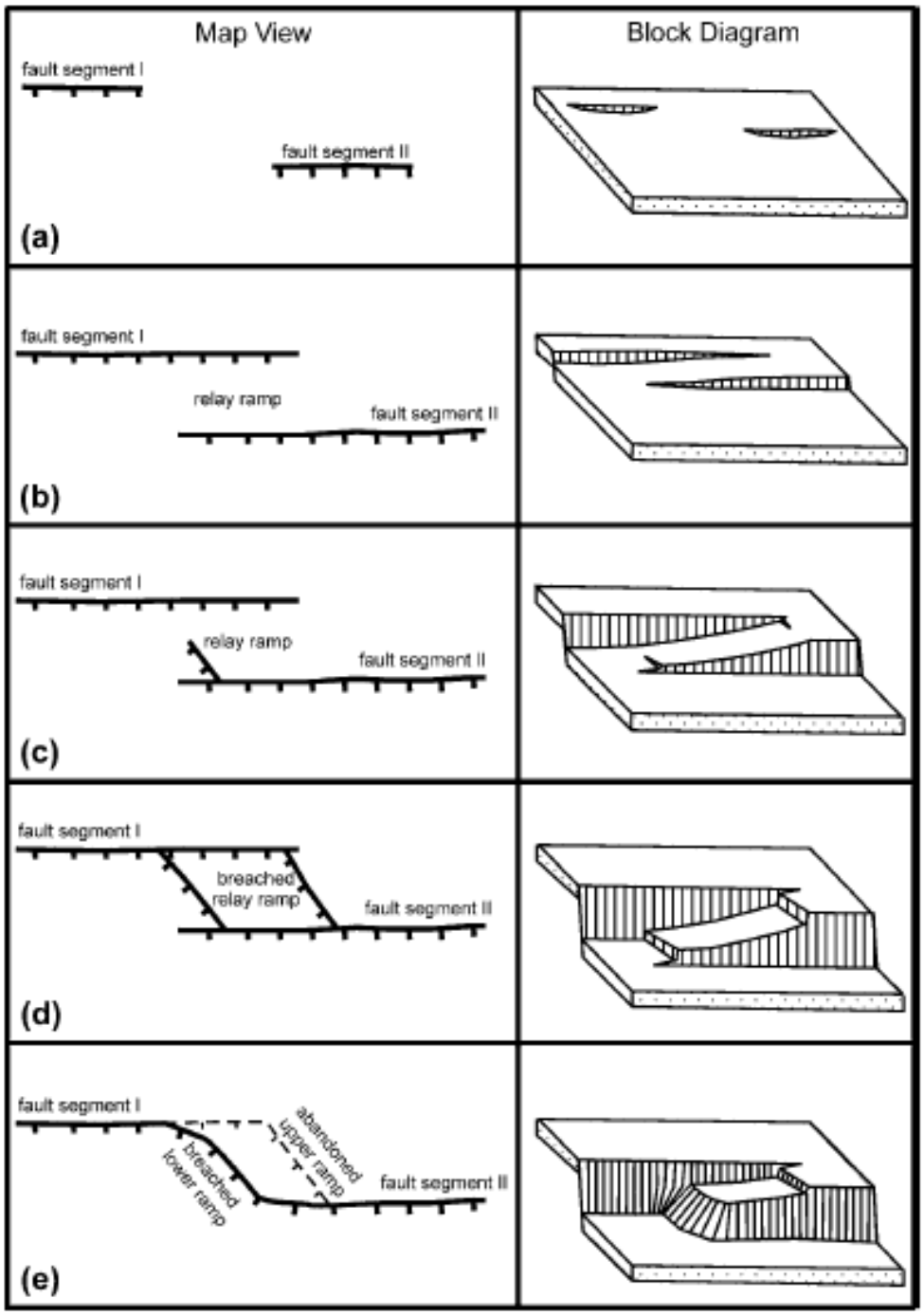

Figure 8a. Typical relay ramp progression from soft-linked to hard-linked. Tick marks show the down-thrown block of the normal fault. (a) Stage 1: fault segments do not interact. (b) Stage II: fault segments begin to propagate past each other and transfer some displacement along the two fault segments, (c) Stage III: strain has accumulated in the relay ramp and has resulted in initial fractures propagating roughly perpendicular away from the fault segments into the relay ramp, (d) Stage IV: the relay ramp is breached by a fault or series or faults, (e) The upper bench is abandoned and previous two fault segments are linked by one continuous fault. Taken from Ciftci and Bozkurt (2007) and Peacock and Sanderson (1994).

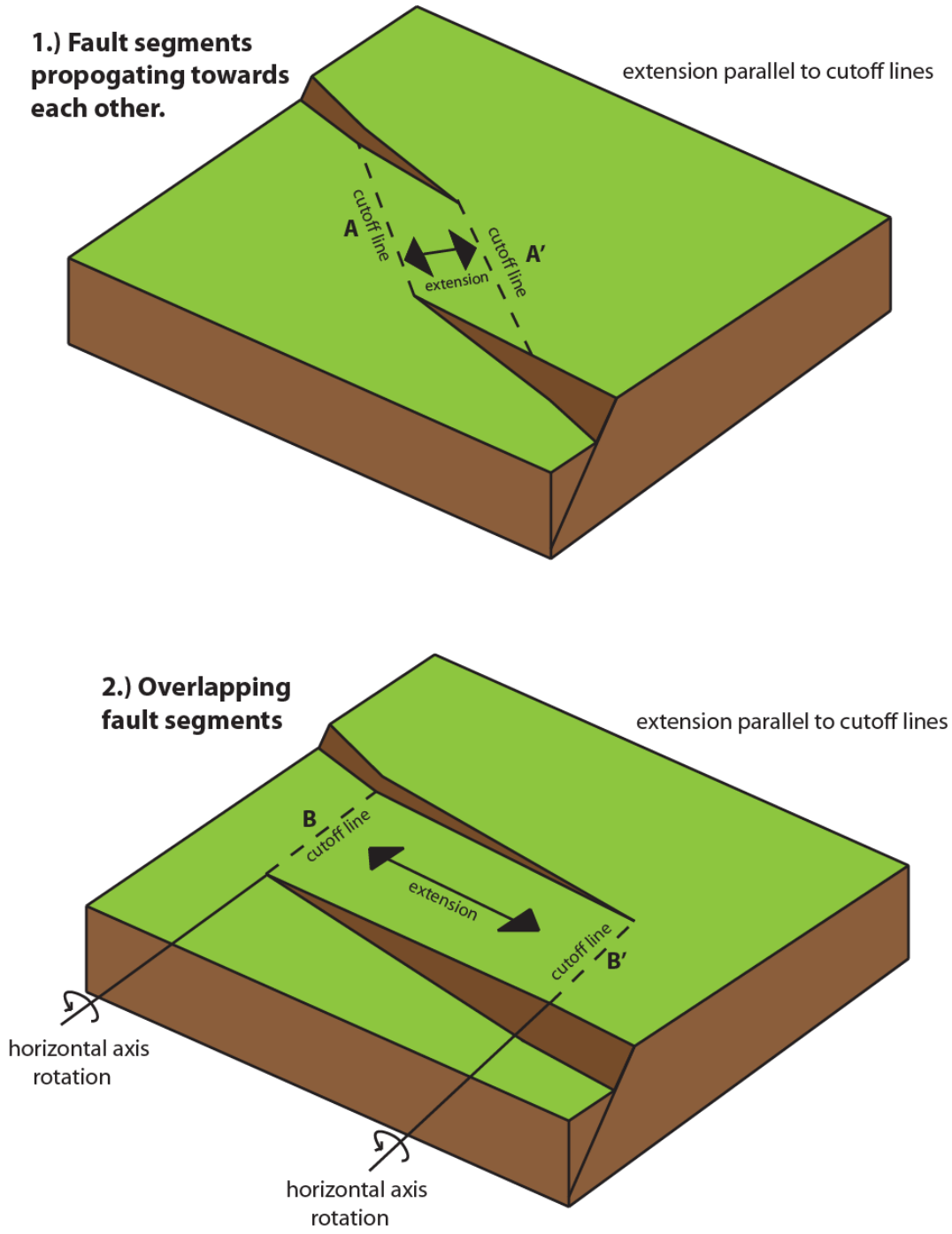

Figure 8b. This figure shows a relay ramp, formed by two overlapping normal faults. The cutoff lines are shown as dashed lines (A and A'), and the actual faults are shown in dark brown. Multiple rotations can occur within the relay ramp that create pervasive fractures. These mainly include horizontal axis rotation and extension oriented perpendicular to the cutoff lines. In this figure, extension oriented perpendicular to the cutoff lines is moving A away from A'. Figure modified from Ferrill and Morris (2001).

Relay Ramps:

Relay ramps were described by Larsen (1988) as strained zones that transfer displacement between normal faults. Larsen (1998) also observed that relay ramps might act as permeable paths for fluids to migrate between the hanging wall and footwall. Permeability within a relay ramp is due to the fault tip-damage zones, as well as the linking-damage zone between the interacting fault segments (Figure 7C).

Relay ramps form in extensional terrains to accommodate strain between synthetic normal faults that overlap in map view (Larsen, 1988; Peacock and Sanderson, 1991; 1994; Ferrill and Morris, 2001; Trudgill and Cartwright, 1994). Soft-linked relay ramps eventually progress into hard-linked segments that contain breaching faults (Figure 8b, e.g., Ciftci and Bozkurt, 2007). Four stages of relay ramp progression were initially described by Peacock and Sanderson (1991; 1994). These stages include (Figure 8a):

(a) Stage I: fault segments do not interact,

(b) Stage II: fault segments begin to propagate past each other and transfer displacement along the two fault segments,

(c) Stage III: strain has accumulated in the relay ramp and has resulted in initial fractures propagating roughly perpendicular away from the fault segments into the relay ramp,

(d) Stage IV: the relay ramp is breached by a fault or series of faults,

(e) The upper bench is abandoned and the previous two fault segments are linked by one continuous fault (Ciftci and Bozkurt, 2007).

During relay ramp progression, ductile strain between the overlapping fault segments is accommodated by a series of rotations within the ramp (Figure 8b). These rotations include rotation about a vertical axis and a horizontal axis (Ferrill and Morris, 2001). In many cases, however, vertical axis rotation is not required as the relay ramp deforms (e.g., Faulds et al., 1992). Extension oriented perpendicular to the fault cutoff lines can also occur within the relay ramp (Figure 8b, Ferrill and Morris, 2001). As the two interacting fault segments move past each other, the cut-off lines rotate (Peacock and Sanderson, 1991; Ferrill and Morris, 2001). The orientations of the dilatant fractures change systematically with time. Complexity within the relay ramp is typically increased by fractures oriented parallel to the actual faults (e.g., Peacock and Sanderson, 1991; Trudgill and Cartwright, 1994). Internal fractures can also be influenced by pre-existing joint sets within the bedrock, as observed in “The Grabens” in Canyonlands, Utah (Trudgill and Cartwright, 1994). The extension and rotations can create pervasive fractures that enhance permeability within the ramp and provide pathways for fluid or hydrocarbon flow (e.g., Trudgill and Cartwright, 1994).

Eventually, a relay ramp can be breached by a hard-linking fault or fault segments; it is then considered a step-over (e.g., Peacock and Sanderson, 1994; Trudgill and Cartwright, 1994, Figure 7D). The process of forming and dissecting a relay ramp in normal fault systems is part of fault growth by segment linkage (Trudgill and Cartwright, 1994). There are many areas of increased permeability within the step-over, as shown in

Figure 7D. These include fractures associated with fault terminations, a linking-damage zone, and fault intersections between the hard-linking segment and the two principal faults (Figure 7D). Dilational quadrants have increased permeability; these are shown in solid red at the fault intersections (Figure 7D).

Combination of Structural Settings:

Commonly, a combination of structures controls the precise location of a geothermal system within the Basin and Range province (e.g., Faulds et al., 2011, 2013; Hinz et al., 2011; Dering and Faulds, 2012; Anderson and Faulds, 2013). Areas with combinations of structural settings are called "hybrid" geothermal systems. For example, a geothermal system located in a step-over within a broader accommodation zone is considered a hybrid. Hybrid systems are more likely to have robust geothermal systems favorable for electricity production, based on data from geothermal power plants in Nevada. There are currently 24 electricity-producing geothermal plants in Nevada, and 10 of those have hybrid structural settings (Faulds et al., 2013).

In addition, Holocene faults are generally associated with geothermal systems in the Basin and Range province (Bell and Ramelli, 2007). Hydrothermal waters typically precipitate minerals that effectively fill voids and fractures, and therefore decrease permeability over time. However, in active fault systems the permeability can be maintained by active fractures, resulting in new or rejuvenated conduits for fluid flow (Curewitz and Karson, 1997). Essentially, in active fault systems, the permeability-inhibiting fault healing commonly associated with geothermal systems either has not had time to develop or is disrupted as the fault slips.

Travertine fissure ridges:

Travertine is a terrestrial calcareous deposit typically found associated with hot springs (e.g., Ford and Pedley, 1996). Travertine deposition is induced by the loss of carbon dioxide (CO_2) in thermal waters through the reaction: $H_2O + CO_2 + CaCO_3 \leftrightarrow Ca(HCO_3)_2$. This reaction is caused by a fluid pressure drop, turbulence of fluid flow, and/or biological activity extracting CO_2 from the water (Chafetz and Folk, 1984; Ford and Pedley, 1996; Brogi and Capezzuoli, 2009). Travertine can have a variety of morphologies; the most common are fissure ridges, cones, and terraces. The dominant travertine morphologies at MacFarlane hot springs are travertine fissure ridges and conical travertine mounds. The active hot springs at MacFarlane flow out of a roughly conical topographic high associated with a travertine fissure ridge.

Travertine fissure ridges are composed of outwardly dipping, bedded travertine flanking a central fissure (Figure 9). The central fissure forms along the crest of the ridge, where water rises (or rose) up nearly vertical fissures (Figure 9). Active travertine fissure ridges typically have a long axis with a hot spring flowing out of one or both of the ridge extremities (e.g., Brogi and Capezzuoli, 2009). This type of travertine is observed in the Pamukkale deposit of Turkey, Rapolano Terme, Italy, Bridgeport, California, and at MacFarlane hot springs.

It has been shown that travertine fissure ridges can be strictly controlled by the geometric setting and kinematics of faults and related damage zones (Altunel and Handcock, 1993; Ford and Pedley, 1996; Cakir, 1999; Handcock et al., 1999; Gruszczynski et al., 2004; Brogi and Capezzuoli, 2009; Brogi et al., 2010; 2012). The location of the fissure ridge typically directly follows damage zones and dilatant fractures

that affect the bedrock beneath the travertine. Thus, fissure-ridges are the most significant travertine masses for tectonic investigations (e.g., Brogi and Capezzuoli, 2009). The orientation of the long axis of the fissure is typically perpendicular to local stretching direction (Handcock et al., 1999). Therefore, the orientations and character of travertine fissure ridges can be used to infer local extension directions and study Quaternary fault systems (e.g., Handcock et al., 1999: Brogi and Capezzuoli, 2009; Brogi et al., 2010; 2012).

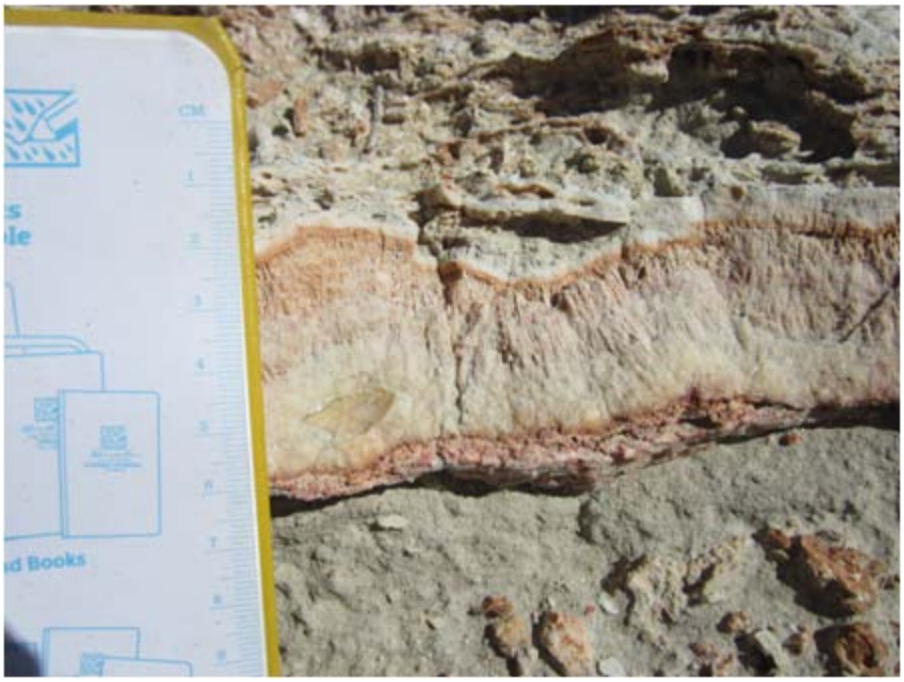

Figure 9. Travertine central fissure ridge. The central fissure forms along the crest of the ridge, where water rose up nearly vertical fissures. The orientation of the long axis of the central fissure ridge is perpendicular to the local stretching direction.

GEOLOGIC BACKGROUND

Mesozoic Tectonics:

Mesozoic rocks are exposed in the Jackson Mountains northeast of MacFarlane hot springs (Figure 10; Willden, 1963; Russel, 1981; Maher, 1989; Quinn et al, 1997). These rocks are part of a Triassic to Jurassic volcanic and plutonic arc system spanning the Mojave Desert, Sierra Nevada, and Klamath Mountains region and are part of an arc system (Figure 10; e.g., Miller, 1987; Quinn et al, 1997). The Jackson Mountains consist of magmatic arc strata, and just to the east of the Jackson Mountains lies a back-arc basinal region (e.g., Quinn et al., 1997, Figure 10). The Luning-Fencemaker fold and thrust belt (Figure 10) was the site of substantial northwest-southeast shortening during the Jurassic and Cretaceous (e.g., Oldow, 1983, 1984; Quinn et al., 1997). Detailed mapping the Jackson Mountains also documents high angle normal faults of late Middle Jurassic age overlapped by Upper Jurassic/Lower Cretaceous King Lear Formation sedimentary rocks (Maher, 1989). These faults generally accommodate dip/slip motion and strike ~100° (Maher, 1989).

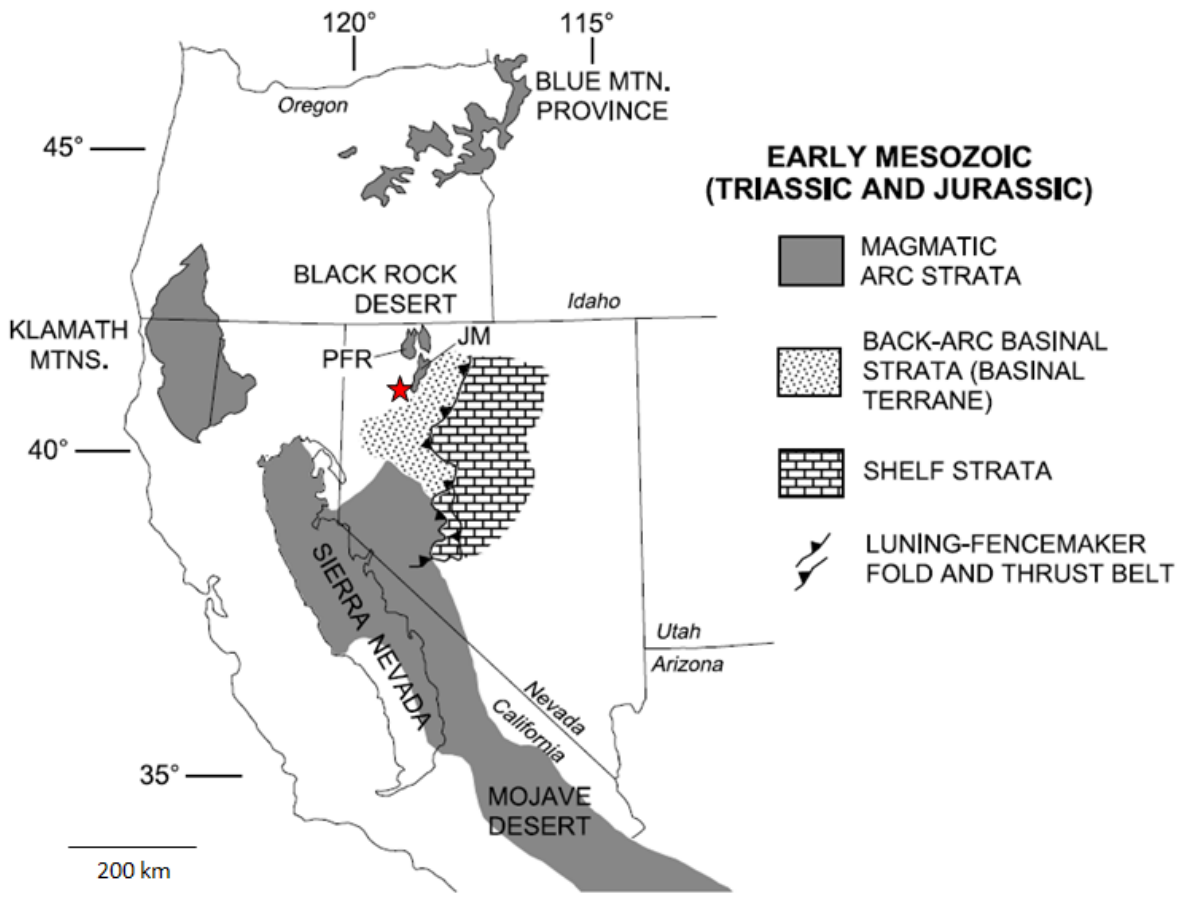

Figure 10. The western U.S. Cordillera, modified from Quinn et al. (1997). This figure shows the distribution of magmatic, back-arc, and shelf strata during the Triassic and Jurassic. The Luning-Fencemaker fold and thrust belt is shown, as well as the Jackson Mountains (JM) and the Pine Forest Range (PRF). The approximate location of MacFarlane hot springs is shown as the red star.

Extension in the Basin and Range (35 Ma to present):

The recent tectonic evolution of the northwestern Basin and Range province is characterized by long-lived west-northwest extension. There was an absence of tectonism between 35 to 12 Ma, followed by west-northwest extension along high angle normal faults that continues today (e.g., Colgan et al., 2006; Lerch et al., 2007; 2008). Faulting in the northwestern Basin and Range began at ~11 – 12 Ma, which is considerably

younger than the rest of the Basin and Range. This extension progressed at a constant rate until about 3 Ma. Sometime between ~3.1 and ~2.61 Ma an intense episode of extension began, giving rise to the Sierra Nevada frontal fault system (Trexler et al., 2000; Henry and Perkins, 2001; Colgan et al., 2006; Cashman et al., 2012;). Many of the mountain ranges in the northwestern Basin and Range show tilting of 25° to 30° that occurred during Neogene extension (Colgan et al., 2006).

Current GPS velocities suggest that the Basin and Range province is extending a total of 11.4 +- .3 mm/yr in a N47W direction (e.g., Hammond and Thatcher, 2007). GPS vector data (Figure 11) show that local extension in the Black Rock Desert (~10 km south of MacFarlane hot springs) is oriented 280°, or approximately east-west.

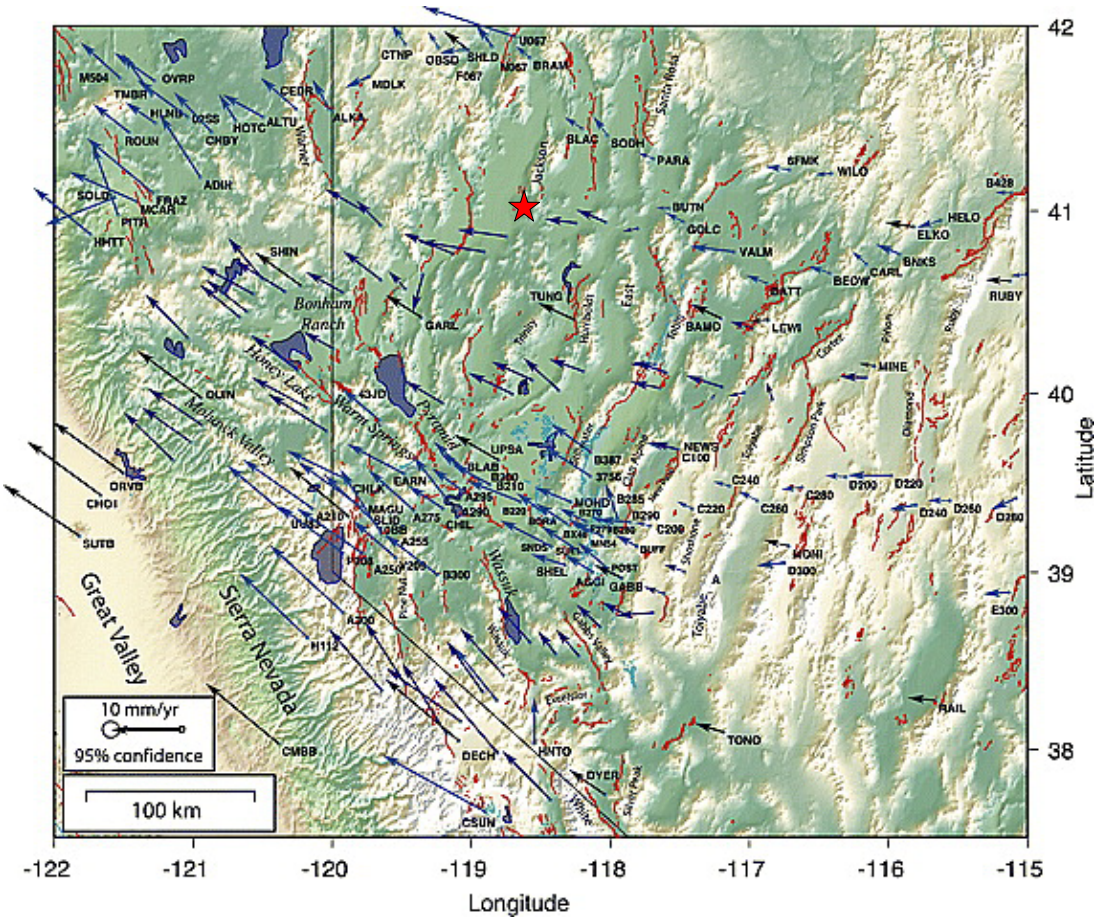

Figure 11. GPS geodetic velocities with respect to stable North America. The red star is the location of MacFarlane hot springs. Velocity vectors near MacFarlane hot springs are oriented approximately east-west. Figure taken from Hammond and Thatcher (2007).

Regional Geology:

MacFarlane hot springs lies within the northwestern Basin and Range on the eastern margin of the Black Rock Desert (Figure 12). The Black Rock Desert is flanked by the north-northeast-trending Jackson Mountains to the east and by north- to north-northwest-trending ranges on the west. The geology in this region is characterized by Mesozoic metavolcanic/metasedimentary units and associated plutonic rocks overlain by a series of Tertiary volcanic and sedimentary rocks. Locally, Neogene sedimentary units

overlie and interfinger with the volcanic rocks. Quaternary lacustrine sediments related to numerous pluvial cycles overlie all bedrock units. Quaternary alluvium and eolian deposits are the most recent units.

Mesozoic Jackson Mountains:

The Jackson Mountains lie to the northeast of MacFarlane hot springs (Figures 12 and 13). They consist dominantly of the Bliss Canyon Formation (siliclastic and volcanogenic sedimentary rocks and limestones), Happy Creek igneous complex, and a suite of intrusive bodies (Willden, 1964; Maher, 1989; Quinn et al., 1997). These rocks are thought to be related to Jurassic/Cretaceous magmatic arc and back-arc environments (e.g., Quinn et al., 1997).

The Bliss Canyon Formation consists of three informal members, which are described by Maher (1989). The oldest member is a dominantly argillite sequence with interbedded cherty and quartzose arenite, calcarenite, and chert-pebble conglomerate. The middle member is a massive limestone interval. The upper member contains quartzose and cherty conglomerate, arenite and argillite. Minor volcanogenic components appear at the top, just below the Happy Creek volcanic complex. There is a gradational and conformable transition into the Happy Creek complex. The Bliss Canyon Formation is dated as Middle to Upper Triassic (Maher, 1989; Quinn et al., 1997).

Overlying the Bliss Canyon Formation is the Happy Creek complex. The majority of the Happy Creek complex consists of a thick volcanic section composed of andesitic flows and related volcaniclastic strata (e.g., Quinn et al., 1997). The andesite is porphyritic with 10%-50% phenocrysts of plagioclase and clinopyroxene (1-2 mm long)

and minor hornblende in an aphanitic to crystalline granular groundmass (Quinn et al., 1997). Vesicular texture is rare. Fragmental andesites are also present and contain angular, unsorted clasts suspended in a porphyritic matrix (Quinn et al., 1997).

A smaller proportion of the Happy Creek igneous complex consists of stratified volcaniclastic rocks. These are dominantly poorly sorted breccias, conglomerate and diamictite in which bedding is very thick to indistinct (Quinn et al., 1997). Finer grained volcaniclastic rocks occur as poorly to well-bedded volcanic-lithic sequences of sandstone and mudstone. Some graded bedding is present, but typically these sedimentary features are obscured by cleavage, metamorphism and hydrothermal alteration (Quinn et al., 1997). The Happy Creek complex is dated as Upper Triassic to upper Middle Jurassic (Maher, 1989; Quinn et al, 1997).

Several intrusive bodies are also observed in the Jackson Mountains. The composition of these plutons includes quartz diorite, granodiorite, gabbro, diorite and monzodiorite with varying mineral compositions (Quinn et al., 1997). These plutons were emplaced in two groups, based on U-Pb zircon ages. Older plutons consist of quartz diorite and cluster between 196 and 190 Ma (late Early Jurassic, Quinn et al., 1997). Younger plutons consist of 170 to 163 Ma diorite to monzodiorite (late Middle Jurassic, Quinn et al., 1997). Both groups intrude country rocks, including the Happy Creek complex the Bliss Canyon Formation.

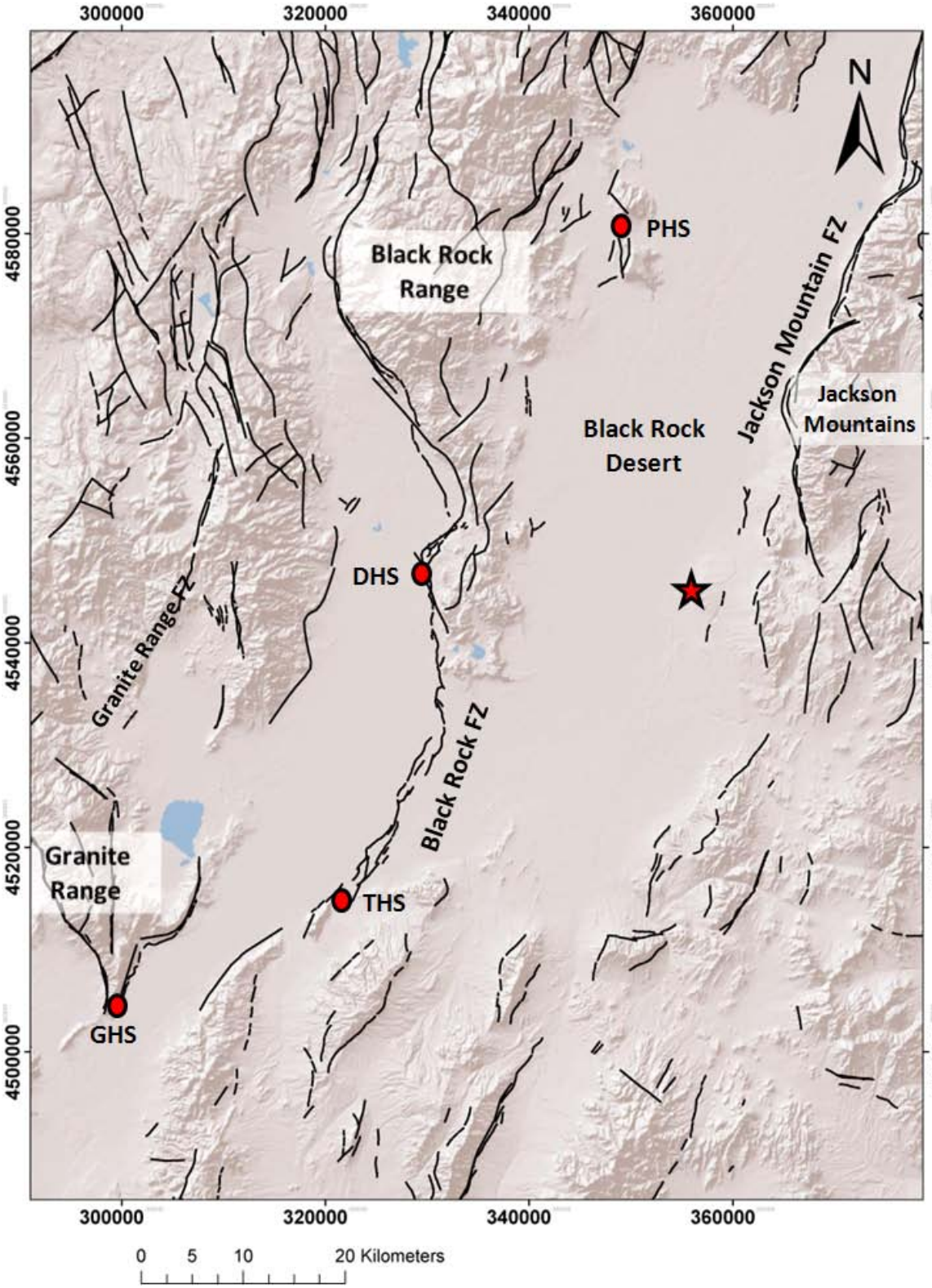

Figure 12. Location of MacFarlane hot springs (shown as star) in relation to the Black Rock Range, the Granite Range, the Jackson Mountains, and the Black Rock Desert. Red dots represent other hot springs (GHS = Gerlach hot springs, THS = Trego hot springs, DHS = Double hot springs, PHS = Pinto hot springs). Both the Black Rock fault zone and the Jackson Mountain fault zone are shown. Faults are shown as black lines and are taken from the U.S. Geological Survey Quaternary fault and fold database (2006).

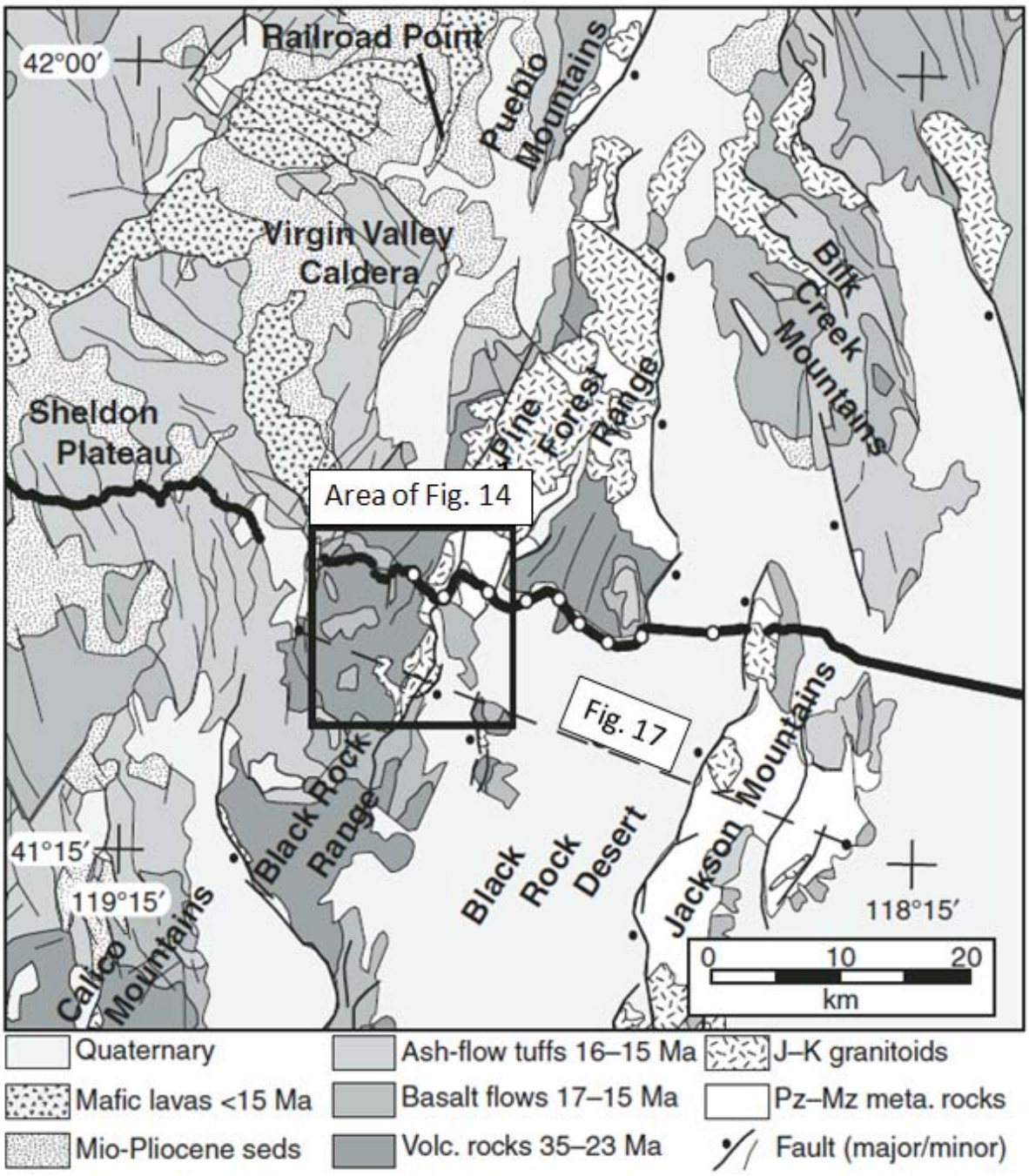

Figure 13. Geology of the Jackson Mountains, Black Rock Range, and surrounding areas. Figure taken from Lerch et al. (2008). The black box indicates the location of a detailed geologic map shown in Figure 14. Solid black line trending ~east-west indicates the location of a seismic reflection/refraction survey completed by Lerch et al. (2008). The location of Figure 17 (cross section) is labeled.

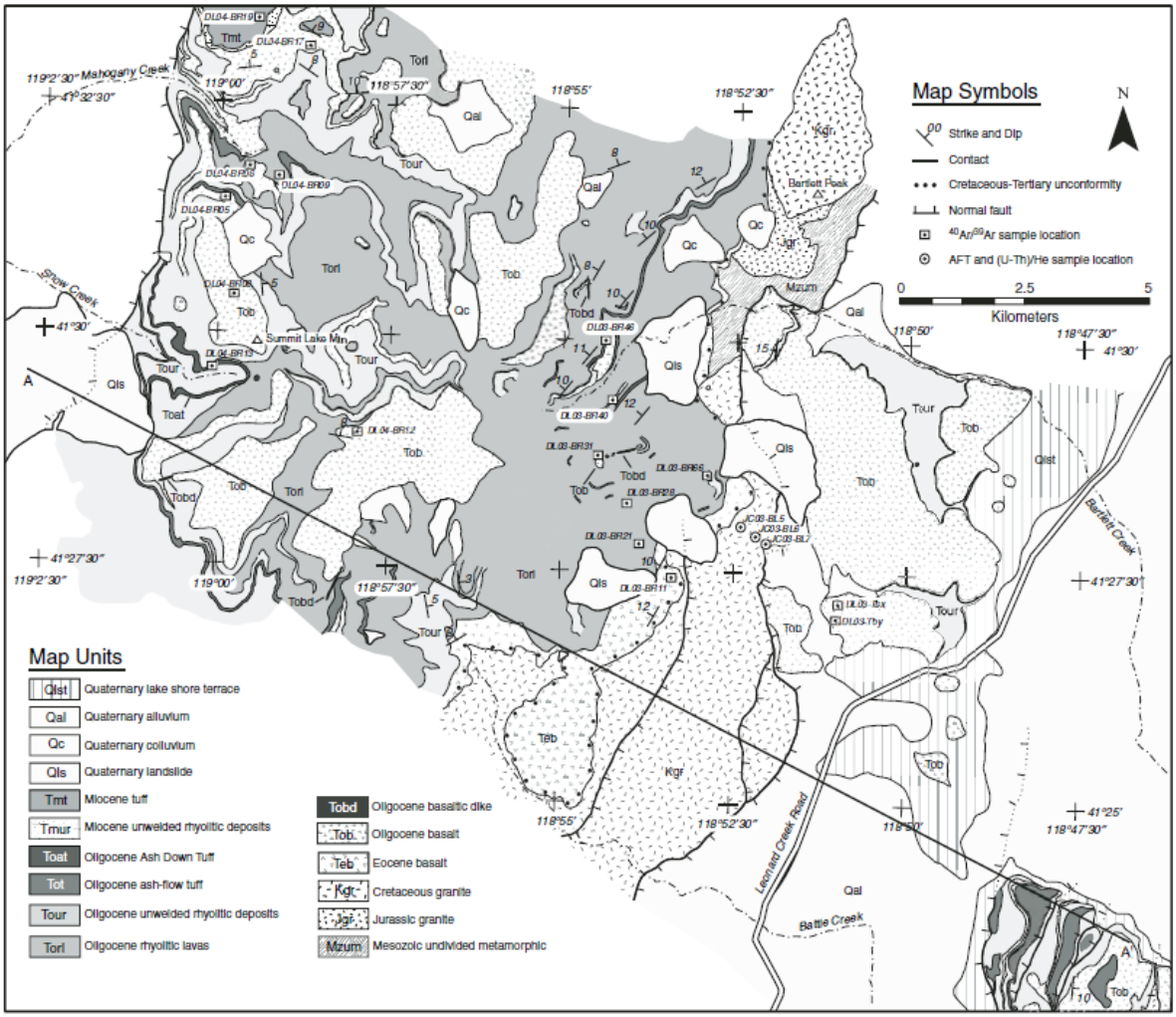

Figure 14. Detailed geologic map of the Black Rock Range, Nevada. The majority of the Black Rock Range consists of Oligocene basalts. Location of this figure shown in Figure 13. Figure taken from Lerch et al. (2008).

Tertiary Basalts:

Tertiary volcanic units are prevalent in northwestern Nevada overlying the Mesozoic strata (e.g., Lerch et al., 2008; Colgan et al., 2006). Geologic mapping ~25 km northwest of MacFarlane hot springs in the Black Rock Range (Figure 13 and 14) documents three groups of volcanic units (Lerch et al., 2008). The volcanic groups include: late Eocene basalt flows; Oligocene to early Miocene bimodal basaltic andesite flows with rhylotic lavas and ash-flow tuffs; and middle Miocene rhyolitic ash-flow tuffs (Lerch et al., 2008). These rocks are of particular interest to this study because of their spatial proximity to MacFarlane hot springs. A sequence of Tertiary basalts lies ~1 km east of MacFarlane hot springs and ~5 km west of the Jackson Mountains (Sibbett et al., 1982; Figure 12).

The oldest basalts in the Black Rock Range are Eocene alkali olivine basalts (Lerch et al., 2008; Figure 14). These were deposited as flows over Mesozoic granite and metamorphic rocks, and the flows vary in thickness from 5 to 200 m. Near the range-bounding fault to the east, the basalts have a maximum dip of ~10° to the west. In thin section, the basalts contain ~10% olivine phenocrysts (.4 mm), set in a microcrystalline groundmass of plagioclase, clinopyroxene and minor olivine (Lerch et al., 2008). A groundmass concentrate of one of the Eocene basalt flows yielded an $^{40}Ar/^{39}Ar$ age of 34.86 ± .75 Ma to 35.7 ± .5 Ma (Lerch et al., 2008).

The majority of the Tertiary bedrock in the Black Rock Range consists of ash-flow tuffs, volcanic breccias, thin basaltic trachyandesite flows, and rhyolitic lavas deposited in the Oligocene to early Miocene (Figure 14, Lerch et al, 2008). The basaltic flows in the sequence weather to red-brown, and range in texture from highly vesicular to

dense and aphanitic (Lerch et al., 2008). Olivine phenocrysts are common, although absent from the microcrystalline groundmass of plagioclase and clinopyroxene (Lerch et al., 2008). Volcanic units in this bimodal sequence range in age from ~23-25 Ma, based on $^{40}Ar/^{39}Ar$ dating.

Middle Miocene basalts have been mapped extensively across much of northwestern Nevada. These relate to either the Columbia River flood basalts, locally known as the Pueblo and Steens Basalts (e.g., Noble et al., 1970; Camp et al., 2003; Colgan et al., 2006) or the Pyramid Lake sequence basalts to the south (e.g., Bonham and Papke, 1969; Faulds and Henry, 2002; Henry et al., 2004). The Columbia River flood basalts have been dated at 16.5 – 16 Ma and are thought to be related to the first eruptions of the Yellowstone hot spot (e.g., Lerch et al., 2008). The Pyramid Lake sequence basalts have been dated at between 13.9 and 15 Ma (e.g., Faulds and Henry, 2002). Although middle Miocene volcanism is widespread, basalts with these ages are absent in the Black Rock Range (Lerch et al., 2008) based on $^{40}Ar/^{39}Ar$ dating.

Neogene sedimentary units:

Neogene sedimentary units have been mapped in much of northwestern Nevada overlying the previously mentioned basalts. These sedimentary units were deposited in lacustrine environments within separate basins that differed spatially and temporally, and thus correlating them is problematic (e.g., Mass et al., 2009). The Neogene units typically include diatomite, sandstone, and interbedded tephras (e.g. Willden, 1964; Mass et al, 2009).

Lake Lahontan Deposits:

Lake Lahontan covered the majority of the basins in northwestern Nevada during its last highstand at ~13 ka (e.g., Adams and Wesousky, 1998; 1999; Bell et al., 2007), (Figure 15). The most recent lacustrine cycle is associated with the Lake Lahontan Sehoo highstand, which receded immediately prior to 13,070 +- 60 years ago. This age was calculated by radiocarbon dating of camel bones found behind a highstand barrier in a paleolagoon (Adams and Wesnousky, 1998; 1999). The maximum elevation of the Sehoo cycle is recorded at 1338.5 m (Adams and Wesnousky, 1999).

Surficial deposits associated with the Lake Lahontan Sehoo cycle can be characterized based on vegetation, clast size, rounding, sorting, rock varnish development, and presence of rodent mounds and shoreline features (e.g., Adams and Wesnousky, 1999; Bell et al., 2007). Surficial clasts are typically subrounded to well-rounded and mainly range in size from 1 – 4 cm, although the clasts vary considerably based on location relative to mountain ranges. Shoreline features are typically visible on the ground as convex-up, positive-relief landforms consisting of well-sorted gravels and sands. Shorelines are also typically visible in aerial imagery as curvilinear features (e.g. Adams and Wesnousky, 1999).

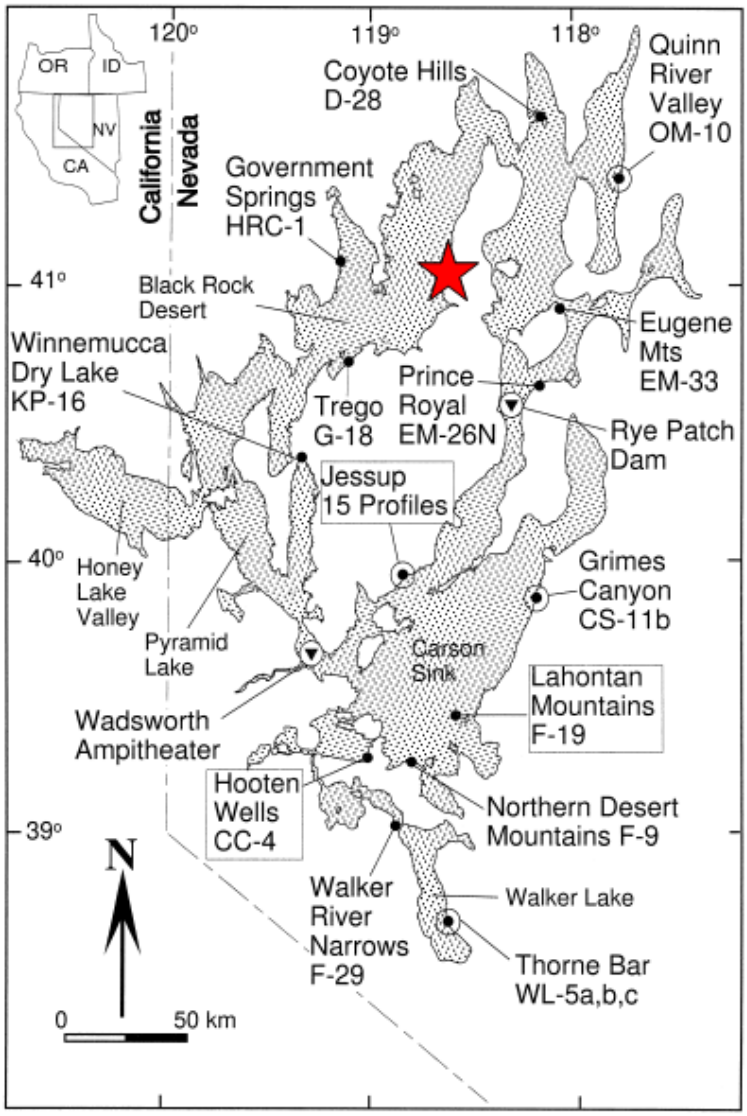

Figure 15. Location of Lake Lahontan highstand (patterned area) at ~13 ka, with MacFarlane hot springs shown as the red star (Adams and Wesnousky, 1999). Soil studies were conducted at each of the labeled locations. Dated Sehoo profiles are delineated by boxes around their labels. Pre-Sehoo soils developed on coarse beach gravels are circled, and pre-Sehoo soils developed on fluvial deposits are designated with circled inverted triangles. The samples sites spatially closest to MacFarlane hot springs are Trego and Government springs.

Soil studies were conducted at sites with Lake Lahontan Sehoo deposits in order to make regional correlations based on soil characteristics and elevations (Figure 15). Two sites along the edges of the Black Rock Desert were studied, the Government springs site and the Trego site (Figure 15). The Government springs site is at an elevation of 1332.7 m. This site consists of an undissected looped barrier that encloses a

small playette. The barrier surface is covered by well-varnished, well-developed pavement of angular to subrounded clasts. The Trego site is found at an elevation of 1333.5 m. This area is characterized by a cuspate barrier complex consisting mostly of well-sorted < 2 mm in diameter granitic gruss deposited by waves travelling south across the Black Rock Desert (Adams and Wesnousky, 1999). This work is especially pertinent because these areas are within the same basin (Black Rock Desert) as MacFarlane hot springs, and thus units should correlate based on paleo-lake elevations.

Alluvial fans:

Multiple cycles of alluvial fans have been mapped in northwestern Nevada and are formed by sheet floods, stream floods and streams (e.g., Blissenback, 1954; Peterson, 1981; Bell et al., 2009). The sorting and roundness of fan sediments can vary greatly. Generally, alluvial fan deposits are stratified with pronounced channel cut-and-fill. Local clast imbrication is also common (e.g., Blissenback, 1954). The relative ages of fans can be determined based on topography (subdued vs. bar and swale), amount of desert pavement and desert varnish, soil development, and crosscutting relationships.

Eolian dunes:

Eolian dune features are common in northwestern Nevada, due to an arid environment, abundance of fine-grained pluvial and alluvial sediments, and wind (e.g., Jewell and Nicoll, 2011). Wind erosion causes mobilization of playa sediments, which are subsequently deposited as dunes. Typical dune morphologies include linear or longitudinal dunes, transverse dunes, parabolic dunes, and star dunes. Grain composition varies from very-well to well sorted silt to sand. Each specific morphology is the result of wind directions and changes in topography (e.g., Jewell and Nicoll, 2011).

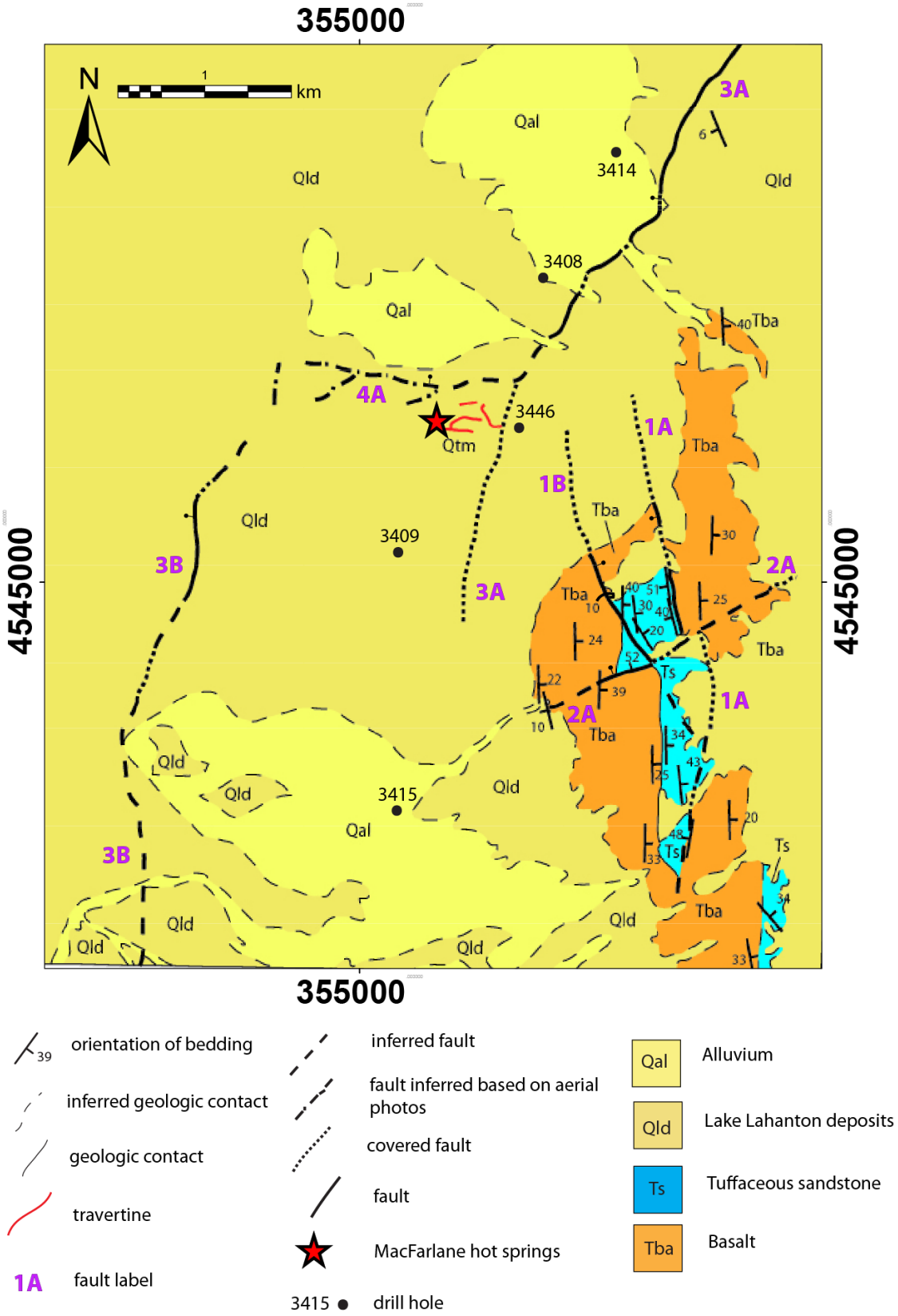

Figure 16. Previous geologic map of the MacFarlane hot springs area, modified from Sibbett et al. (1982). Faults are labeled in purple.

Geology of MacFarlane hot springs:

Geologic mapping and temperature gradient exploration drilling were done in the early 1980s in order to test the viability of the MacFarlane geothermal system (Sibbett et al., 1982; Swanberg and Bowers, 1982; Figure 16). Tertiary basalts and sedimentary units, as well as Quaternary sediments, surrounding MacFarlane hot springs were mapped (Sibbett et al., 1982), (Figure 16). Numerous faults were also mapped and proposed as controls on the permeability in the geothermal system (Sibbett et al., 1982; Figure 16). This section summarizes the results of these previous studies and then poses questions about the MacFarlane geothermal system that were not addressed in previous research.

An east-dipping sequence of Tertiary basalts is exposed ~1 km east of MacFarlane hot springs (Sibbett et al., 1982; Figure 16). A minimum basalt thickness of 366 m crops out on the ridge east of MacFarlane hot springs. The basalt varies in texture from vesicular to scoriaceous. Coarsely crystalline, yellow-brown calcite is locally present in the basalt. The depth to the top of the basalt was measured at numerous drill hole locations; this helps track fault offset throughout the area.

A Neogene sedimentary unit overlies the basalt ~ 1 km east of MacFarlane hot springs (Sibbett et al., 1982; Figure 16). This unit consists of diatomite, tuffaceous siltstone, sandstone and conglomerate. Diatoms were dated as late-middle Miocene to early Pliocene (Willden, 1964; Sibbett et al., 1982). Coquina was dated as late Miocene to early Pliocene (Sibbett et al., 1982). These deposits appear to represent a shallow lacustrine environment that changes to near-shore and fluvial environments locally.

Pleistocene Lake Lahontan sediments overlie the Tertiary units along an angular unconformity (Sibbett et al., 1982), (Figure 16). These consist of bar and shoreline

deposits, as well as deeper water sands and clays (Sibbett et al., 1982), (Figure 16). Recently deposited alluvial fans and active stream channels locally overlie all Lake Lahontan deposits (Sibbett et al., 1982), (Figure 16). Although these units are included on the preexisting map of the MacFarlane area, descriptions of these units are absent in the literature.

There are remaining questions about the details of the geologic units and their relationships to the structures in the area. The Quaternary units in this area are important, because they constrain the age and location of the youngest faults. Sibbett et al. (1982) does not give detailed unit descriptions for any of the Quaternary units. There are multiple Quaternary units in the area that were not included on the previous map, including eolian dunes, tufas, and different ages of alluvial fans. In this study, special attention is given to all ages of stratigraphy and their regional correlations in order to create a more complete geologic map. These details are important for constraining the ages of faults controlling permeability in the geothermal system.

Previously Mapped Structural Framework

The Jackson Mountain fault zone forms the western boundary of the Jackson Mountains, and its southern extent is about 6 km east of MacFarlane hot springs (Figures 12 and 17). This fault zone exhibits mainly normal to normal-oblique motion, down to the west. The Jackson Mountain fault zone has been documented using geologic mapping, gravity surveys, and seismic reflection/refraction surveys by Lerch et al. (2007; 2008). These surveys were completed in an east-trending transect ~ 45 km north of

MacFarlane hot springs (shown as a thick black line in Figure 13). The dip of the fault is unknown, but assumed to be about 40° west based on analogy to the major faults in the nearby Santa Rosa and Pine Forest Ranges (Figure 17, Colgan et al., 2006). Slow seismic velocities (Vp <- 3.0 km/s), indicating basin fill sediments, extend to a ~0.6 km depth across the Black Rock Desert and reach a maximum thickness nearing the Jackson Mountain fault zone (Figure 17, Lerch et al., 2008). This indicates considerable offset (>0.6 km) along this fault zone. This fault system has slipped in the past ~13,000 years based on scarps expressed in Lake Lahontan sediments. The fault system has been active since the Mesozoic, because the fault is expressed offsetting Mesozoic stratigraphy in the Jackson Mountains.

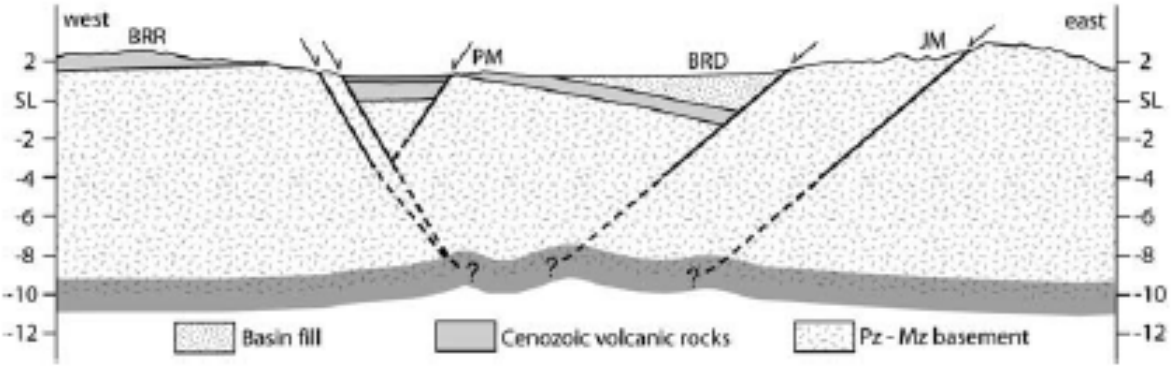

Figure 17. Simplified cross section of the faults in the Black Rock Range, Black Rock Desert, and Jackson Mountains (Lerch et al., 2008). Location of transect is shown in Figure 13. BRR – Black Rock Range, PM – Pinto Mountain, BRD – Black Rock Desert, JM – Jackson Mountains. No vertical exaggeration, depths are given in kilometers relative to sea level (SL).

The faults directly surrounding MacFarlane hot springs are grouped here in four categories based on ages and orientations (1A and 1B; 2A; 3A and 3B; and 4A; Figure 16). For ease of reference, the older fault system (1A, 1B, and 2A) will be referred to as

the Rattlesnake fault domain. The younger fault system (3A, 3B, and 4A) will be referred to as the MacFarlane fault zone.

A series of faults was previously mapped in Tertiary bedrock ~ 1 km east of MacFarlane hot springs (Sibbett et al., 1982). The faults form a north-trending graben expressed in Tertiary bedrock (Figure 16, faults 1A and 1B). A minor northeast-striking, west-side-down Tertiary fault post dates faults 1A and 1B (Figure 16, fault 2A). Fault 1A dips to the west and has accommodated 305 m of offset of the sedimentary beds (Sibbett et al., 1982). The sedimentary beds (Ts, Figure 16) have been warped into an asymmetrical syncline due to drag folding along fault 1A (Sibbett et al., 1982). The antithetic normal fault 1B is not further described in previous literature. Fault 2A is shown on the map but not further described in the previous literature.

The MacFarlane fault zone directly surrounds MacFarlane hot springs (Sibbett et al., 1982), (Figure 16, faults 3A, 3B and 4A). This fault zone consists of a series of north-northeast-trending, right-stepping scarps expressed in Lake Lahontan sediments (Sibbett et al., 1982). Fault 3A accommodates ~6 m of down-to-the-west offset of algal tufa mats (Sibbett et al., 1982). The top of a sequence of basalt flows is offset ~ 400 m down to the west just south of MacFarlane hot springs along the same fault, based on drill hole data (Sibbett et al., 1982). An east-west striking dextral step connecting faults 3A and 3B was mapped based on a lineament visible in aerial imagery (Sibbett et al., 1982), (Figure 16, fault 4A).

There are many unanswered questions about the geometry, kinematics and locations of the specific faults, which are important in understanding fluid pathways for

the geothermal system. Very limited kinematic data were collected by Sibbett et al. (1982). Kinematic data are especially important to constraining movement on the Tertiary fault system, which is expressed in bedrock. Because the Quaternary faults are expressed in unconsolidated Quaternary sediments, it is difficult to measure kinematics. Detailed Quaternary mapping and geophysical surveys would greatly help to constrain the MacFarlane fault zone.

Previous Geothermal Exploration at MacFarlane Hot Springs:

Temperature Gradient Wells:

Forty-four temperature gradient boreholes were drilled near MacFarlane hot springs by Teledyna Geotech (Garland, TX) and Hunt Energy Corporation (Dallas, TX) in the early 1980's (Swanberg and Bowers, 1982). The raw drilling data are owned privately and were not available for this thesis project. The wells covered an area of

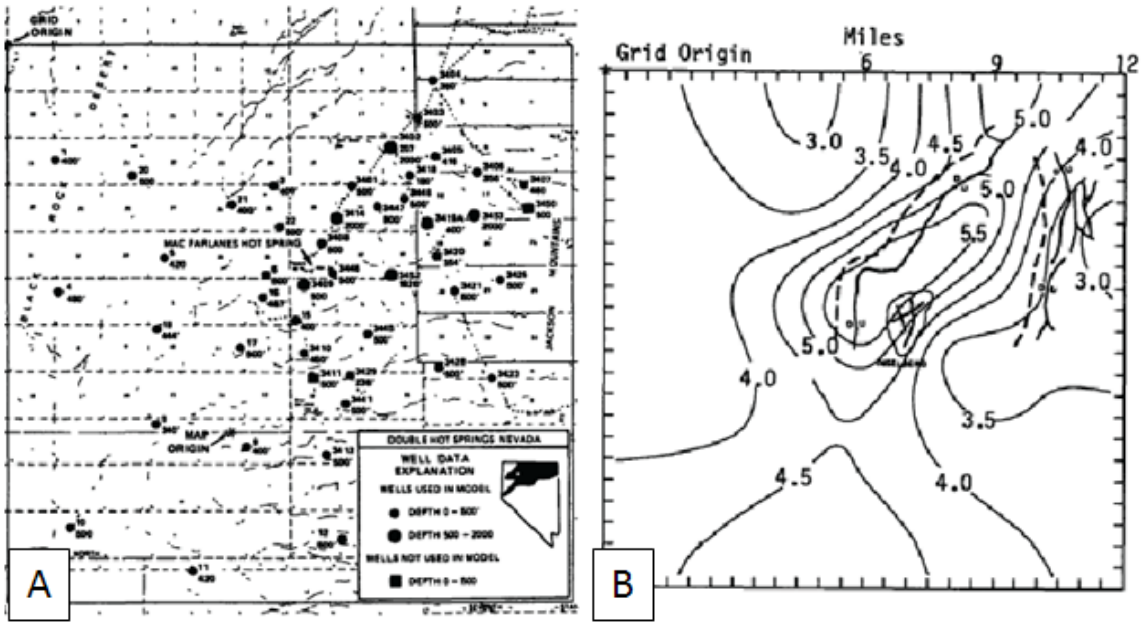

Figure 18. Original temperature gradient map and location of drill holes, from Swanberg and Bowers (1982). A. Shows the actual number and location of drill hole. B. Shows the low-order polynomial fit (trend surface) to temperature gradients (°F/100 ft). Mapped faults are shown as black lines. The wells vary in depth from 30-150 m to 460-610 m (small and large black dots respecively). These figures are combined and projected onto a topographic map in Figure 19 for ease of viewing and interpretation.

about 370 km^2 and directly surround MacFarlane hot springs (Figures 18 and 19). The results, as summarized by Swanberg and Bowers (1982) and Sibbett et al. (1982), are presented here.

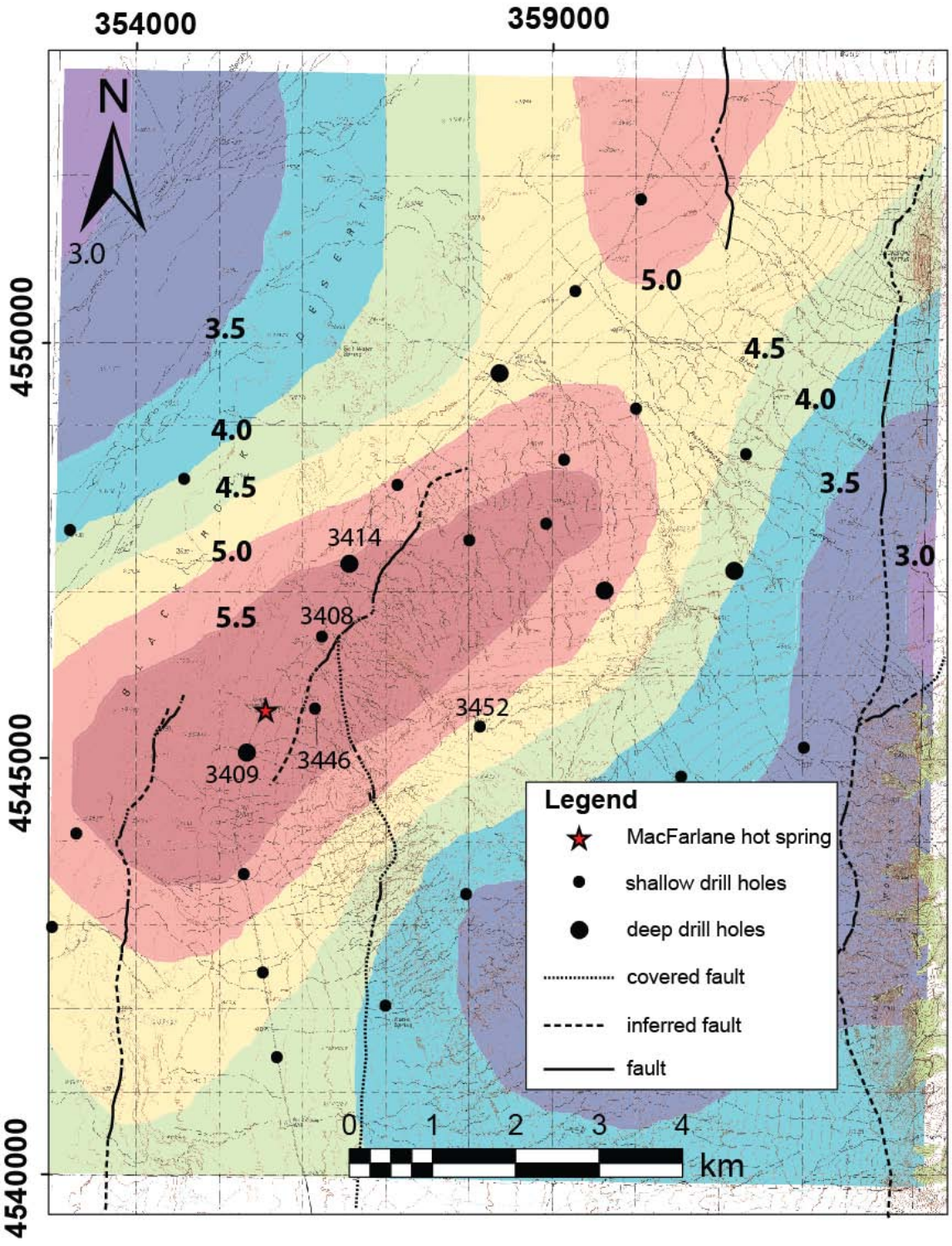

Figure 19. Low-order polynomial fit (trend surface) to temperature gradients (°F/100 ft) of MacFarlane hot springs area. Figure modified from Swanberg and Bowers (1982) and Sibbett et al. (1982). Faults shown were mapped in this study. Shallow drill holes are 30-150 m in depth, and deep drill holes are 460-610 m in depth. Wells with measured depth to the top of basalt (Tb) are labeled above the drill hole (3414, 3408, 3452, 3446, 3415 and 3409). MacFarlane hot springs is shown as a red star, due west from drill hole 3446, to the west of the north-northeast striking fault.

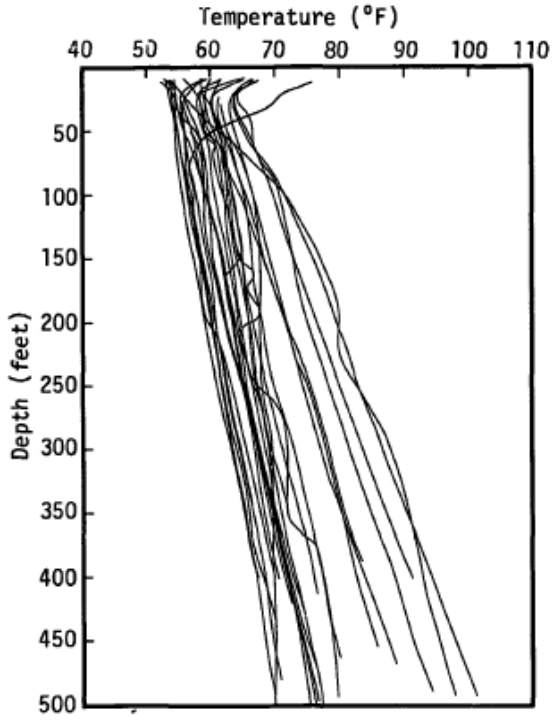

Figure 3a.

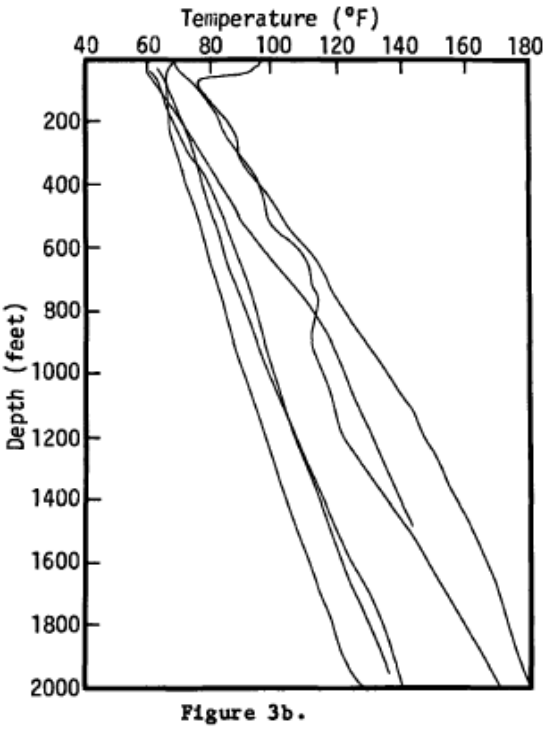

Figure 3b.

Most of the temperature logs show strong linear relationships between temperature and depth (Figure 20). Only the temperature gradients that showed a linear relationship (and were not influenced by groundwater) were used in the temperature gradient map. Linear temperature/depth curves indicate conductive heat transfer and can be used to find geothermal upwelling. Specific temperature logs for each drill hole are not available in this dataset.

An east-northeast-trending high temperature gradient anomaly (shown in red, Figure 19) surrounds the hot springs. This high temperature anomaly is 8.5 km long and up to 3.5 km wide (Figure 19). The highest temperature gradient is about 189° C/km (Swanberg and Bowers, 1982), which was observed at well 3408 (Figure 19). The maximum actual temperature measured is 81° C at a depth of 610 m.

Figure 20. Temperature gradients measured at MacFarlane hot springs (Swanberg and Bowers, 1982). Shallow wells are shown at the top and deep wells are shown below.

Although this temperature gradient anomaly is large spatially, the temperatures are considered low in relation to other high-temperature geothermal systems in the Basin and Range.

Structural Controls:

The structural controls have been proposed for the north-northeast-trending high temperature gradient anomaly found surrounding MacFarlane hot springs (Swanberg and Bowers, 1982; Sibbet et al., 1982). The anomaly was proposed to be associated with the projected intersection of the north-northeast-striking fault of the MacFarlane fault zone and the older fault exposed in Tertiary bedrock (Sibbett et al., 1982; Swanberg and Bowers, 1982). This location is consistent with the location of the highest temperature gradient drill hole 3408 (Figure 19). The actual hot springs were thought to be associated with a step-over in the MacFarlane fault zone (Sibbett et al., 1982; Swanberg and Bowers, 1982; Figure 16).

Geochemistry:

One water sample from the hot springs was analyzed to determine the geothermal reservoir temperatures. The water was sodium-bicarbonate-chloride type and contains 3650 TDS (Sibbett et al., 1982). Geothermometry using Na-K-Ca and quartz were concordant and gave a maximum reservoir temperature of ~140° C (Sibbett et al., 1982). Quartz, Na/K and chalcedony calculations were also done and gave reservoir temperatures of 80° - 120° C (Sibbett et al., 1982). High temperature geothermal systems have reservoir temperatures >160° C (e.g., Arehart et al., 2004; Coolbaugh et al., 2006).

MacFarlane thermal anomaly is not considered a high temperature system, but could be developed using current technologies as a binary power plant system.

Further Research Questions:

There are still questions remaining about the details of the structures that control the MacFarlane geothermal system. Based on recent studies on the structural controls of geothermal systems in the Basin and Range, Holocene faults are most likely to control upwelling. The Holocene fault geometries at MacFarlane hot springs need to be considered as possible controls on the geothermal upwelling. The details of the right step-over have not been mapped nor discussed. The anomalous east-west trending orientation of the travertine fissure ridge also is not discussed. The major and minor travertine deposits provide crucial structural information regarding the formation and geometries of the Holocene faults and fractures that might control the geothermal system.

RESEARCH DESIGN

This study was designed to test between different structural settings that could control the MacFarlane geothermal system and associated anomalously oriented travertine fissure ridges. The unusual orientation of the travertine fissure ridges has not been discussed and is imperative to the structural controls of the geothermal system. The possibilities that are tested in this study include:

1) an east-striking fault intersecting the MacFarlane fault zone at the travertine fissure ridges,

2) a single southward fault termination on fault 3A in the MacFarlane fault zone,

3) single northward fault termination on fault 3B,

4) a partially dissected relay ramp formed between two terminating faults 3A and 3B,

5) a hard-linking step-over (fault 4A) linking faults 3A and 3B,

6) an intersection between faults 1A and 3A near the location of the travertine and high temperature gradient (Figure 21),

7) Lithologic controls on the travertines, such as a linear paleochannel or dilation related to previous jointing in the underlying basalt.

Previous work suggests that the travertine ridges are related to a right hard-linking step-over in the MacFarlane fault system (Sibbett et al., 1982), (fault 4A, Figure 16) and that the geothermal upwelling is related to a fault intersection between faults 1A, 2A and 3A (Sibbett et al., 1982; Swanberg and Bowers, 1982; Figure 16).

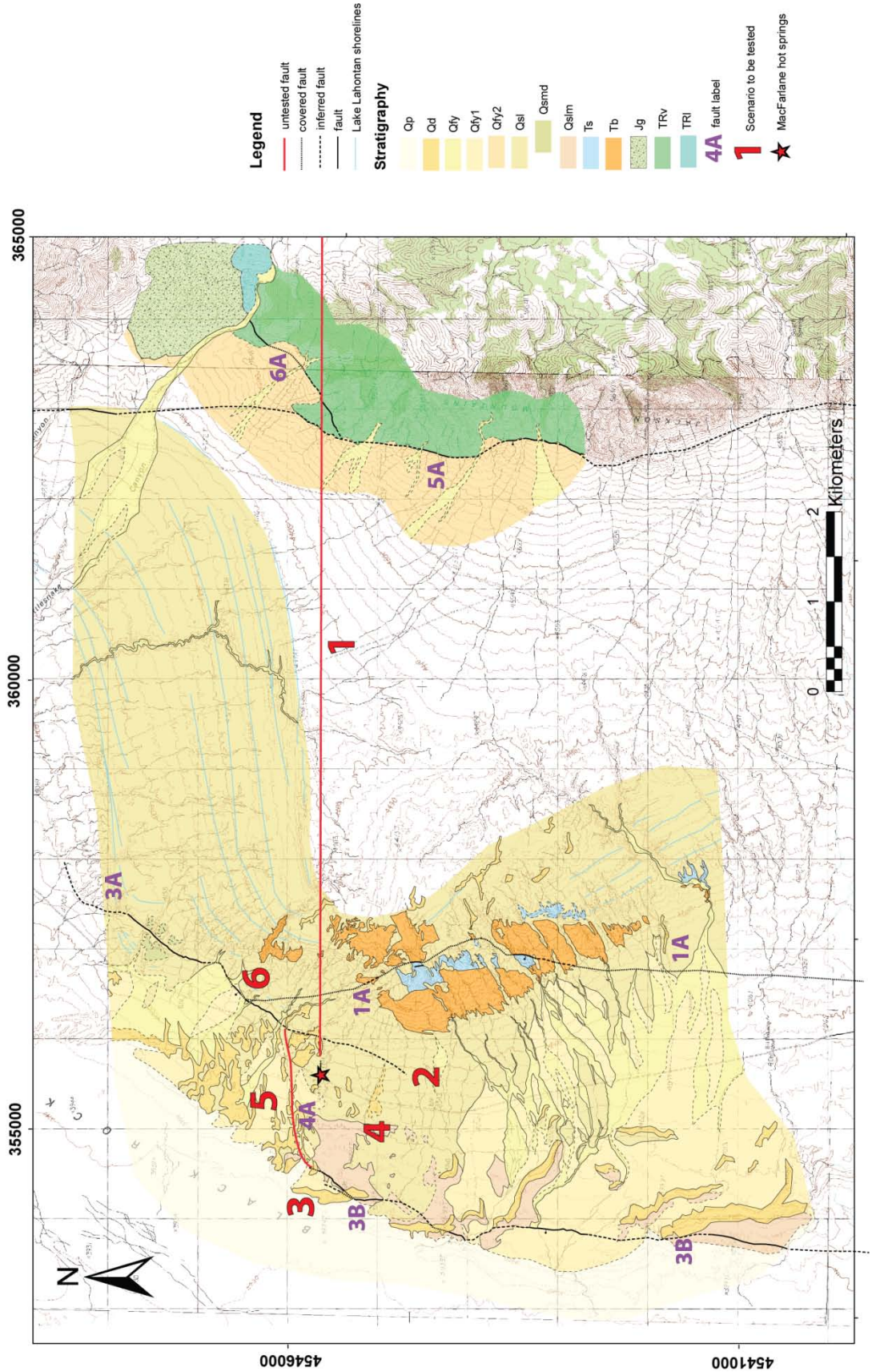

Figure 21. Different structural scenarios tested in this study in order to determine the structural controls of the MacFarlane geothermal system are labeled in red (1-6). The faults are labeled in purple. MacFarlane hot springs is shown as a red star. The geology and faults shown in black were mapped as a part of this study. The faults in red were tested but not found.

A variety of methods was used to test these structural scenarios. Geologic mapping was conducted to show age relationships between structures and to constrain fault kinematics and offset. All Quaternary and bedrock units were described and mapped in detail so that regional correlations could be made. The amount of offset on fault 1A can be determined based on detailed geologic mapping. The locations and orientations of faults 3A and 3B were mapped in detail as part of the Quaternary mapping. The southern Jackson Mountains were mapped in order to test for a proposed east-west striking fault. Kinematic data were gathered from all observed fault surfaces.

As a second phase of the project, two-meter and one-meter temperature surveys were conducted to: 1) test hypotheses on locations of shallow fluid flow related to faults or other permeable units, and 2) discover areas of high temperature that might have been overlooked in previous work. Traverses were done perpendicular across known faults, as well as down-topography from the faults, in order to see if certain faults were controlling hot fluids at a shallow depth. One-meter surveys were completed in areas that were designated Black Rock Desert Wilderness (no motorized vehicles allowed) or in areas with extremely rough topography. This method was also used as a reconnaissance technique in order to explore for previously missed high temperature areas.

In addition, a magnetic survey was completed to test specific fault terminations. After compiling all the data, the specific locations of the terminations on faults 3A and 3B were still questionable. This is based on limited surface expression, degradation of fault scarps expressed in sediments, and a limited shallow temperature signature. First, a ground-based magnetic traverse was done perpendicular to locations on the fault with

documented offset to assess whether the faults had distinct magnetic signatures. The magnetic signatures of faults 3A and 3B were not distinct enough to warrant further magnetic surveys.

RESULTS

In this section, new data collected throughout this project are presented. This includes new geologic mapping data from the southern Jackson Mountains and from the area directly surrounding MacFarlane hot springs. Next, all of the kinematic data and fault observations are presented. New shallow temperature survey data are also shown and related to faults in the area. Lastly, results from a ground-based magnetic survey and their implications are summarized.

Stratigraphic Framework:

Overview:

Geologic mapping focused on the location, orientation, kinematics and timing constraints on the faults in the area. Detailed mapping was also used to correlate units regionally. An overview of the stratigraphy, from oldest to youngest, is presented below.

A small part of the southern Jackson Mountains was mapped to test for a regional east-striking fault along strike of the travertine ridge (Scenario #1, Figure 21). The Mesozoic stratigraphy here includes a heavily veined and altered limestone unit overlain

by a slightly metamorphosed volcaniclastic sequence and intruded by a dioritic pluton (Figure 21). These units strongly resemble the Permian - Triassic Bliss Canyon Formation limestone, the Happy Creek volcanic complex, and a suite of Jurassic intrusive bodies mapped ~ 3 km to the north by Willden (1964), Maher (1989), and Quinn et al. (1997).

The Tertiary bedrock ~1 km southeast of MacFarlane hot springs provided kinematic data on fault 1A (Figure 21). These rocks consisted of basalts and a tuffaceous sedimentary unit. Both of these units are difficult to correlate with regional stratigraphy. The Tertiary basalt texture at MacFarlane is distinct from the nearby Pyramid sequence and Columbia River flood basalts based on its large pyroxene phenocrysts (1-3 cm). It does contain similar coarse mafic pyroxenes as a late Oligocene basalt mapped in the Fox and Lake Ranges (Anderson et al., 2013), but further mineralogy and 40Ar/39Ar dating is needed to confirm this correlation. The sedimentary units were deposited within separate paleo-basins that are difficult and problematic to correlate regionally.

Detailed Quaternary mapping provided locations and relative ages of faults 3A and 3B (Figure 21). Quaternary mapping also tested structural scenarios relating to the travertine orientations, including a relay ramp, fault terminations, lithologic controls, and/or a hard-linking step-over (fault 4A, Figure 21). Quaternary units include lacustrine deposits with shoreline features, deeper lake sediments, relict alluvial fans, travertine fissure ridges, eolian dunes, and active stream channels. The lacustrine sediments resemble those of the Lake Lahontan Sehoo cycle mapped in nearby basins by Bell et al. (2009), based on clast composition, rounding and size, morphology of deposits, and

elevations. The network of travertine fissure ridges was mapped to evaluate relationships between orientations, locations, and relative ages of the fissure ridges.

Mesozoic Stratigraphy:

The bedrock units exposed in the southern Jackson Mountains were mapped along strike of the travertine fissure ridges to test the possibility of a regional east-striking fault controlling the location of the travertine fissure ridges (Scenario #1, Figure 21). Age relationships were found between all units and are presented below.

Bliss Canyon Formation Limestone

The oldest unit is a grey limestone. The limesone is heavily fractured, with extensive white calcite veins and local greenish-blue malachite (Figure 22). The surface shows extensive spitzkarren weathering. Local brecciated areas with angular to sub-angular pebble to cobble size clasts are present; the brecciated areas have local areas of greenish-blue malachite and deep red to brown hematite mineralization in the matrix. No marine fossils were observed. This unit is likely related to the limestone sequence of the Bliss Canyon Formation, which is Middle to Upper Triassic (Maher, 1989; Quinn et al., 1997). This correlation is based on similar rock compositions and position relative to the overlying Happy Creek Volcanic unit.

Happy Creek Volcanic Complex

A stratified metavolcanic sequence overlies the limestone unit. This sequence ranges from welded tuff, to conglomerate, to sandstone. The volcanic unit consists of green, brown and red pyroclastic welded tuff. Locally, feldspars have been altered to a

reddish-brown clay. The conglomerate unit consists of subrounded gravel to pebble size chert and other lithic clasts. Local clasts up to cobble-size of the underlying limestone were found interbedded within the conglomerate, confirming the relative ages of the two units (Figure 23). The sandstone/mudstone unit is reddish brown to grey and has a fine to very fine grain size. This unit has been slightly metamorphosed, but preserved bedding is also present. This sequence appears to have similar rock compositions to the upper crustal stratified volcanic sequences of the Happy Creek Volcanic complex, mapped to the north in the Jackson Mountains by Maher (1989) and Quinn et al. (1997).

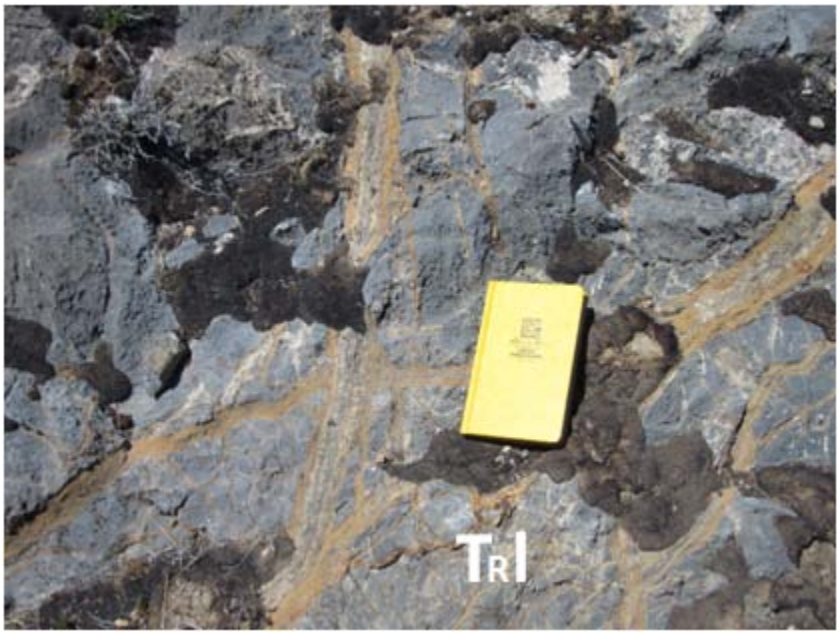

Figure 22. Heavily fractured and weathered Middle to Upper Triassic limestone of the southern Jackson Mountains (TRl). This unit resembles the Bliss Canyon Formation.

Figure 23. Clast of limestone (Trl) incorporated into the overlying metavolcanic sequence (TRv).

Granodiorite

A light-green porphyritic slightly-metamorphosed granodiorite intrudes the volcaniclastic and limestone sequences. This unit is composed of quartz, hornblende (1-5 mm in length), pyroxene, and feldspars; the composition of the rock is 50-60% mafic minerals. Local secondary epidote is also present. Greenschist facies metamorphism has occurred based on green color and presence of epidote. This unit likely correlates to the plutons previously mapped by Maher (1989) and Quinn et al. (1997) in the Jackson Mountains to the north, based on similar mineral assemblages and stratigraphic relationships. U/Pb data indicate that these plutons are between 196 to 190 Ma, or Early Jurassic (Quinn et al, 1997).

Tertiary Stratigraphy:

Basalt (Tb) and a Neogene sedimentary unit (Ts) were mapped ~1 km east of MacFarlane hot springs at a detailed scale, to better constrain kinematics on fault 1A (Figure 21). The fault kinematics and ages of fault 1A are especially important, because the geothermal water might be controlled by fault 1A intersecting fault 3A. It is also useful to attempt to correlate the basalt with regional units.

Basalt

The basalt unit (Tb) covers an area of ~ 4 km^2. The flows vary from black to dark grey and exhibit local columnar jointing (Figure 24). The unit is extensively weathered to dark to light reddish-brown. The basalt ranges in texture from coarsely porphyritic to aphanitic. Phenocrysts of dark black pyroxene (1-3 cm), plagioclase (5 mm – 1 cm in length) and small phenocrysts of olivine (<4 mm) are found within the porphyritic flows. The plagioclase is dark grey and opaque in color and forms thin, tabular crystals. The olivine is commonly weathered to a brownish red. Vesicles up to 1 cm in diameter are found near the stratigraphic top of each local flow sequence. Needle-shaped, light green quartz crystals locally fill vesicles. The entire unit has been tilted and dips 22° – 40° to the east and strikes mainly north to north-northwest.

Veins of light orange calcite and white silica cut the basalt (Figure 24C). The veins were measured in most basalt outcrops throughout the map area, although certain areas (m scale) had higher concentrations of veining. The orientations of silica veins

vary from north-northeast-striking to southwest-striking, and are discussed further in the next section. Silica veins range from 1 cm to ½ m in thickness and show amorphous to botriodial textures. Calcite veins range from 1 cm to 6 m in thickness and show dog-eared texture. No obvious cross-cutting relationships were found between the calcite and silica veins, so their relative ages are unknown. These veins are found throughout the basalt (Tb) but do not cut the tuffaceous sedimentary (Ts) unit. Based on this observation, the veins predate Ts.

This basalt (Tb) has phenocryst assemblages (e.g. coarse pyroxene phenocrysts) that resemble late Oligocene sequences in the Fox and Lake Ranges (Anderson et al., 2013) rather than the Pyramid Sequence (e.g., Bonham and Papke, 1969; Faulds et al., 2003; Henry et al., 2004). The large (1-3 cm) pyroxene phenocrysts found in the basalt at MacFarlane resemble basalt in the Fox Range that is dated at 27.39 +- 0.09 Ma (R. Anderson, unpublished data, 2014). However, the Oligocene to early Miocene volcanic strata mapped in the Black Rock Range by Lerch et al. (2007) lack mafic phenocrysts, which is not consistent with Tb. Thin section analysis and 40Ar/39Ar dating would be required to confirm a correlation between Tb and the late Oligocene basalts in the region.

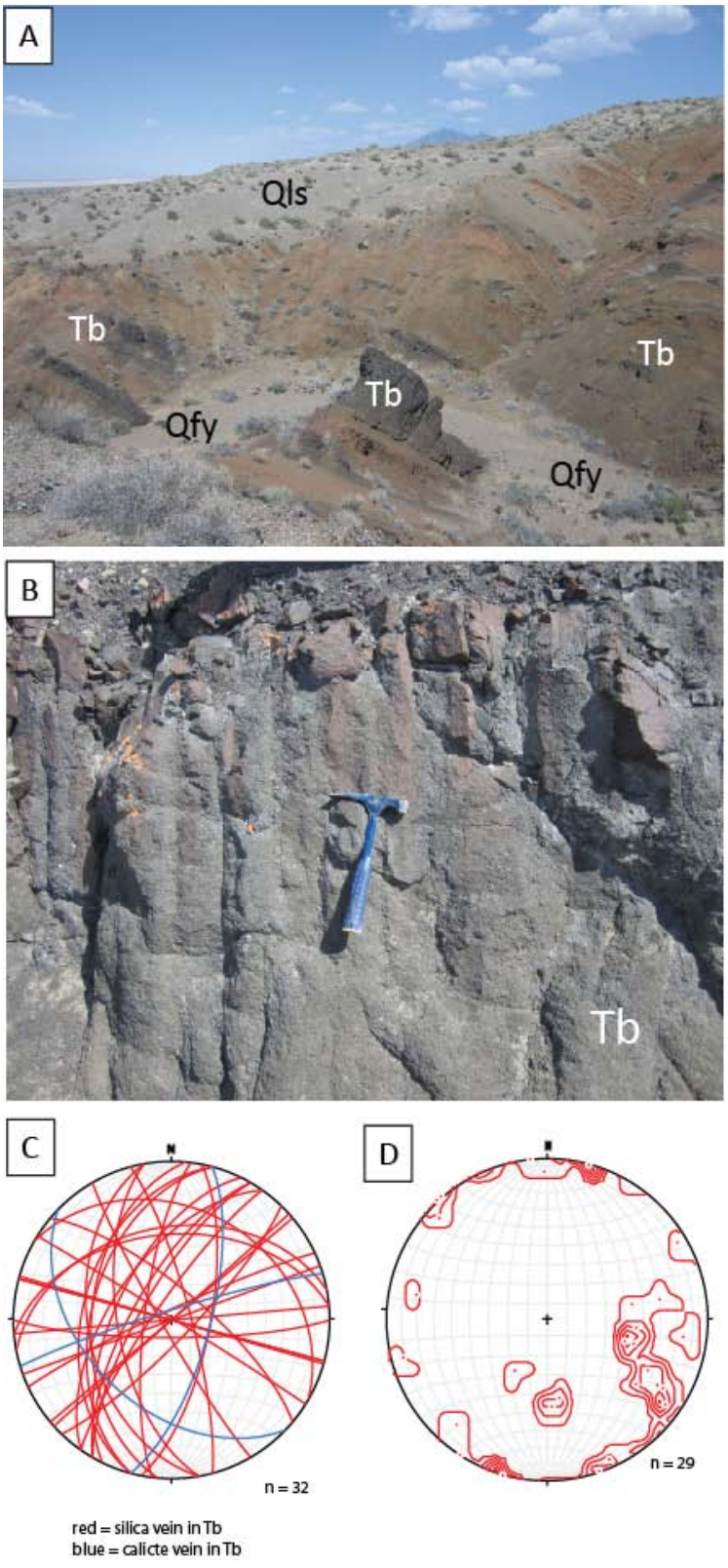

Figure 24. Photo A: "Tb" basalt. Photo taken looking north at basalt (Tb) overlain by Lake Lahontan sediments (Qsl) in an angular unconformity. B: columnar jointing in Tb. These photos are typical of Tb and show its extensive weathering. C: Great circles of calcite and silica veins that cut Tb. D: Density contour of poles to veins. Contours are 2% per 1% area. Data were compiled in the Stereonet 9 program (Rick Allmendinger, 2013).

Diatomite and Tuffaceous Sandstone

A sedimentary sequence (Ts) overlies the basalt (Tb). This unit is a moderately weathered tuffaceous sandstone and diatomite, with local coquina and resistant silicified layers. The sandstone is light tan to reddish-brown, coarse-grained, moderately sorted, and 1-10 cm thick. Bedding is well-preserved in some of the sandstone sequences. The interbedded tuffaceous layers are light tan to brown and ~ 1 cm thick. The diatomite is white, very fine-grained and chalky in texture. In much of the area, this unit is severely weathered. No veins were observed in this unit.

There are three distinct white-to-tan coquina horizons within the Ts unit that range in thickness from 6 – 20 cm. The actual coquina shells range from 2 - 5 mm in diameter (Figure 25). Local reddish brown silicified sandstone with round nodules that are ½ - 1 cm in diameter are found associated with the coquina. This unit forms a distinct marker bed that can be traced throughout the map area and used to constrain fault movement. It also provides a reliable resistant bed on which bedding orientations can be measured.

The contact between Ts and Tb is depositional. The contact is exposed in a canyon wall of a recent drainage. Bedding in Ts and flow surfaces in Tb have similar orientations near the contact. The contact between the basalt and sedimentary unit lacks evidence of faulting, such as a higher concentration of veining and silicification, drag folding, or deformed beds. The contact is also irregular and records paleotopography on the surface of Tb.

Figure 25. Photo A: resistant coquina layer in outcrop. Photo B: coquina shells in hand sample. This unit is distinct and provides a reliable marker bed within Ts that can be traced throughout the area. It is offset by fault 1A.

This sedimentary unit (Ts) resembles other Neogene units in the region. However, correlating their ages is problematic because of inadequate age control. The units were deposited in basins that varied spatially and temporally. The presence of mollusk shells in the coquina provides a general age for this unit, which is late Miocene (Sibbett et al., 1982). Diatoms collected in the Jackson Mountains were dated as late-middle Miocene to early Pliocene, in accord with the inferred ages of the coquina shells (Willden, 1964; Sibbett et al., 1982). 40Ar/39Ar geochronology on the tuffaceous horizons is needed to confirm the age of the Ts unit.

Quaternary Units:

Late Pleistocene and Holocene units, including Lake Lahontan lacustrine deposits, travertine fissure ridges, and post-Lahontan deposits, constrain the latest movement on the faults in the study area. The Lake Lahontan deposits can be separated into three main units: recessional barrier beach and bar deposits, lake sediments, and tufa (Plate 1). These units correlate with the Lake Lahontan Sehoo highstand mapped by Adams and Wesnousky (1999) in the Black Rock Desert. This correlation is based on the elevations of the deposits and similarity of sediment types and morphology. The post-Lahontan units include alluvium, eolian dunes, and ephemeral playa and stream channel deposits.

Figure 26. Fine-grained lacustrine sediments (Qslm) shown on the left. This photo is taken looking south. This photo shows the distinctive white color, fine-grained sediment size, lack of vegetation and low-lying topography of Qslm relative to other units. Reddish-brown dendritic tufa associated with Qslm is also present in the foreground. Eolian dunes (Qd) are in the background.

Lake Lahontan Deposits

A fine-grained lacustrine package is the stratigraphically lowest of the Lake Lahontan units in the study area. This unit is characterized by white to light tan very-fine grained silts and clays (Figure 26, Qslm). The sediments in this unit are loosely to moderately consolidated, with little vegetation. This unit is somewhat dissected by drainages, probably due to its easily erodable sediments. This unit is distinguishable in the field by a light to white albedo in aerial imagery, low-lying topography, and lack of shoreline-related rounded clasts. Local reddish brown dendritic tufa (up to 2-4 cm thick)

is associated with this unit. The tufa is somewhat laterally continuous, covering areas up to ~5 m^2. These sediments and associated tufas are confined to a distinct elevation between ~1190 – 1220 m.

Figure 27. Photo shows typical ground surface of the Sehoo Lake Lahontan recessional shorelines. The clasts here are subrounded to rounded and are covered by moderately developed rock varnish.

Lake Lahontan recessional beach and bar deposits (Qsl) overlie the fine-grained lacustrine sediments (Qslm) along a depositional contact. On the ground surface, these deposits consist of moderately to well-sorted subrounded to rounded gravel-to pebble-size clasts (Figure 27). Locally, these deposits form convex up topographic highs (up to 2-3 m) with rounded crests. These topographic highs consist of well-rounded clasts with moderately to well-developed desert pavement. These topographic highs form thin, curvilinear traces visible in aerial photographs and on the ground (Figure 28a and 28b).

This unit overlies the Tertiary basalts and sedimentary unit along an angular unconformity.

Tufa (Qsmd) is present along the Lake Lahontan recessional shorelines. These algal tufa mats are typically dark brown to red, laterally continuous, and up to 7 cm thick (Figure 29). The tufa mats are more resistant than the surrounding Lake Lahontan sediments. The tufa mats exhibit dendritic textures and local tufa-cemented, well-rounded beach pebbles and gravel. The largest laterally continuous tufas are found between 1245 and 1255 m elevation and cover ~ .8 km^2 (Plate 1). These specific tufas document offset along fault 3A. They provide a resistant layer that preserves the fault scarps, records amount of offset, and shows the locations and orientations of the faults.

The Lake Lahontan recessional beach deposits (Qsl) and associated tufas (Qsmd) correlate with the Sehoo highstand, previously mapped in the Black Rock Desert by Adams and Wesnousky (1999) and mapped in nearby basins by Bell et al. (2007). This is based on similar elevations, shoreline morphology, and sediment characteristics. The extensive dentritic tufa is also consistent with Lake Lahontan Sehoo deposits. Based on field observations, this unit is interpreted to be slightly younger than the fine-grained sediments, and deposited on top of the fine-grained lacustrine sediments as the lake levels receeded ~ 13,000 years ago.

Based on sediment characteristics and similar elevations of this deposit, lacustrine unit Qslm also correlates with the Lake Lahontan Sehoo highstand mapped by Adams and Wesnousky (1999). The depositional setting of this unit is a deeper water lake environment, based on very fine grain size and low, uniform elevation relative to other

lacustrine deposits. This is the thickest lake-cycle unit of the Sehoo member, with high proportions of silt and clay in the lowlands (e.g., Morrison and Frye, 1965). Dendritic tufa members are also a defining characteristic of these young Sehoo lacustrine cycles. The Sehoo highstand receded immediately prior to 13,070 +- 60 years ago (Adams and Wesnousky, 1998; 1999).

Alluvial Fans

The inactive alluvial fan unit (Qfy1) overlies bedrock and lacustrine sediments (Figure 28b). Qfy1 is found associated with lower-elevation areas near MacFarlane hot springs. These fan deposits are composed of sandy matrix with mainly pebble-to cobble-size subrounded to subangular clasts. The clast are composed of locally derived bedrock. Well-rounded beach cobbles are also present. There is local moderately to well-developed desert pavement on the fan surface, with moderately to poorly developed rock varnish. Cryptobiotic soils are locally developed on the surface as well. These older fans are characterized by subdued, smooth topography, and slightly darker albedo in aerial photos (Figure 26a). This fan unit covers all Lake Lahontan deposits, yet is cut by Holocene fault scarps associated with fault 3A. This indicates that it is younger than ~13,000 years.

Inactive alluvial fan unit (Qfy2) occurs at the foot of the southern Jackson Mountains ~ 6 km to the east of MacFarlane hot springs. This unit can be distinguished from Qfy1 based on clast composition and rounding. This unit is characterized angular to

sub-angular gravel- to cobble-size clasts that are moderately to poorly sorted. Composition of clasts mainly includes bedrock from the southern Jackson Mountains. This unit can also be distingushed from Qfy1 by its distinct lack of reworked beach cobbles. Local moderately- to well-developed desert pavement and rock varnish are present. There is minor development of cryptobiotic soils.

Ephemeral stream channel and fan deposits (Qfy) overlie the bedrock, lacustrine sediments, and older alluvial fans (Figure 28 and 30). The stream channels are typically 2 – 8 m wide, and gradually widen and fan out as the topography flattens to the west. Meanders are present in many stream channels. These deposits have a silty to sandy matrix, with clasts that are gravel to boulder-size, poorly-sorted, and angular. The clasts are composed of locally derived basalt, sandstone, coquina, diatomite, travertine, and limestone. Well-rounded reworked beach cobbles are present locally. This unit can be distinguished from the older fan cycle based on its angular, poorly-sorted clasts and rough fan surface topography. This unit also typically has a darker albedo in imagery than the older fan cycle, and there is minimal development of desert pavement and rock varnish. This fan cycle covers all fault scarps and Lake Lahontan sediments in the area, indicating that Qfy is younger than ~13,000 years (Figures 28 and 30).

Eolian Dunes

Eolian dunes (Qd) locally overlie the bedrock, lacustrine, and alluvial fan units. The dunes are up to ~1.5 km long and up to ~300 m wide. They are typically associated with the fine-grained lacustrine sedimentary units (Figure 30b, Qd) and are also found flanking the playa. The area directly surrounding MacFarlane hot springs and the

travertine fissure ridges has longitudinal and transverse dunes (Figure 30a and 30b). Local star dunes are also located on the eastern side of the Tertiary bedrock.

This eolian unit is composed of tan to light brown, well-sorted, non-cemented fine- to medium grained sand that forms topographic highs of up to ~ 5 m. Dunes have linear crests (mainly oriented east-west) and wave-like textures in aerial view (Figure 30a). The dunes vary from inactive to active, commonly proximal to one another. Local cross-bedding is present in some inactive dunes. Silty, unconsolidated sediments are also locally present. The majority of the dunes are inactive. These dunes are partially stabilized by vegetation and have numerous animal burrows (Figure 31). This unit also overlies all fault scarps and structural features expressed in the lacustrine sediments. The eolian dunes can be easily distinguished from the other Lake Lahontan sediments and alluvial units by their distinct uniform grain size and dune morphologies.

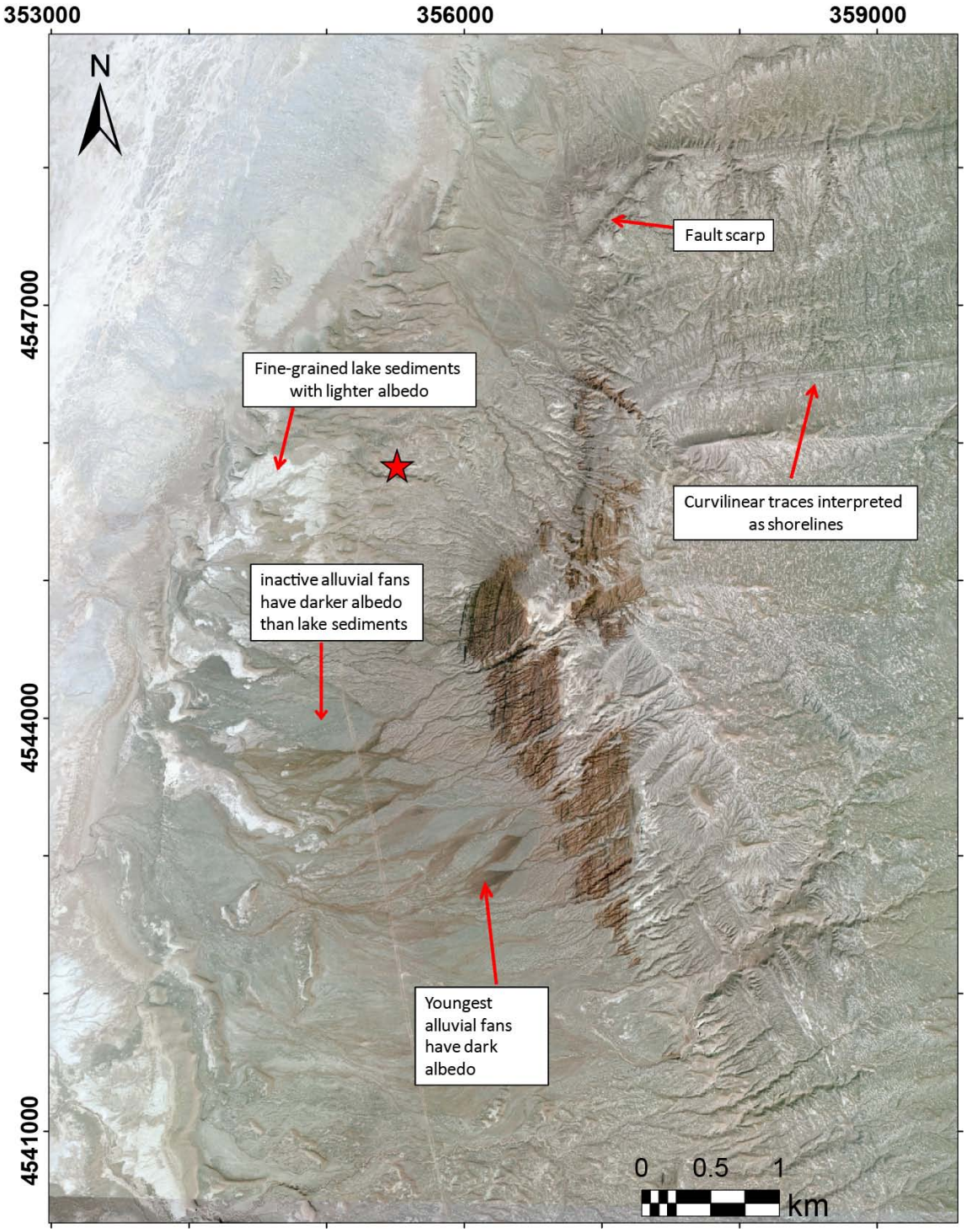

Figure 28a. Aerial imagery of the MacFarlane hot springs area. Note distinguishing characteristics visible in aerial imagery of lacustrine and alluvial units. Hot springs shown as red star.

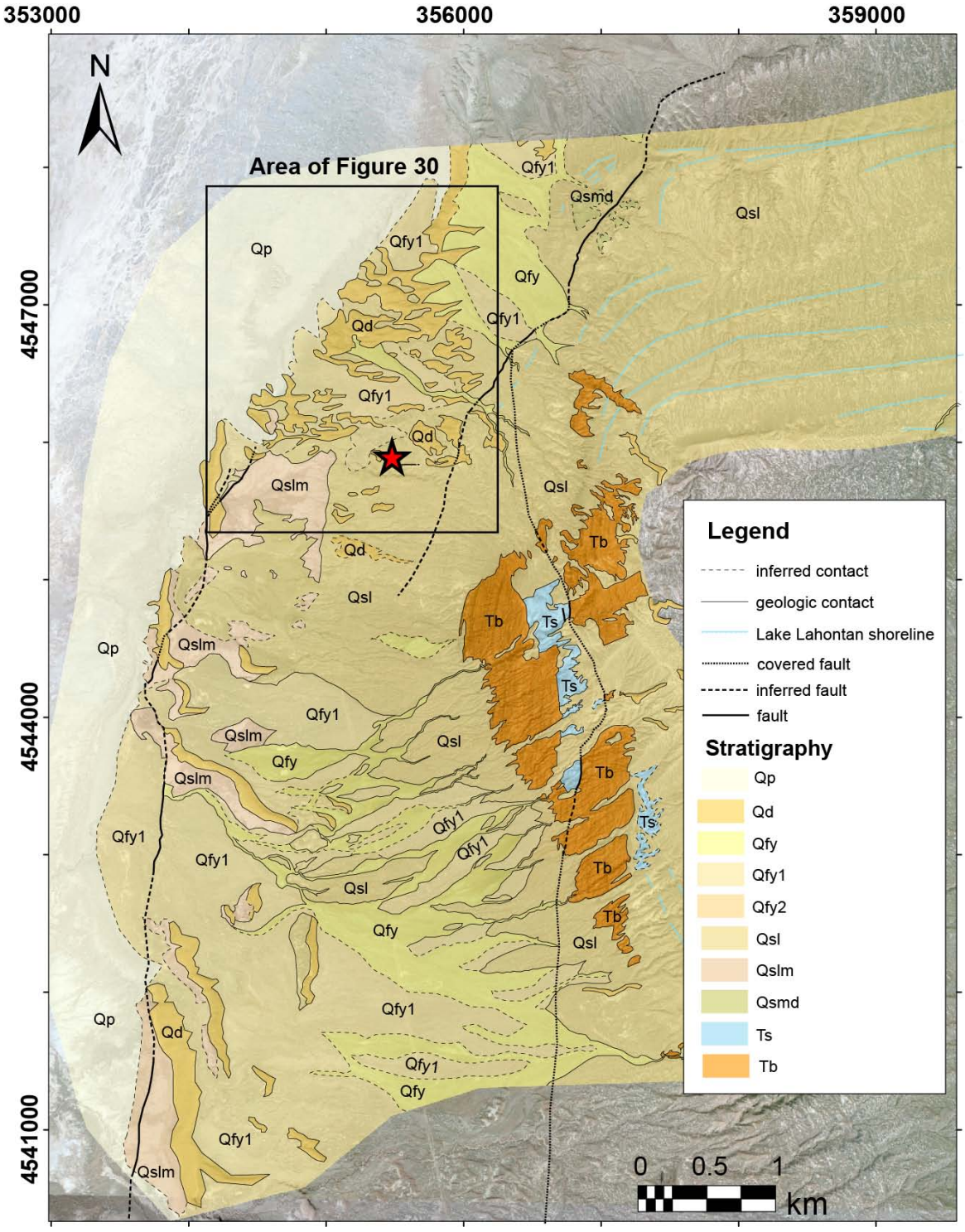

Figure 28b. Geology mapping from this study overlain on aerial imagery at MacFarlane hot springs area. Actual hot springs shown as red star. Area of Figure 30a and 30b shown in black box.

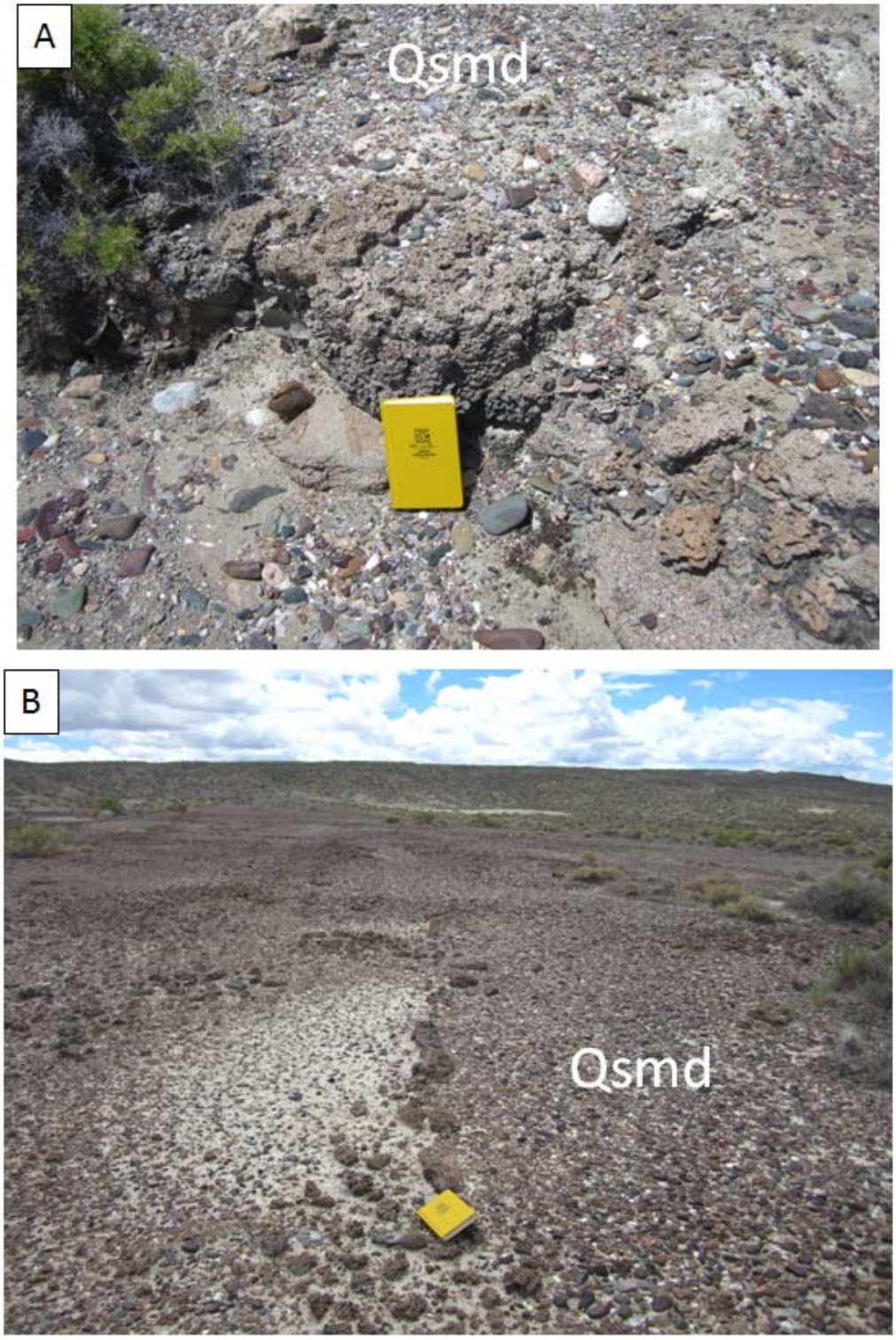

Figure 29. Both photos show the algal tufa mats (Qsmd). These photos document the thickness and continuous lateral extent of Qsmd.

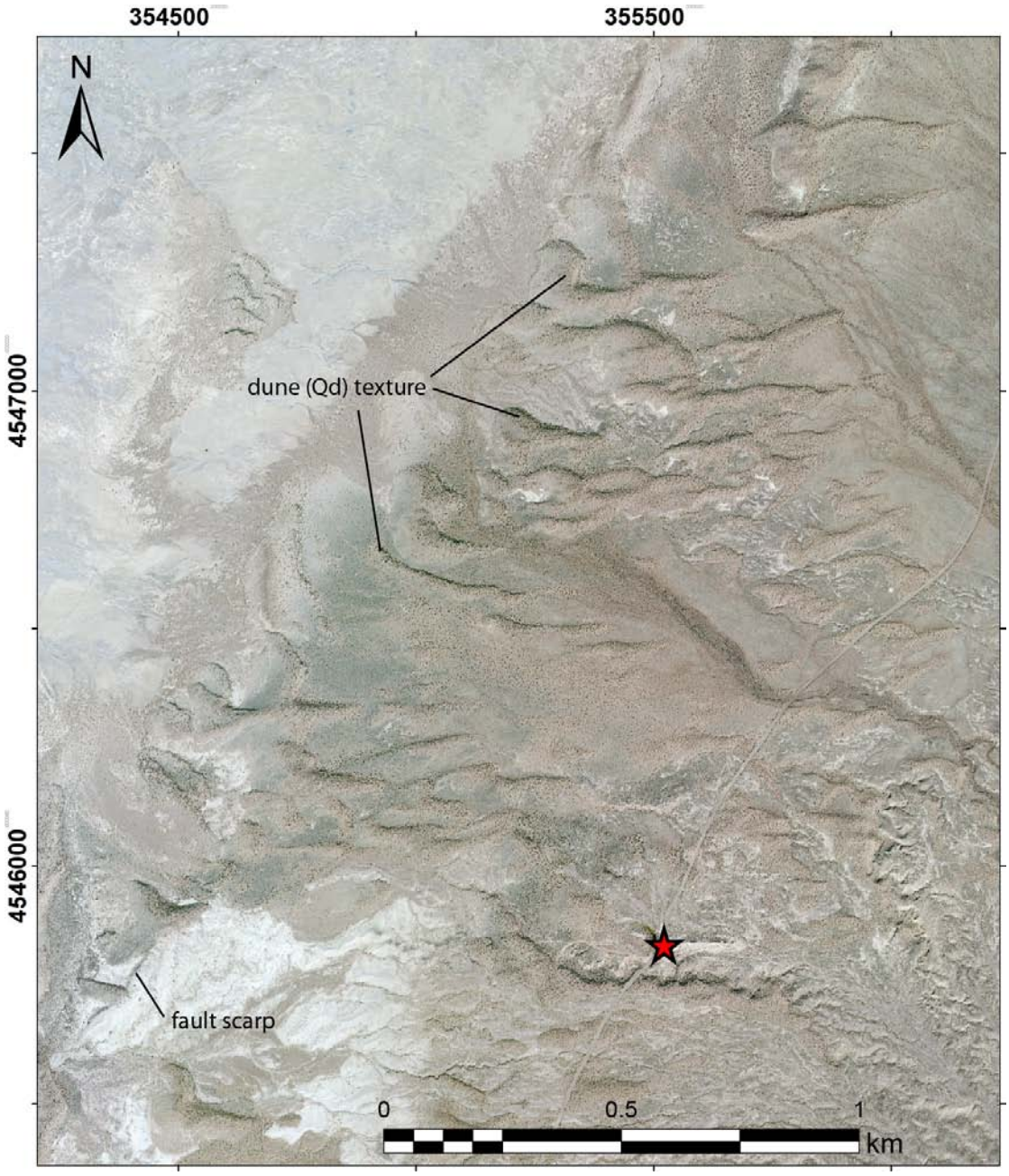

Figure 30a. Aerial imagery of the dune field located near MacFarlane hot springs. Linear dune texture is evident in this imagery. One side of the dune has darker albedo, with a lighter, gradually sloping side. The mapped locations of the dunes are shown in Figure 30b. The location of this map is shown as black box in Figure 28b. MacFarlane hot springs is shown as red star.

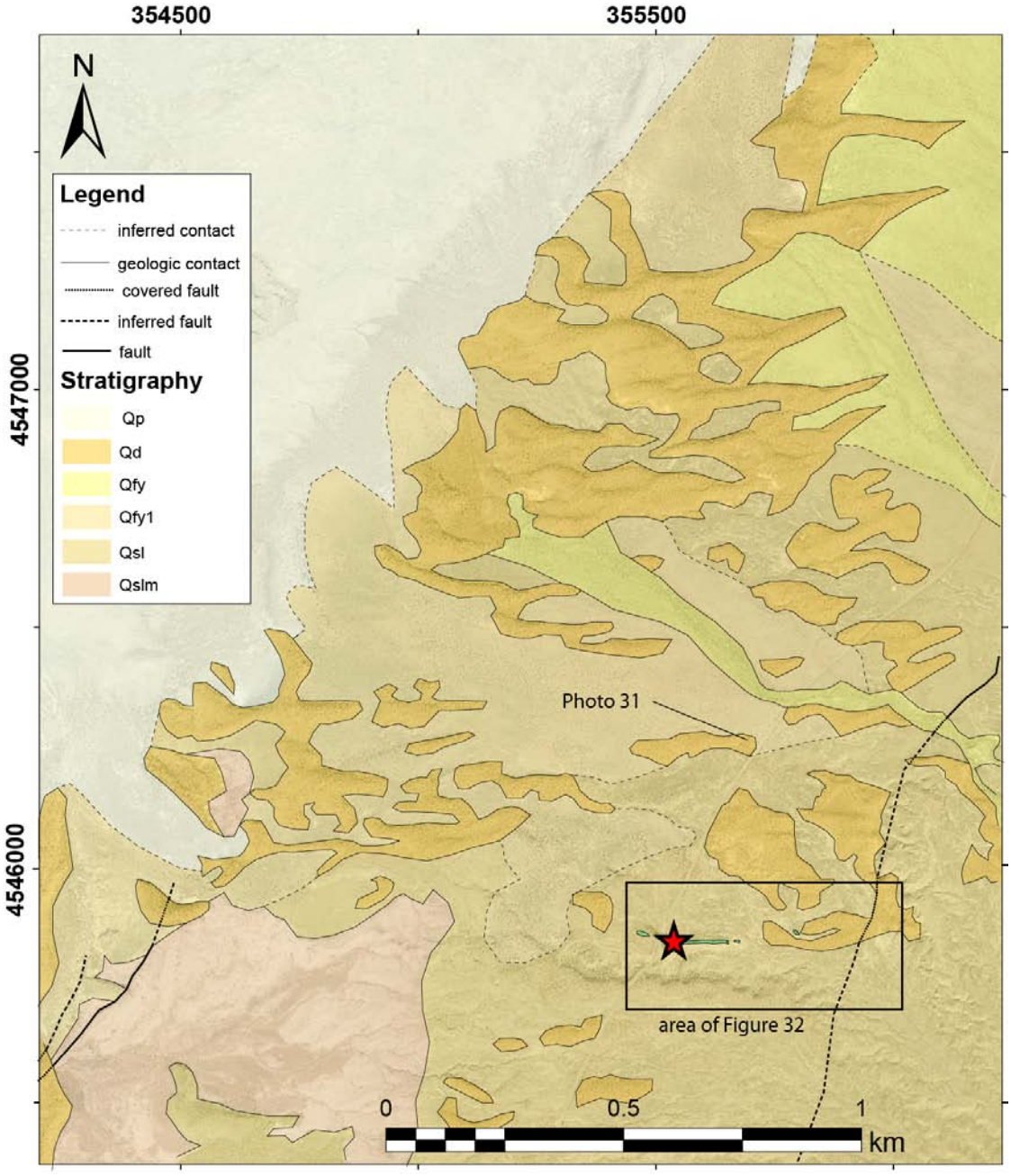

Figure 30b. Geologic units overlain on aerial imagery at MacFarlane hot springs. This area shows the extensive dunes (Qd) that cover all other units. The dunes mapped here are shown in aerial imagery in Figure 30a. MacFarlane hot springs is shown as a red star, and travertine mound as green line. The location of photo 31 is shown. The area of this map is shown as a black box in Figure 28b.

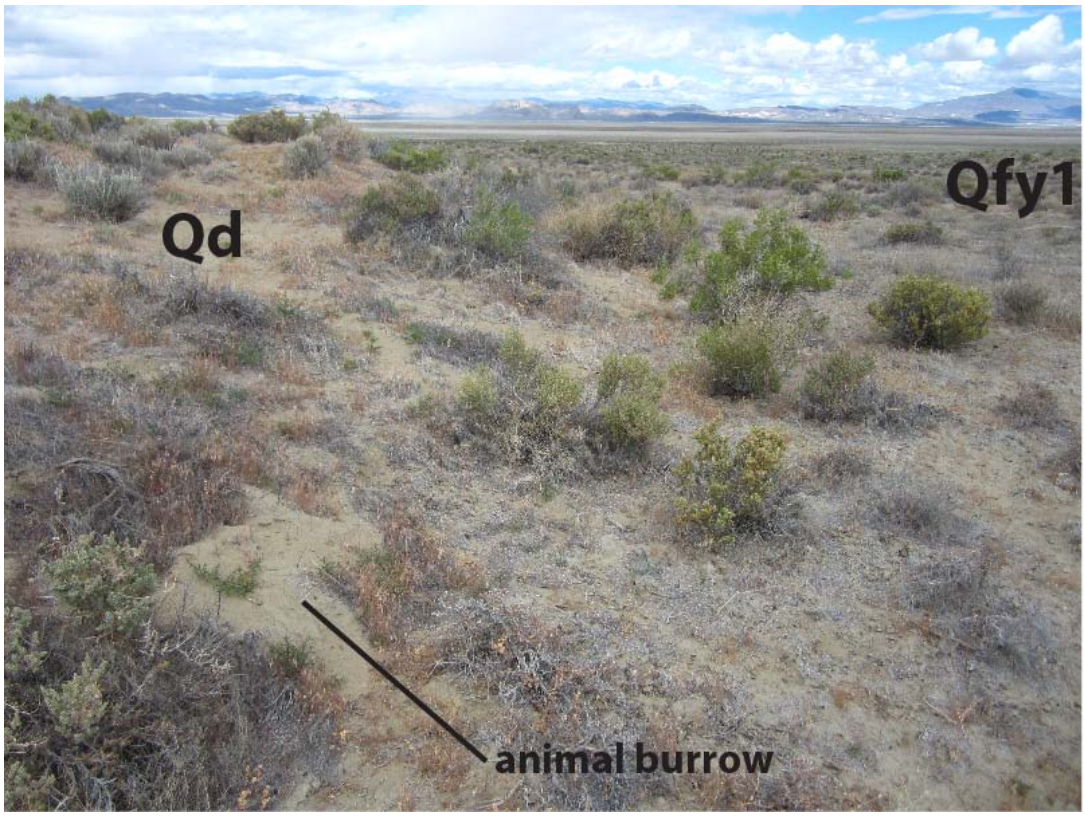

Figure 31. Photo of eolian dune. Photo was taken looking to the west-northwest. Note the absence of clasts within the dune and topographic high formed by the dune. Most dunes at MacFarlane hot springs are heavily vegetated and have numerous animal borrows, as shown here.

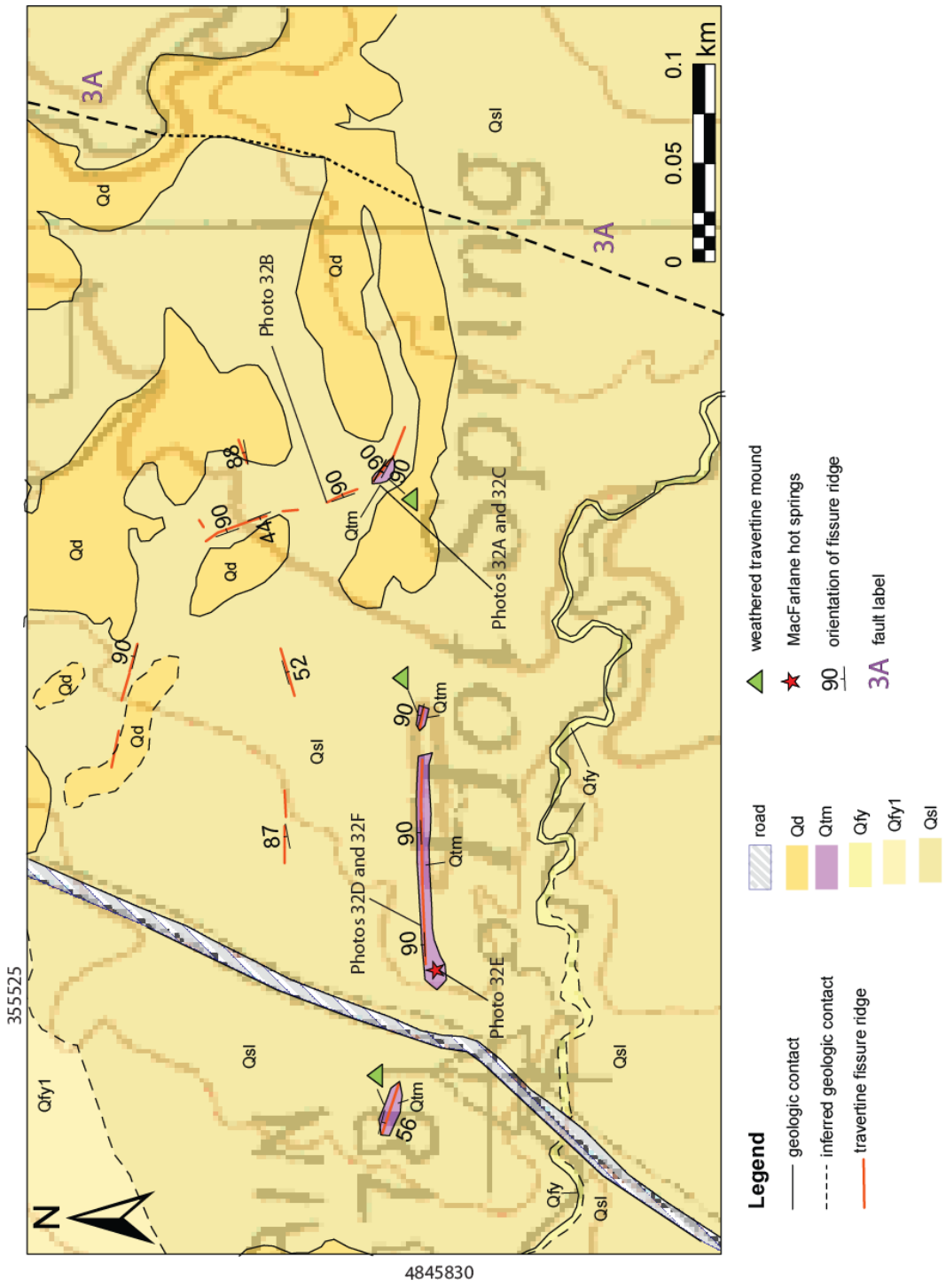

Figure 32. Map of travertine mounds and fissure ridges at MacFarlane hot springs. Travertine mounds are shown in purple, with the fissure ridges shown in red. Severely weathered travertine mounds are indicated by the green triangles. MacFarlane hot springs is shown as a red star. Location of this figure is shown in Figure 35.

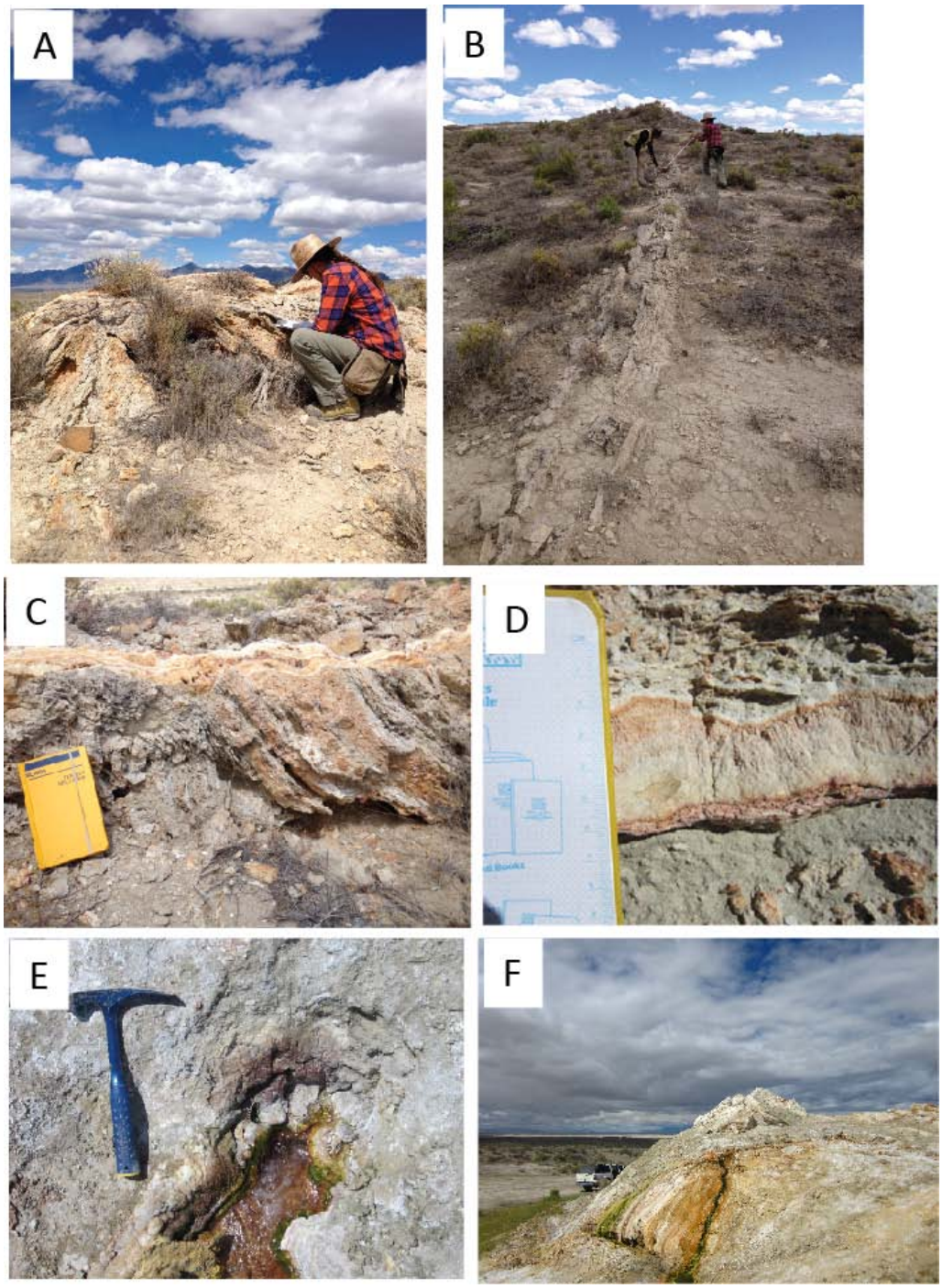

Figure 33. A; Inactive travertine fissure ridge. Photo is taken facing northeast. Note extensive weathering and vegetation cover. B: Travertine fissure ridge adjacent to inactive ridge. Notice the limited lateral extent of the fissure ridge. C: Internal lamination on the inactive travertine ridge. Notice how the younger vertical fissures cut through the older subvertical deposits. D: Travertine central fissure. The internal crystals have grown perpendicular to the orientation of the fissure ridge, into the dilatant fissure. The internal laminations made by layers of these crystals are parallel to the fissure ridge orientation and indicate multiple episodes of dilation. E and F: The active travertine mound and associated hot springs. *Photo credit (A, B, and C): Patricia Cashman*

Travertine Fissure Ridges:

The travertine fissure ridges exposed at MacFarlane hot springs cut through Lake Lahontan sediments and occur within an area of ~.04 km^2 (Figures 32 and 33). The location of the travertine fissure ridges corresponds to the southward termination of fault 3A, based on its expression in Lake Lahontan sediments (Figure 32). The travertine fissure ridges exhibit a variety of orientations and sizes (Figures 32 and 33). Detailed mapping shows four dominant travertine fissure ridge orientations.

The majority (if not all) of the travertine fissure ridges were active during the Lake Lahontan lacustrine cycle, and one mound is still active today. The evidence showing the travertines were active during the Lake Lahontan pluvial event include the presence of wave-rounded travertine clasts (Sibbett et al., 1982) and calcium-carbonate-cemented ooids associated with some travertine fissure ridges. All travertine deposits also cut through Lake Lahontan sediments (Figure 32). It is difficult to determine the relative ages of many of the fissure ridges, because they have similar morphologies and degrees of weathering. However, the largest travertine fissure ridge is distinctly younger than three other travertine fissure ridges based on lack of weathering and an active hot springs flowing out of its west end (Figure 33D, E and F).

Morphology

Most travertine deposits show a vertical, planar central opening, or fissure, though which water flowed and deposited calcium carbonate on the walls of the fissure. Water flowed out the top of the fissure and down the sides, depositing layers of travertine on the

flanks of the fissure ridges. In some cases, large, sloping mounds were formed through this process (purple, Figure 32, Figures 33A, C and F). Most fissure ridges contain internal laminated veins made by layers of crystals that parallel the fissure ridge (Figure 33D). These indicate multiple episodes of dilation. Local crystal growth within the veins is perpendicular to the long axis of the ridge, indicating dilation, with no lateral motion (Figure 33D). Three travertine fissure ridges showed dips of <60° (Figure 32).

Active Travertine Mound and Associated Fissure Ridge

The largest travertine fissure ridge has a hot spring continuously flowing from its west end (Figures 32, 33E and 33F). The hot spring flows out a slight depression in the travertine, which is flanked by a roughly conical travertine mound (Figures 33E and 33F). The travertine fissure ridge is ~140 m long and up to ~1.5 m high. The central fissure and associated vein that runs along the long axis of the ridge varies in width from ~1 cm to ~20 cm (Figure 33D). The actual mound with the active hot springs is ~ 2.5 m high and 7 m wide (Figure 33F). The travertine fissure ridge, mound, and hot spring are located ~250 m directly east of fault 3A. The travertine fissure ridge is composed of white to orange/red to grey calcium carbonate and shows a variety of textures. These include smooth lithified surfaces, with local terraces, and grey woody/porous to botryoidal tufa-like textures. This fissure ridge has the most internal laminations, indicating more episodes of dilation than the other travertine fissure ridges.

Orientations

Each travertine fissure ridge records a dilational orientation. There are four major populations of travertine orientations, including 1.) east-west striking, 2.) east-northeast striking, 3.) north-northwest striking and 4.) east-southeast striking (Figure 32). The largest four travertine fissure ridges (shown in purple, Figure 32) are aligned east-west of each other in a general en echelon pattern. The largest travertine fissure ridge is oriented east-west, and the three smaller purple travertine fissure ridges are oriented east-southeast. A group of travertine fissure ridges with small widths (<1 m) is oriented north-northwest and east-northeast (red lines, Figure 32). No cross cutting relationships between travertine fissure ridges were observed.

Weathered Travertine Fissure Ridges

Severely weathered travertine fissure ridges are mainly found along strike and to the east of the large travertine fissure ridge (purple mound indicated by green triangles, Figure 32, Figures 33A, B, and C). These travertine fissure ridges range in color from white to tan to grey. The travertine fissure ridges vary in length from 10 m to 25 m, and are 1-3 m wide (Figure 32). The ridges have up to 2 m of vertical topography. Local calcium-carbonate-cemented ooids are associated with inactive travertine fissure ridges, indicating that the travertine deposits were active during the Lake Lahontan pluvial cycle. These fissure ridges are older than the active travertine mound and associated fissure ridge and show a younging age progression from east to west, with the exception of the westernmost travertine fissure ridge. This interpretation is based on distinctly different degrees of weathering and the presence of the active hot springs.

Structural Framework:

Based on kinematic and geologic data, there are three main fault areas near MacFarlane hot springs (Figure 21). These include faults in the southern Jackson Mountains (faults 5A and 6A), a single fault expressed in Tertiary bedrock (fault 1A), and faults within the MacFarlane fault zone (faults 3A and 3B). Specific fault sets can be distinguished based on ages and orientations. The fault sets include (from oldest to youngest):

6A.) a northeast-striking, down-to-the-northwest, normal fault exposed in Mesozoic bedrock in the southern Jackson Mountains;

1A.) a north-striking, down-to-the-west, normal fault expressed in Tertiary bedrock and covered by Lake Lahontan sediments;

5A.) a north-striking, down-to-the-west, normal motion, Jackson Mountain fault zone, expressed in Lake Lahontan sediments;

3A and 3B.) a north-northeast-striking, down-to-the-west, normal motion, MacFarlane fault zone, expressed in Lake Lahontan sediments and tufa mats.

Three additional faults previously mapped by Sibbett et al. (1982) were not found in this study (faults 2A, 2B and 4A, Figure 16). Each of these was studied to test possible controls on the travertine and geothermal upwelling at MacFarlane hot springs (Figure 21).

Southern Jackson Mountains (faults 5A and 6A)

A part of the southern Jackson Mountains was mapped (Figure 34) to test for an east-striking fault, or intersection of such a fault with another fault, controlling the location of the travertine (scenario #1, Figure 20). No regional east-striking faults were found. Two faults were observed in the southern Jackson Mountains (5A and 6A). Fault 6A is located at the northern tip of the southern Jackson Mountains (Figure 34). The fault is expressed in the Triassic Happy Creek volcanic complex. The fault is not expressed in any alluvial fans, Lake Lahontan deposits, or ephemeral steam channels. The fault crops out as brecciated zones and as fault planes with slickenlines. This fault is east-northeast-striking, normal, and down-to-the-northwest. Kinematic data show dip-slip motion and a dip of 56° to the northwest (Figure 34). This fault is younger than Triassic and older than the Lake Lahontan deposits (~13,000 yrs). This fault might correlate with an episode of high-angle normal faulting that occurred in late Middle Jurassic, documented ~1 km to the north in the Jackson Mountains by Maher (1989). This is based on conjugate strike orientations and similar dips.

Fault 5A is located at the range front bounding the southern Jackson Mountains (Figure 34) and is expressed as a slight change in topography in Lake Lahontan sediments. This fault is visible as lineaments that cut shorelines at an oblique angle in aerial photos. These lineaments typically have a slightly darker albedo. The fault is north-striking, and down-to-the-west, and normal. Fault 5A correlates with faults of the Jackson Mountain fault zone mapped to the north. This is based on spatial proximity, similar orientations, and kinematics. The faults of the Jackson Mountain fault zone have

been active since Basin and Range extension began in northwestern Nevada (~12 Ma) and have been active in the past ~13,000 years (e.g., Lerch et al.,2008).

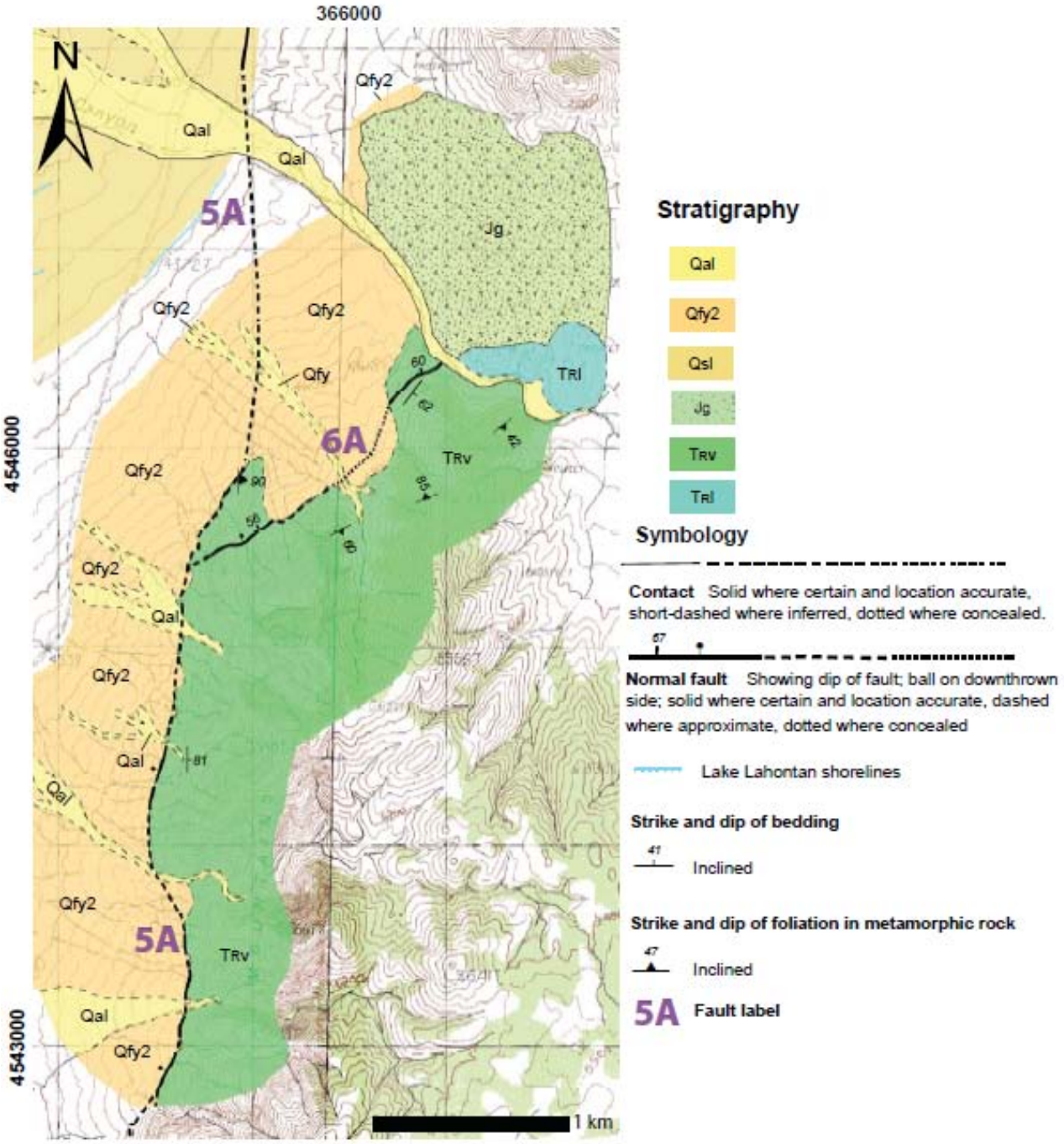

Figure 34. Geologic map of the southern Jackson Mountains. Faults shown are 5A and 6A.

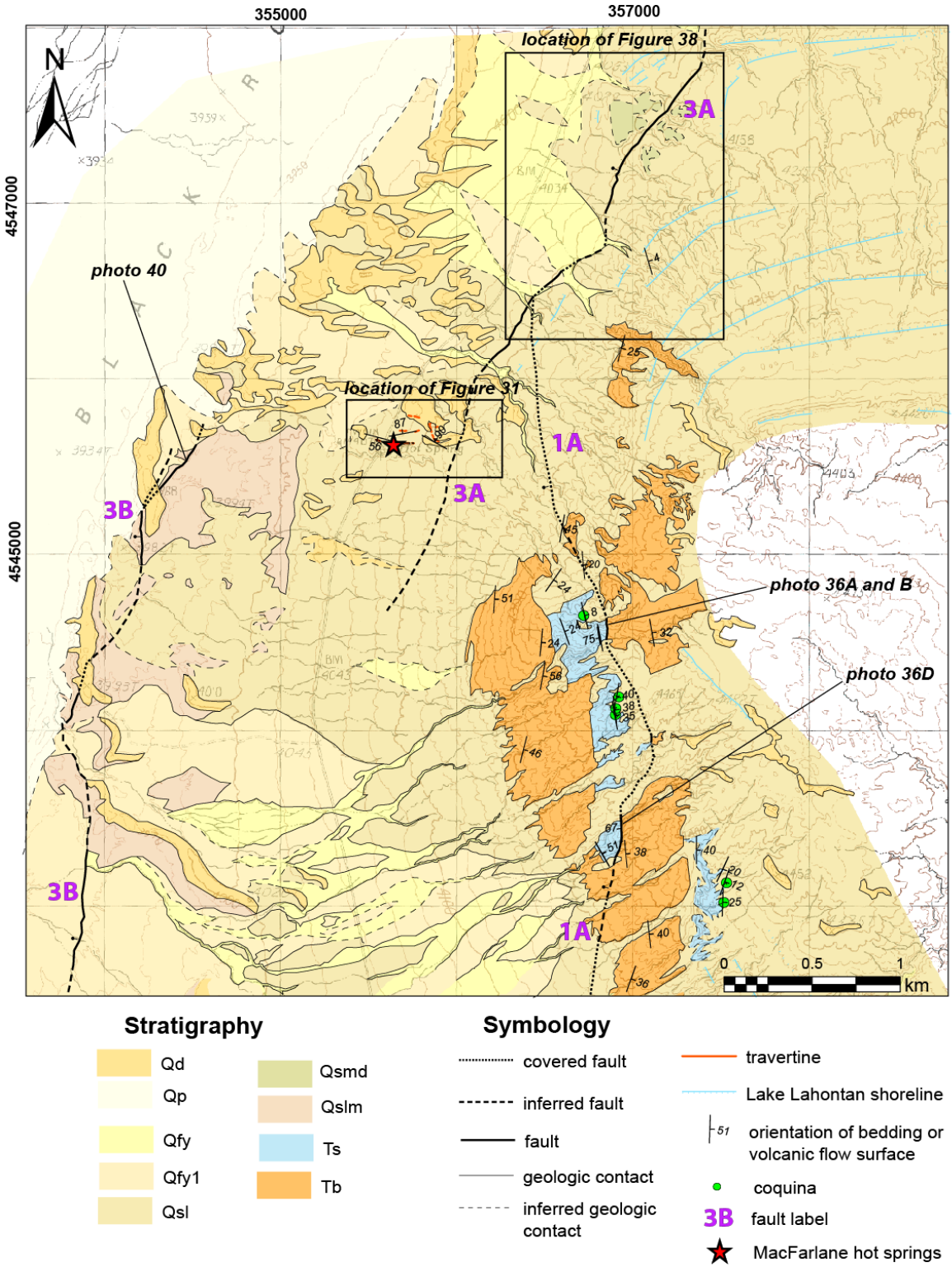

Figure 35. Overview map of the faults proximal to MacFarlane hot springs. Faults shown are 1A, 3A, and 3B.

Tertiary Bedrock (fault 1A)

The Tertiary bedrock east of MacFarlane hot springs was mapped to determine kinematics and assess offset on fault 1A. This fault is important to this study, because it might control the upwelling in the geothermal system (Scenario #6, Figure 20). In this scenario, fault 1A is projected to continue north and intersect fault 3A near the highest temperature gradient borehole (Sibbett et al., 1982).

Fault 1A cuts the Tertiary bedrock units ~2 km southeast of MacFarlane hot springs (Figure 35). The fault is exposed for ~300 m and accommodates offsets between Tb and Ts. Exposed fault planes are overlain by Lake Lahontan sediments (Figure 36A and 36B). Kinematic data on fault planes include slickenlines and drag folding; mapped separation of coquina beds was used to determine displacement.

Fault 1A contains slickenlines that show mainly dip-slip motion, with a minor sinistral-oblique component trending southwest (Figure 36C). The main fault strikes between 186° and 206° and dips between 61° and 76° west. Drag folding in Ts also indicates down-to-the-west motion (Figure 36D). A minor fault with 0.5 m of offset was observed in Ts with a similar sense of motion.

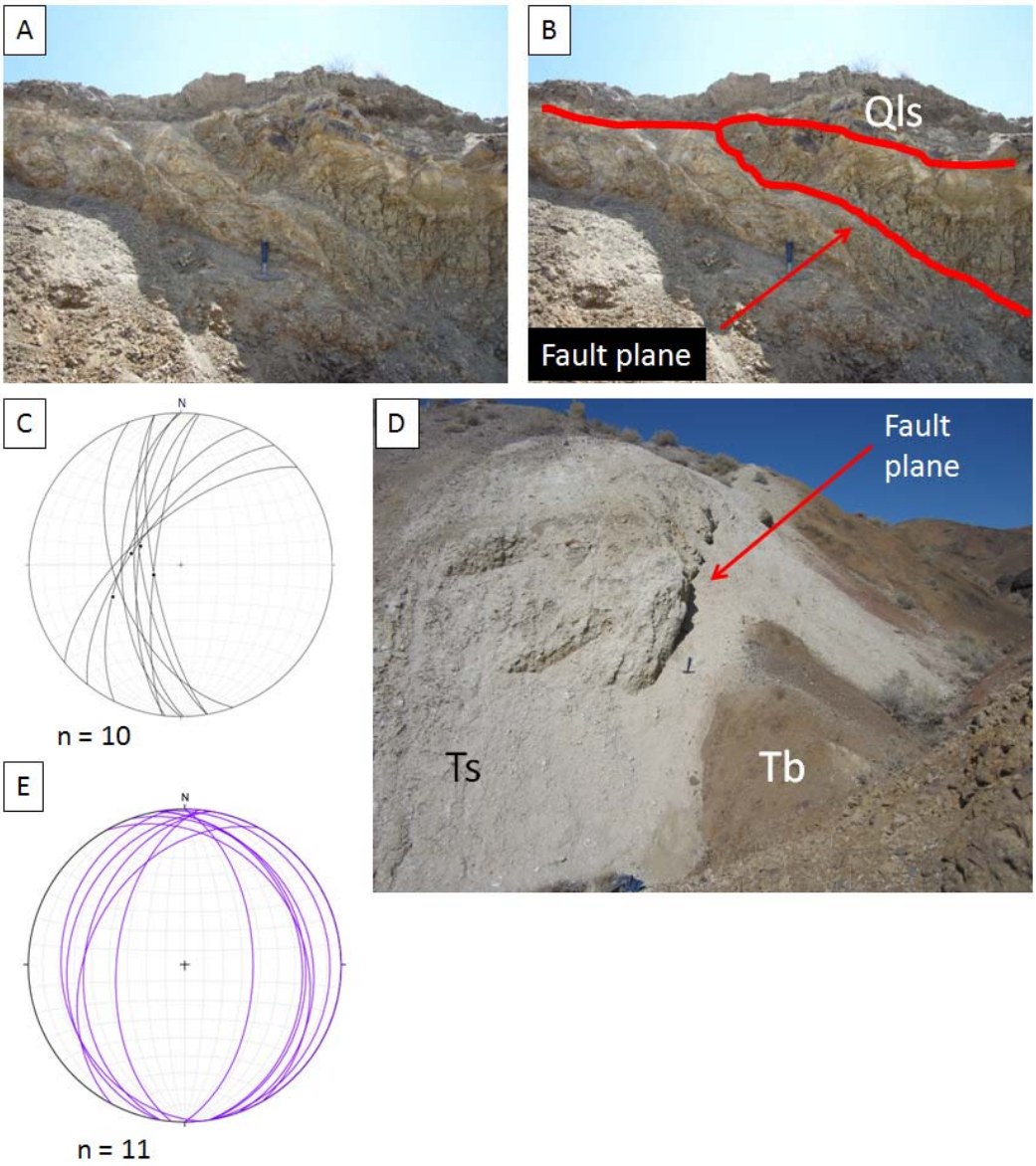

Figure 36. A: Fault 1A exposed in a drainage. Photo is taken looking south. B: Interpretations from photo A. West-dipping fault plane expressed in the tuffaceous sedimentary unit (Ts). Fault plane is covered by Lake Lahontan sediments (Qsl), giving age constraints on this fault. C: Fault plane (great circle) and slickenline (dots) orientations plotted on equal-area stereonets. D: Drag folding along fault 1A. The fault forms the eastern contact between the basalt (Tb) and the tuffaceous sedimentary unit (Ts). This photo was taken looking north, so the fault is dipping to the west. E. Bedding orientations of Ts are deformed by drag folding along fault 1A and shown as great circles in purple.

The coquina horizon within Ts provides a reliable marker bed that documents fault offset (Figure 35). The coquina is repeated across the fault. Based on cross-sections drawn in areas with the most reliable kinematic data (B-B', Plate 1), this fault has accommodated ~335 m of normal offset. The age of fault 1A is older than older than ~13,000 years but younger than 4-11 Ma (Late Miocene to early Pleistocene), based on the inferred ages of the Lake Lahontan and Ts units, respectively.

MacFarlane Fault Zone (faults 3A and 3B)

The MacFarlane fault zone was mapped in detail to test scenarios involving geothermal upwelling and the locations of the travertine ridges. Specifically, mapping tested for terminations on faults 3A and 3B (scenarios #2 and #3, Figure 21), and for the development of a relay ramp with or without a hard-linking stepover (scenarios #4 and #5, Figure 21). This fault zone is in closest proximity to MacFarlane hot springs and contains the youngest offsets in the area.

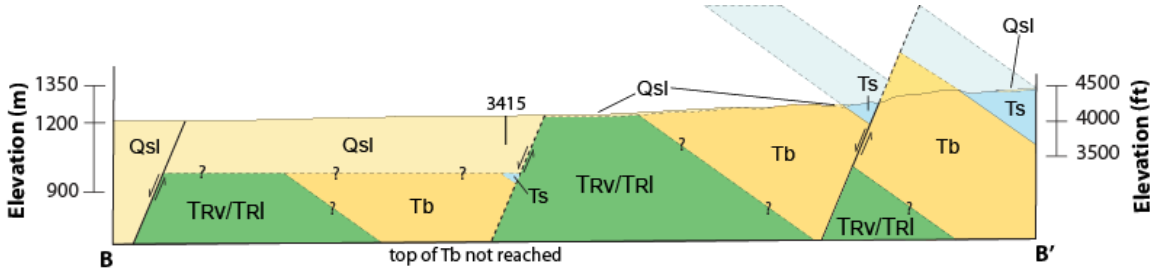

Figure 37. Cross section from B-B' on Plate 1. Dip of fault 1A is based on field measurements. Unit Ts records offset on this fault, which is ~335 m.

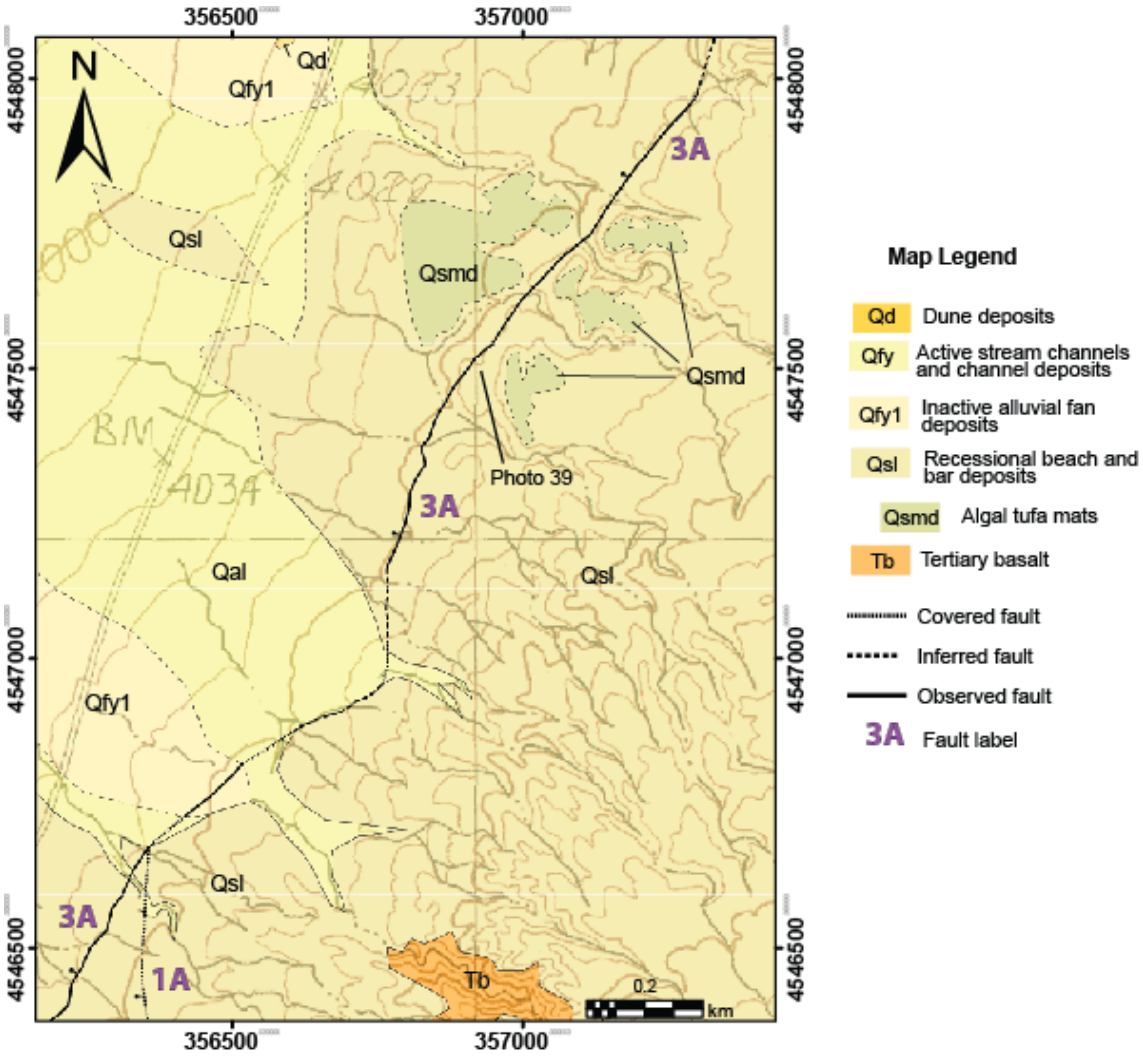

Figure 38. Offset tufa mats along Fault 3A. Tufa mats are shown in light green and are offset ~6 m down to the west.

Figure 39. Photo showing the fault scarp of Fault 3A and offset tufa mats (Qsmd). Photo is taken looking to the northeast, and its location is indicated on Figure 38. Mike Schmidt (~1.7 m) is shown in red for scale.

The MacFarlane fault zone is located ~ 7 km west of the southern Jackson Mountains (faults 3A and 3B; Figure 21). The MacFarlane fault zone consists of two synthetic faults that overlap in map view and are together at least 15 km long. The faults are expressed as scarps visible on the ground and as linear features that cut shorelines in aerial photographs. These faults strike north-northeast and dip west.

Fault 3A is located northeast of MacFarlane hot springs. This fault accommodates ~6 m of down to the west offset of resistant Lake Lahontan algal tufa mats, ~2 km northeast of MacFarlane hot springs (Figures 38 and 39). A scarp along strike of the offset tufa has minimal offset (visible only in aerial imagery) ~ 1000 m northeast of MacFarlane hot springs. The lineation in the aerial imagery of this scarp dies out ~ 650 m northeast of the travertine. This amount of offset (6 m) terminating in ~2 km laterally records an increased displacement gradient consistent with fault 3A termination scenario #2 (Figure 21).

Sibbett et al (1982) suggested ~400 m of offset in Tb, based on drill data, to the southeast of MacFarlane hot springs (offset shown in Figure 37). This interpretation contradicts the southern termination mapped on fault 3A. This offset can be explained by pre-Lake Lahontan movement along fault 3A. There is no surface expression of fault 3A cutting Lake Lahontan sediments (Qsl) in this location. This area is not covered by recent alluvial fans or dunes, so it would be expected that movement in the past ~13,000 years would be recorded as a scarp. Thus, Holocene slip on fault 3A terminates southward and is constrained to the locations presented in Figure 35.

Fault 3B is located ~1 km west and southwest of MacFarlane hot springs (Figure 35). Fault scarps cut Lake Lahontan unit Qslm. Scarp traces are also visible in aerial imagery cutting through units Qsl and Qfy1. Tufa mats are continuous along areas of the hanging wall (2-4 cm thick) and are clearly truncated by the fault (Figure 40). Similar tufa mats are less continuous and severely eroded on the footwall. These tufa mats record ~ 2 m of offset, down-to-the-west (Figure 40). Scarps are covered by recent eolian deposits and show substantial degradation and drainage dissection. Fault 3B splays and terminates ~1 km directly west of MacFarlane hot springs. This is consistent with the 3B fault termination scenario #3 (Figure 21).

Figure 40. Photo taken looking southwest along the fault scarp of fault 3B. The scarp is expressed in deep water lake sediments (Qslm) that show local offset tufa (Qsmd) down to the west. Eolian dunes (Qd) are in the background.

Travertine Deposits:

All travertine fissure ridges are ~100 – 500 m west of fault 3A, and ~1 – 1.4 km east of the tip of fault 3B (Figure 35). The fault segments overlap in map view, forming a relay ramp; the travertine fissure ridges reside within the relay ramp. The orientations of the travertine fissure ridges provide kinematic data related to this relay ramp. Each travertine fissure ridge records a dilational orientation (Figure 41).

The orientations of the travertine fissure ridges are compared to the orientations of veins measured in Tb (Figures 41 and 24C) to assess whether fracture orientations in Tb controlled the fissure ridges. Some vein orientations correlate with the travertine ridges, but many do not. There are distinct northeast and north-northeast striking vein populations in Tb that are not observed in the travertine fissure ridges.

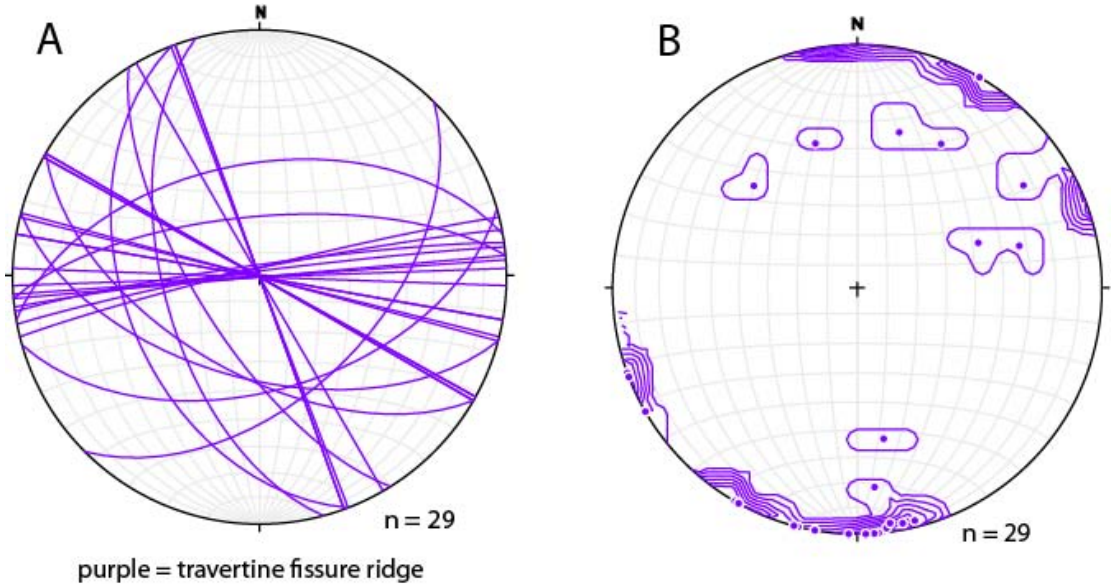

Figure 41. A. Great circle plots of travertine fissure ridges (purple). Most travertine fissure ridges are subvertical and strike: 1.) east-west, 2.) east-northeast, 3.) north-northwest and 4.) east-southeast. B. Density contour plot of poles to veins, with contours at 2% per 1% area.

Previously Mapped Faults

Three additional fault sets mapped by Sibbett et al. (1982) were reinterpreted by this study. These are shown in Figure 16 and include:

1B.) a north-northwest-striking, down-to-the-east normal fault cutting the western contact between the Tertiary basalt and sedimentary unit;

2A.) a northeast-striking, down-to-the-north normal fault expressed in Tertiary bedrock; and

4A.) an east-striking, down-to-the-north, normal step-over fault within the MacFarlane fault zone expressed in Quaternary sediments.

Fault 1B was reinterpreted to be a depositional contact in this study (fault 1B, Figure 16). This fault was interpreted to form a graben with fault 1A, and continue to the north to intersect fault 3A of the MacFarlane fault zone near the highest temperature gradient borehole (Sibbett et al., 1982). This area was mapped in detail in this study to assess the structural framework (Figure 35). No kinematic indicators (slickenlines, drag folds, reidel shears) were observed in bedrock. The strike and dip of Ts and Tb in the area are concordant, with Ts overlying Tb. An irregular depositional contact between Tb and Ts was observed just east of fault 1B. The contact between Ts and Tb is irregular due to paleotopography and basalt flow variations. The western contact between Tb and Ts is therefore interpreted to be depositional (Figure 35), and a fault is not necessary to explain any apparent offset.

New mapping for this study reveals no evidence for fault 2A, a northeast-striking fault east of MacFarlane hot springs (Figure 35). Previous mapping showed this fault cutting through Tb and Ts units, and covered by Lake Lahontan sediments (Sibbett et al., 1982). In this study, the area with this mapped fault was carefully analysed. A lineament in Tb with lighter albedo is visible in the aerial imagery where this fault was mapped. However, the lineament is actually a northeast-striking silica vein (~10-30 cm wide and ~ 20 m long) in Tb. No kinematic indicators (slickenlines, drag folding, reidel shearing) were observed in the silica vein or adjacent bedrock. Further, there is no offset of bedding or geologic contacts across the vein. The apparent offset visible in aerial imagery and on the ground is due to an irregular depositional contact between Ts and Tb. The offset coquina marker bed within the Ts unit records a single west-dipping normal fault; it forms the eastern contact between the Tb and Ts units. Continuity of bedding is confirmed by the locations and orientation of coquina beds mapped throughout the area. The coquina beds match up along strike across the previously mapped fault 2A.

The east-striking fault 4A, within the MacFarlane fault zone, was not found in this study (fault 4A, Figure 16). Fault 4A was previously mapped based on air photo lineations (Figure 16, fault 4A, Sibbett et al., 1982). This area was mapped in detail in this study specifically to find all fault scarps. A number of eolian dunes with east-west crests overlie Lake Lahontan recessional beach deposits (Figure 30a and 30b, Qe and Qsl). A large, linear dune crest in the area is ~600 m long, near where the previous fault was mapped (Figure 30a and 30b). No fault scarps were visible on the ground and there is no change in the surficial deposits. No faults are present; the lineation visible in aerial

imagery is a dune margin. Based on lack of evidence for fault 4A, a hard-linking step-over fault, at least in the Quaternary units, contributing to the geothermal upwelling and travertine orientations (scenario #5, Figure 21) is ruled out.

Two-Meter Temperature Data:

Shallow temperature surveys were conducted at MacFarlane hot springs in order to: 1) test hypotheses on locations of shallow fluid flow related to faults or other permeable units, and 2) discover areas of high temperature that might have been overlooked in previous work. Both one-meter and two-meter surveys were done; the methodology for both surveys is described in the appendix of this paper. Shallow temperature was chosen as an exploration tool based on ease of data collection and interpretation, as well as usefulness in locating shallow temperature anomalies.

Survey Locations

The first two-meter temperature survey stations were picked based on the locations of Quaternary fault scarps from geologic mapping and of elevated temperature gradients (Swanberg and Bowers, 1982). This survey was designed as a reconnaissance with widely spaced data points. The temperature readings were taken down-topography from fault 3A to pick up any warm outflow related to fluid flow along the fault. Shallow temperatures were also measured up-topography, along strike, and around the active travertine fissure ridge in order to test the location of shallow fluid flow related to this feature. All of these measurements lie within the greater high temperature gradient anomaly found by Swanberg and Bowers (1982), shown in Figure 19. Subsequently,

temperature measurements were taken to the south and north of the travertine to look for any other high temperature areas outside of the high temperature anomaly.

A subsequent series of shallow temperature surveys was undertaken to better define the high temperatures found along strike of the major travertine fissure ridge. A one-meter survey was completed in areas that were too rugged for an ATV or were located in the Black Rock Desert Wilderness Area. Two-meter temperatures were taken in all other accessible areas. Temperature readings were taken along strike and up-topography from the previous hot temperatures, as well as north and south of the high temperatures. Temperature readings were also taken down-topography from the hot springs to trace outflow patterns.

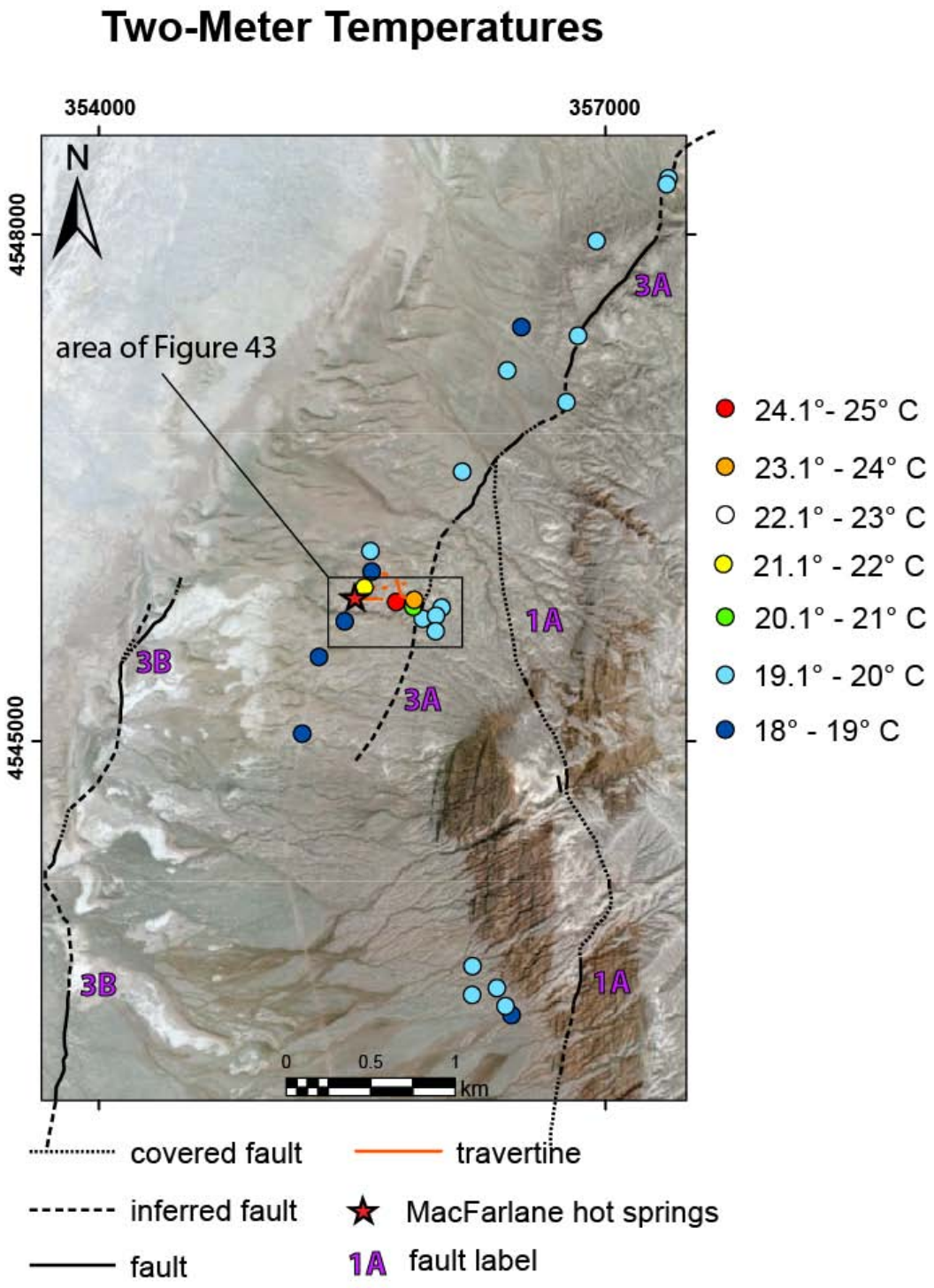

Figure 42. All two-meter data points. Elevated temperatures were found along strike and up-topography from the main travertine mound. These elevated temperatures terminate across Fault 3A. Surveys were completed in November of 2012.

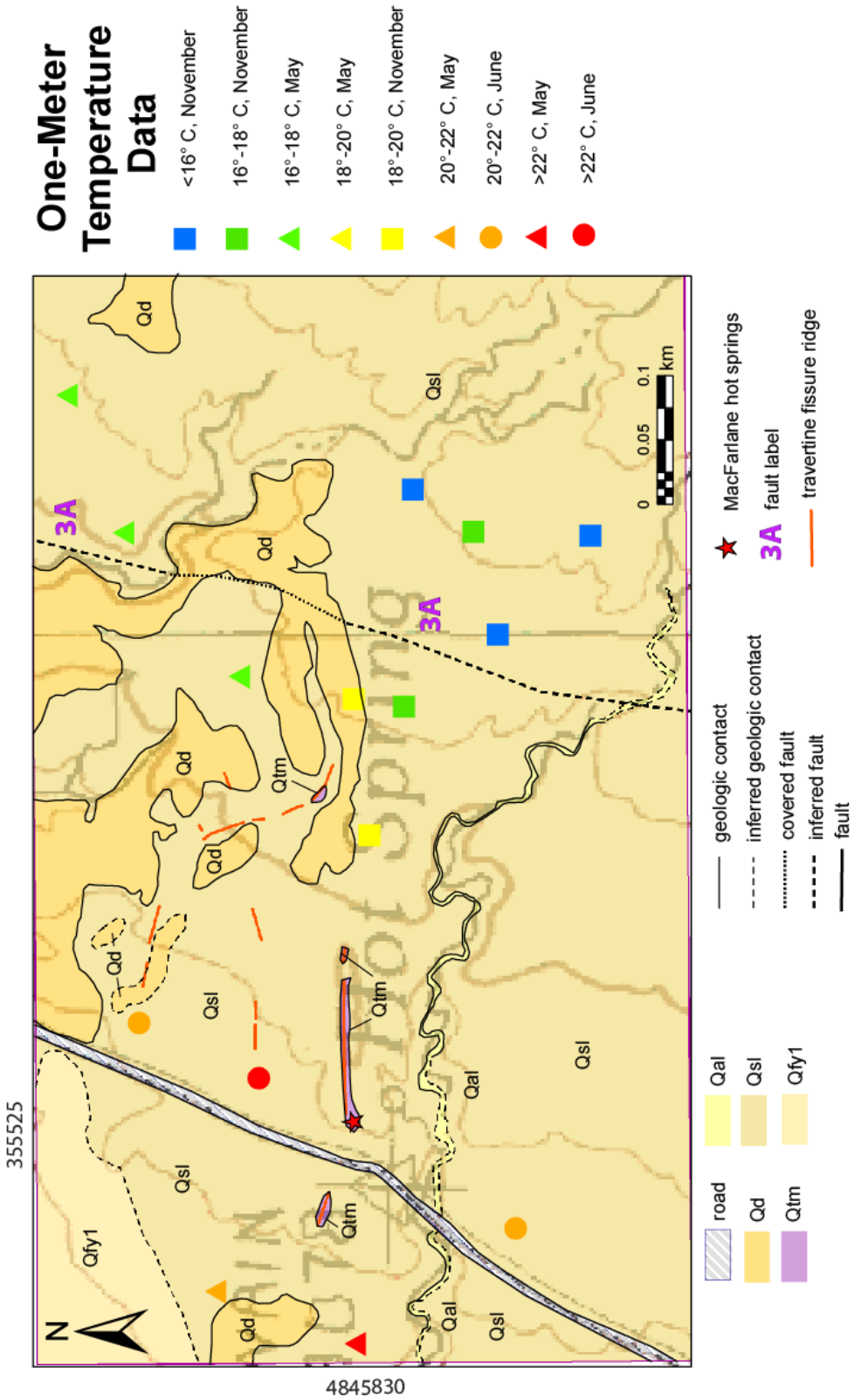

Figure 33. One-meter data points. This figure includes one-meter temperatures from three separate surveys done in November of 2012, May and June of 2013. This figure shows the elevated temperatures down-topography of the travertine mound which are due to outflow. The termination of elevated temperatures across Fault 3A is also shown.

Shallow Temperature Results

The first reconnaissance survey showed elevated two-meter temperatures only along trend and up-topography of the main travertine fissure ridge (Figure 42). The highest temperature, 25°C, was 200 m directly east of the hot springs. A temperature of 23° C was recorded 330 m uphill directly east of the hot springs. Temperature readings along the scarp of fault 3A and down-topography of fault 3A were cold. Temperature readings at the location of the highest temperature gradient drill hole, corresponding with the projected intersection of fault 1A and fault 3A (Swanberg and Bowers, 1982) were also cold. This may result from the upwelling hot fluids not reaching a two-meter depth. Temperature readings south of the hot springs at the location of the previously mapped northeast-striking fault 2A (Sibbett et al., 1982; Figure 16) were also cold (Figure 42).

The second series of surveys showed elevated one-meter temperatures down-topography of the hot springs (Figure 43). These temperatures form a broad anomaly, rather than a linear trend. This is to be expected from outflow. The surveys also found a cold point (<16° C) ~500 m east of the travertine fissure ridge, which shows that the elevated shallow temperatures do not extend east of fault 3A (Figure 43).

The shallow temperature data are useful in tracing hot water at a shallow depth. The lack of high shallow temperatures in most of the field area shows that hot water is not present at 1-2 m depths. The high shallow temperatures found up-topography and along strike of the travertine show that hot fluid moves west before reaching the surface spring. This might indicate a through-going east-west fracture that increases

permeability. The termination of high two-meter temperatures at fault 3A (Figure 42; Figure 43) suggests that this fault controls upflow of geothermal fluid at a shallow depth.

Magnetic Data:

A magnetic survey was completed to assess whether the magnetic signature could be used to map covered faults (faults 3A and 3B, Figure 44) in the vicinity of the relay ramp. The methodology is described in the appendix of this paper. There is some uncertainty of the locations of the fault terminations associated with the relay ramp because of possible burial under Quaternary alluvium and eolian dunes. This survey was designed to first test the magnetic signature of known faults and then to map the locations of these fault terminations if the fault had a reliable magnetic signature.

Magnetic Survey Locations

First, magnetic data were collected in areas where the fault could be confirmed by detailed geologic mapping or previous drill data in order to assess whether the faults had a recognizable magnetic anomaly. The three locations that were chosen include: 1) the offset algal tufa mats associated with fault 3A to the northeast of the hot springs, 2) the southern termination of fault 3A, where previous offset is suggested by drill data, and 3) the location of minor offset tufa to the southwest of the hot springs on fault 3B (Figure 44). The surveys were completed in east-west transects (optimal for a magnetic signature) perpendicular to the mapped fault traces, in order to obtain the best magnetic signature of the faults. The data were then corrected for the base station and reduced to

the pole for the most accurate results. By reducing the data to the pole, dipole anomalies are removed and a single anomaly over the magnetic body is shown. The reduced data were modeled in Oasis Montaj.

Magnetic Survey Results

Overall, magnetic gradients found in this survey trend north-northeast and are both steep and gradual (Figure 44). The steep gradients are interpreted to mark magnetic reversals in the underlying volcanic rocks. The gentle gradients are interpreted to indicate fault offset in volcanic rocks with consistent magnetic polarity. Changes in magnetic signatures due to geochemistry (related to faulting) are explained in the appendix of this paper.

A steep magnetic gradient is found trending north-northeast ~ 500 m to the east of the fault scarp on fault 3A (Figure 44). The gradient is associated with a ~1000 nT magnetic low. A similar steep gradient is observed to the south. The trace of the gradient is irregular and angular, forming “v”-like patterns. Both of these steep gradients are interpreted to be related to magnetic reversals recorded in the remnant magnetism in the underlying basalt unit. This interpretation is based on their locations and the character of the gradient. The v’s formed by the gradient are consistent with the documented east dip of the underlying Tb flows as it interacts with topography.

There are over 50 documented magnetic reversals that occurred in the Neogene (LeBrecque et al., 1977). Based on unpublished paleomagnetic data, there is a magnetic reversal mapped in basalt west of the Jackson Mountains on the eastern margin of the

Black Rock Desert (J. Glen, personal communication, March 6, 2014). This is consistent with the steep magnetic gradient observed in this magnetic survey.

A gradual north-northwest trending magnetic gradient is observed in the hanging wall of fault 3A (Figure 44). The magnetic signature changes from high to low moving west away from the surface expression of the fault scarp. A similar magnetic gradient is observed in the hanging wall of fault 3B (Figure 44). Both of these gradients might be due to mineral alteration along the fault plane due to fluid flow or the west-side-down fault geometries. Coupled with other geophysical data, the observed gradient would be a convincing fault indicator. Further geophysical surveys would be needed to confirm these interpretations.

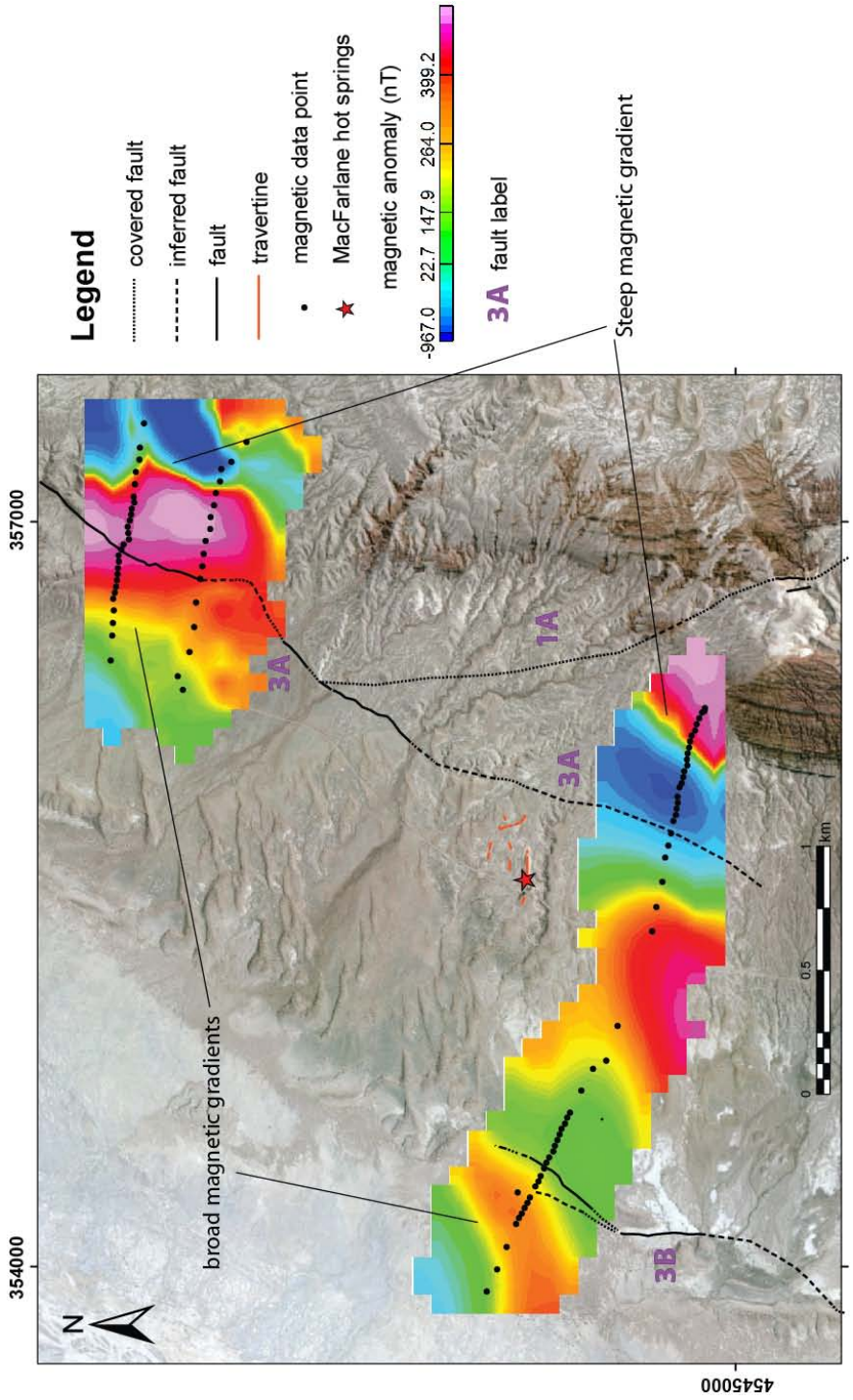

Figure 44. Magnetic data collected at MacFarlane hot springs. Data have been corrected for the base station and reduced to the pole. Survey locations are shown as black dots. The steep magnetic gradients are interpreted as remnant magnetic signatures representing a magnetic reversal. Note that the "v" patterns are consistent with the documented east-dip of the Tb flow. The broad magnetic gradients found in the hanging wall of fault 3A and 3B are interpreted as related to faulting.

DISCUSSION

In this section, the new data from geologic mapping, structural analysis, shallow temperature surveys, and magnetic data are integrated with previous work to describe structural controls on the travertine fissure ridges and the overall geothermal system at MacFarlane hot springs. First, the timing of deformation surrounding the hot springs is summarized. Then, the shallow temperature data are related to the overall geothermal system. Next, the structural controls on the anomalously oriented travertine fissure ridges are discussed. The spatial and temporal progression of the travertine fissure ridges is described and related to their position within the relay ramp. Finally, the structural controls on the overall geothermal system are summarized.

Tertiary Bedrock (fault 1A):

The timing of the fault 1A is constrained by field relationships. The fault cuts the tuffaceous sedimentary (Ts) unit, which has been broadly constrained to late-middle Miocene to early Pliocene (Dall, 1924; Firby, 1967; Willden, 1964; Sibbett et al., 1982). The fault trace is also clearly covered by Lake Lahontan recessional beach and bar deposits, which are ~13,000 years old (Adams and Wesnousky, 1999). This constrains the movement on this fault to between ~16 Ma and ~13, 000 years ago.

MacFarlane Fault Zone:

Based on detailed Quaternary mapping, the timing of recent deformation on faults 3A and 3B in the MacFarlane fault zone directly surrounding MacFarlane hot springs has been determined. Fault scarps are expressed in the Lake Lahontan recessional shoreline and bar deposits, which are ~13,000 years old (Adams and Wesnousky, 1999). The scarps also cut inactive alluvial fan deposits (Qfy1, Figure 39). Although the exact age of this alluvial cycle is unknown, it does show well-developed surface features, such as desert pavement and rock varnish, that indicate it is not currently active. This indicates that faults 3A and 3B slipped sometime in the late Pleistocene or Holocene, within the past ~13,000 years.

Shallow Temperatures:

Shallow temperature data from MacFarlane hot springs show elevated temperatures directly along strike and up-slope from the active travertine fissure ridge. This indicates that the hot springs are related to fluid that flows east to west, most likely as part of an outflow system. These high temperatures terminate eastward across a fault (Figures 42 and 43, fault 3A), which suggests that the fault controls upflow of hot fluids at that location.

Structural Controls of the Travertine:

The travertine fissure ridges at MacFarlane hot springs strike dominantly east-west, and record multiple dilational events. The orientations of the dilational fissure ridges do not match extensional trends in the northwestern Basin and Range. As discussed above, possible controls on the east-west striking travertine fissure ridges were tested in this study. Each scenario is ruled out except for #4, which involves a Holocene relay ramp.

Scenario #1, fault intersection of an east-striking fault

The possibility of an east-west striking fault intersecting the MacFarlane fault zone at the location of the travertines was considered. Such a fault was not found in geologic mapping in the southern Jackson Mountains. No Quaternary scarps indicating such a fault were present. Further, no indication of such a fault was found in the magnetic data, nor in two-meter temperature data. This scenario is ruled out based on absence of supporting evidence.

Scenario #2, southward termination of fault 3A

Fault 3A terminates to the south, based on detailed Quaternary mapping. The southward termination of fault 3A is suggested by progressively decreasing offset on Quaternary scarps to the southwest. A scarp with ~6 m of offset is mapped ~2 km northeast of MacFarlane hot springs. A scarp along strike of the 6 m scarp minimal offset (visible only in aerial imagery) ~1000 m northeast of MacFarlane hot springs (Figure 45). The lineament in the aerial imagery of this scarp dies out ~ 650 m northeast of the

travertine. The location of the travertine fissure ridges corresponds to the displacement gradient at the inferred tip of fault 3A. This also explains why the travertine fissure ridges are proximal to this fault termination (between 100 and 500 m away).

Scenario #3, northward termination of fault 3B

Fault 3B appears to terminate to the north, as evidenced by scarps in Quaternary units. The northern termination of fault 3B is suggested by a scarp with ~ 2 m of offset ending ~ 1 km directly west of MacFarlane hot springs (Figure 35). This fault termination appears to have less of a displacement gradient at the fault tip than fault 3A. Because fault 3B is located basinward, the scarp exposure is limited due to erosion or cover by eolian dunes and alluvial fans. Fault 3B is also downslope of the hot springs, so it is unlikely to be the source of the hot upwelling fluids.

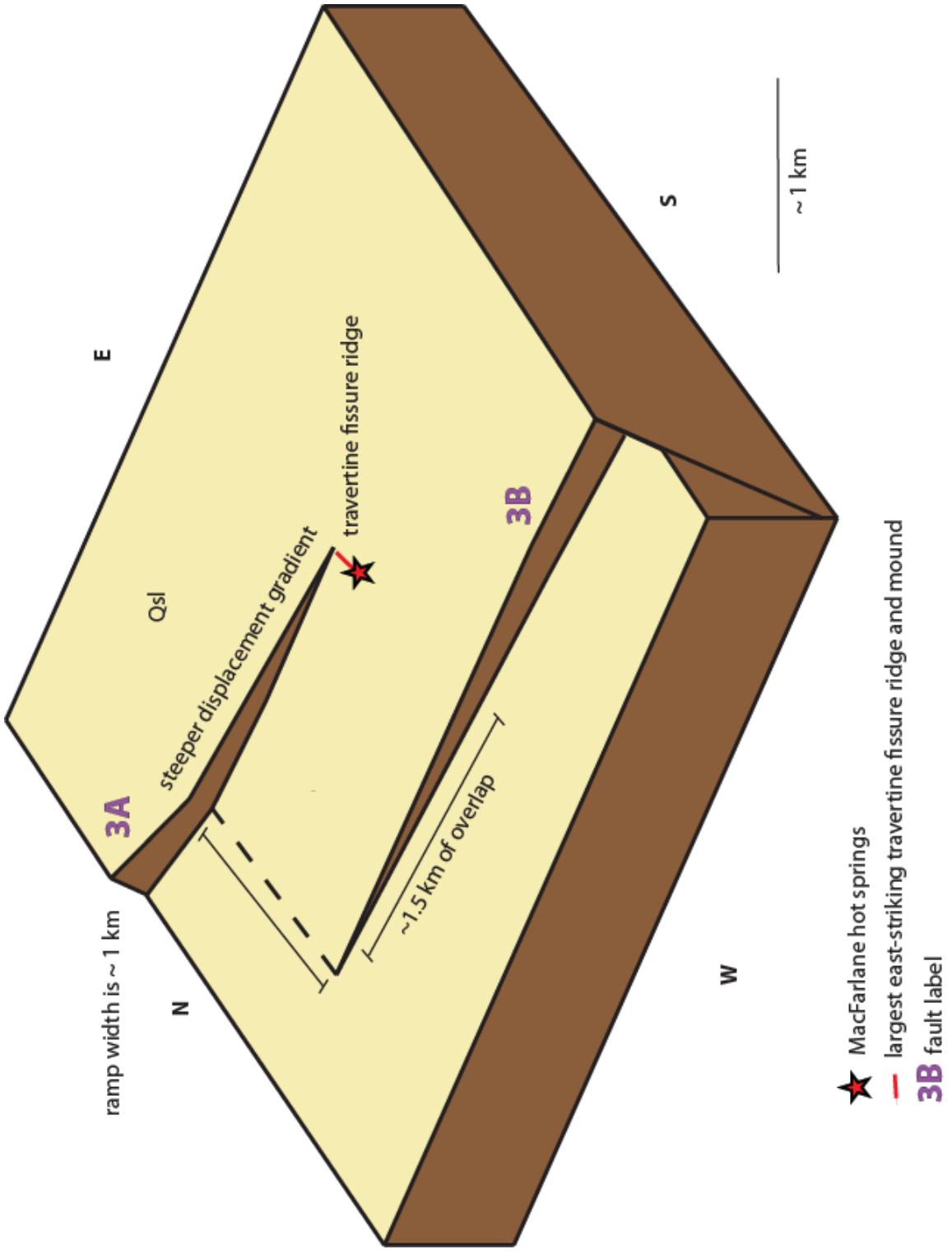

Figure 45. Schematic diagram of the relay ramp at MacFarlane hot springs. Fault segments 3A and 3B overlap ~ 1.5 km. The width of the relay ramp is ~ 1km. The largest travertine fissure ridge is shown in red, and MacFarlane hot springs is shown as a star.

Scenario #4, relay ramp

A relay ramp between the overlapping fault segments fault 3A and 3B can be defined based on geometrical criteria (Figure 45). Fault segments 3A and 3B are estimated to overlap ~1.5 km, and the width of the relay ramp is ~ 1 km, based on detailed Quaternary mapping. The hot springs and related travertine fissure ridges lie between the fault segments on the ramp, between 100-500 m west of fault 3A and between 1 – 1.4 km east of fault 3B. Deformation within the relay ramp directly controls the location and orientation of the travertine fissure ridges.

The east-west orientation of the active travertine fissure ridge is consistent with dilational fractures formed during a typical relay ramp progression. The orientations of the cutoff lines (or hinges) of the relay ramp and the stresses within the relay ramp change as the overlapping fault segments propagate past each other (e.g., Peacock and Sanderson, 1991). The current geometries of the overlapping faults are consistent with bending at the hinge of the relay ramp, which is roughly perpendicular to the faults (Figure 45). The active travertine fissure ridge progressed east to west, based on degrees of weathering and the location of the active hot springs (as recorded by abandoned travertine fissure ridges). This is consistent with fracturing that propagates away from the faults into the relay ramp. This is typical near fault tips with displacement gradients.

The east-northeast orientations of five inactive travertine fissure ridges north of the active travertine fissure ridge are also consistent with a typical relay ramp progression (Figure 32). Before faults 3A and 3B overlapped, the projected cutoff lines (or hinge of the relay ramp) would have been oriented between north-northeast and east-northeast

(Figure 8b). Bending along this cutoff line is consistent with a population of inactive dilational fissure ridges oriented east-northeast.

Three severely weathered travertine fissure ridges are oriented east-southeast (green triangles, Figure 32), which is not fully compatible with the typical relay ramp cutoff line orientations. These travertine fissure ridges are not active today. Although the travertine fissure ridges are oriented east-southeast, they are aligned roughly east-west and subparallel to one another, almost directly along strike of the active travertine ridge. These travertine fissure ridges show an age progression from east (oldest) to west (youngest), with the exception of one travertine ridge. These age progressions and orientations are consistent with a fault propagating from east to west. The displacement gradient observed in fault 3A may account for initiation of the fault breaking the ramp at this location and propagating from east to west (step (c) in Figure 8a), (Figure 45).

Scenario #5, step-over

A step-over fault (fault 4A) breaching the relay ramp was considered as a possible control on the travertine fissure ridges. No fault scarps cutting the relay ramp were observed in this study. An east-striking step-over was previously mapped by Sibbett et al. (1982) based on lineaments visible in aerial imagery. There are numerous dune crests in the direct area, which also form lineaments visible in imagery. This similarity might explain the previous interpretation. The magnetic and shallow temperature data also do not indicate any step-over fault. Therefore, scenario #5 is ruled out based on lack of evidence.

Scenario #6, intersection between fault 1A and fault 3A

An intersection between faults 1A and 3A was previously considered as a control on the location of the travertine fissure ridges (Sibbett et al., 1982; Swanberg and Bowers, 1982). Based on field data obtained in this study, a fault intersection probably does not control the geothermal upwelling. Fault 1A projects to intersect fault 3A on the ground surface ~1.1 km to the northeast of MacFarlane hot springs and the travertine fissure ridges (Figure 35). The surface location of this fault intersection is down-topography of the travertine fissure ridges. The elevation of the fault intersection on the ground surface is ~6 m lower than the elevation of the highest travertine fissure ridge. This makes it unlikely that any fluid flowing up through this fault intersection would influence the formation of the travertine ridges.

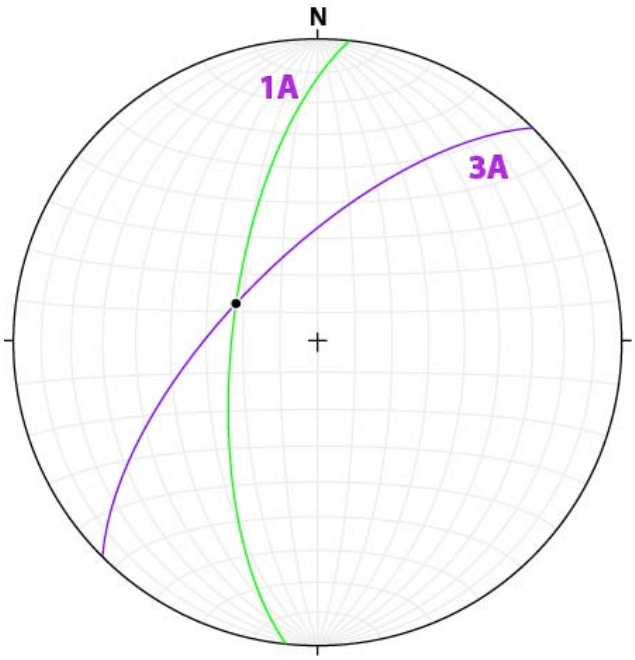

Figure 46. Projected intersection of fault 3A and fault 1A. The line of intersection plunges northwest, which is inconsistent with the northeast-trending temperature anomaly mapped by Swanberg et al. (1982).

The orientation of the previously proposed fault intersection is also inconsistent with the orientation of the high temperature gradient anomaly. The line of intersection between faults 3A and 1A plunges to the northwest (Figure 46). This is based on a measured 67° dip for fault 1A, and assumed similar dip of 67° for fault 3A. The orientation

of this line of intersection does not match the northeast-trending high temperature gradient anomaly shown in Figure 19.

Scenario #7, Stratigraphic Controls

Stratigraphic controls on the location of the travertine deposits were also considered. These specifically included a paleochannel or permeable unit underlying the travertines. Ephemeral stream channels are mapped near the travertine fissure ridges but do not have morphologies that could produce the fissure ridges. One stream channel mapped just south of the travertine (Qfy, Figure 32) might be more permeable than the surrounding Qsl deposits based on grain composition, sorting, and rounding. The stream channel meanders along an east-west trending down-slope axis. The stream channel exhibits considerable sinuosity along its long axis and varies in width between 6-8 m. This is inconsistent with the majority of the travertine fissures, which are typically between 1-20 cm wide and straight. No observed travertine fissure is curved or sinuous.

The unit that underlies the majority of the travertines is Qsl (Lake Lahontan recessional beach and bar deposits). The Lake Lahontan deposits are laterally homogenous, with the exception of north-northeast-trending shoreline deposits in the vicinity of the travertine. These deposits do not have high permeability, based on grain size, and they have curvilinear traces. The shorelines are much broader features than the travertine fissures and do not have similar orientations to the travertine ridges.

Jointing anisotropy in the underlying basalt was considered as a control of the travertine fissures. The travertine fissures are underlain by basalt at a depth of ~ 455 m, based on drill data (Sibbett et al., 1982). Dilational joints and veins are observed in the basalt throughout the mapping area. They have a variety or orientations (Figure 41). In this case, pre-existing joints and fractures in the basalt might preferentially accommodate slip and/or dilation related to the relay ramp between faults 3A and 3B. However, it seems more likely that the travertine fissure ridge orientations are explained by relay ramp flexure, without the influence of pre-existing joints. Joints were not observed in Ts overlying Tb, which makes it unlikely that the joints propagated into the overlying Quaternary sediments. The joints might also be expressed in units that are more competent, and non-existent in less competent units such as the Quaternary sediments.

CONCLUSIONS

New shallow temperature data, geologic mapping, kinematic data and a magnetic survey integrated with previous work were used in this study to evaluate the structural controls of the MacFarlane geothermal system. The following section summarizes the new findings and outlines possibilities for further work.

- The main travertine fissure ridge at MacFarlane hot springs has a central dilational fissure oriented east-west, which does match extensional trends in the northwestern Basin and Range. Data suggest that the travertine ridges at MacFarlane hot springs are related to Quaternary relay ramp

geometries. The travertine fissure ridges are near the displacement gradient at the fault tip of fault 3A. The orientation of the large travertine fissure ridge is consistent with extension observed in relay ramps perpendicular to the cutoff lines (or hinges) of the relay ramp. The main travertine fissure ridge appears to have propagated from east to west, based on relative degrees of weathering and the location of the active hot springs. This is consistent with a fault beginning to breach the relay ramp; the fault initiates at the fault tip with a sizeable displacement gradient and propagates across the relay ramp (step (c), Figure 8a).

- High shallow (1 and 2 m) temperatures uphill and east of the travertine fissure ridges show that the hot springs are related to fluid that flows east to west, most likely as part of an outflow system. These high temperatures terminate eastward across fault 3A, which suggests that this fault controls hot fluid upflow at that location.
- The line of intersection between fault 3A and fault 1A plunges northwest. This is inconsistent with the orientation of the high temperature gradient anomaly.
- Offset and kinematics can be constrained on fault 1A. The fault strikes between 186° and 206°, dips 61° to 76° west, and has accommodated ~335 m of normal offset.
- The previously unmapped southern Jackson Mountains consist of a heavily veined and weathered Mesozoic limestone overlain by a slightly metamorphosed volcaniclastic sequence, both intruded by a dioritic

pluton. No east-west-striking fault systems are observed in these units, which rules out a regional east-west striking fault controlling the orientation of the travertine fissure ridges. These units have similar lithologies to the Upper Triassic to Jurassic Bliss Canyon Formation, the Happy Creek volcanic complex, and intrusive granodiorites of the Jackson Mountains to the north.

- Sibbett et al. (1982) suggests ~400 m of offset in Tb along fault 3A, based on drill data, to the southeast of MacFarlane hot springs (offset shown in Figure 37). This offset contradicts the apparent southern termination inferred for fault 3A. This offset can be explained by pre-Lake Lahontan movement along fault 3A. There is no surface expression of fault 3A cutting through Lake Lahontan sediments (Qsl) in this location. This area is not covered by recent alluvial fans or dunes; so it would be expected that movement in the past ~13,000 years would be recorded as a scarp. Thus, Holocene slip on fault 3A terminates southward and is constrained to the locations presented in Figure 35.
- Further work at the fault terminations associated with the MacFarlane fault zone and relay ramp would be useful. Geophysics, especially gravity and seismic reflection/refraction, could help to constrain the geometries of these faults. Specifically, several seismic lines perpendicular to fault 3A and fault 3B in the area where surface scarps terminate would be very useful. LiDAR would also be useful to constrain the locations of the subtle Quaternary fault scarps.

APPENDIX:

Lithologic Unit Descriptions:

Quaternary Stratigraphy

Qd – eolian dunes. Tan to light brown, well-sorted, non-cemented fine-grained sand in intermittently active to inactive dunes, partially stabilized by vegetation. Local cross-bedding and silty unconsolidated sediments.

Qp – playa deposit. Light tan, fine-grained, well-sorted silts and clays. Loosely consolidated. Distinguished by low-lying flat topography and light albedo in aerial photos.

Qtm – travertine fissure ridges. White to tan calcium carbonate deposited in linear ridges with a central fissure along its long axis. CaCO3 is deposited due to changes in chemistry, temperature and pressure as hot springs water flows out of the fissure ridges. Internal laminations present paralleling main fissure ridge. Some fissure ridges are filled with light orange to white calcite crystals that are oriented perpendicular to the ridge. Local travertine mounds are up to ~2 meters high. Textures of the mounds are mainly smooth lithified surfaces with local terraces and vary from woody/porous to botryoidal. Brown and green algae present in current spring.

Qfy– ephemeral stream channel deposits. Silty to sandy matrix, clasts are gravel to boulder-size; poorly sorted; angular to subangular; clasts are composed of locally derived basalt, sandstone, coquina, diatomite, travertine, limestone volcanic bedrock, and clasts of reworked beach cobble. Local stream channels are sinuous.

Qfy1 – alluvial fan remnants. Characterized by subdued, smooth topography and darker albedo in aerial photo. Silty sediment with pebble-to cobble-size subangular clasts; composition of clasts includes locally derived bedrock to reworked beach cobbles. Local moderately to well-developed desert pavement, rock varnish and development of cryptobiotic soils.

Qfy2 – alluvial fan remnants at the foot of the southern Jackson Mountains. Characterized by a silty matrix, angular to sub-angular gravel- to cobble-size clasts that are moderately to poorly sorted. Composition of clasts includes bedrock from the southern Jackson Mountains, and distinctly lacks reworked beach cobbles. Local

moderately- to well-developed desert pavement, rock varnish and development of cryptobiotic soils.

Qsl – Lake Lahontan lacustrine deposits. Grey, white to tan, silty loosely consolidated sediments with subrounded gravel-to pebble-size clasts. Characterized in aerial photo by thin, curvilinear traces interpreted as shorelines, and a lighter albedo. Local bar deposits consisting of well-rounded clasts and desert pavement. Local white surficial evaporite deposits.

Qsmd – Tufa member. Dark brown to red laterally continuous algal tufa mats, up to 7 cm thick. Dendritic textures, local tufa-cemented, well-rounded beach pebbles and gravel.

Qslm – Lake Lahontan deep-water sediments. Characterized by white to light tan silts and clays. Loosely to moderately consolidated, with little vegetation. Some sediments have been mobilized by wind, and this unit is typically in close proximity to eolian dunes. Unit distinguishable in the field by it light to white albedo in aerial imagery, low-lying topography and lack of shoreline-related rounded clasts. Sediments are confined to a distinct elevation between ~1190 – 1220 m.

Tertiary Stratigraphy

Ts – Sedimentary diatomite unit with a series of distinct silicified sandstone and coquina beds. The diatomite is white with interbedded light tan to reddish-brown tuffaceous sediments and sandstone. Sandstone is coarse-grained and 1-10 cm thick. This unit was dated as late-middle Miocene to early Pliocene based on diatoms collected in the southern Jackson Mountains (Willden, 1964), and mapped by Sibbett et al in 1982. There are two distinct coquina units, white to tan, that range from 6 – 20 cm thick and consist of about 5 mm diameter-sized shells. Reddish brown silicified sandstone has round nodules that are ½ - 1 cm in diameter. Coquina contains shells that were dated as late to early Pliocene (Dall, 1924 and Firby, 1967). Unit also mapped by Sibbett et al, 1982.

Tb – Basalt flows. Black to dark grey, weathers dark reddish-brown and exhibits local columnar jointing. The basalt ranges in texture from coarsely porphyritic to aphanitic. Phenocrysts of dark black pyroxene (1-3 cm), plagioclase (7 mm – 1 cm in length) and small olivines (>4 mm) are found within the porphyritic sequences. Vesicles up to 1 cm in diameter are found near the stratigraphic top of each local flow sequence. Secondary needle-like light green quartz crystals are present filling the vesicular unit. Local veins of light orange calcite and white silica. Calcite ranges from 1 cm to 6 m in thickness and

shows dog-eared texture, silica ranges from 1 cm to ½ m in thickness. Previously mapped by Sibbett et al, 1982.

Late Paleozoic to Mesozoic Stratigraphy

Jg – slightly metamorphosed igneous intrusive unit. Light green porphyritic slightly-metamorphosed granodiorite composed of quartz, hornblende (1-5 mm in length), pyroxene, epidote, feldspars. Mafic minerals comprise 50-60% of rock. Slight greenschist facies metamorphism based on green color and epidote; no foliation present. Age might be similar to intrusive dioritic plutons in the Jackson Mountains, dated as between 196 and 190 Ma based on U/Pb ages, or Early Jurassic (Quinn et al, 1997).

TRV – slightly metamorphosed interbedded volcanic tuffs and sediments. Ranges from green, brown and red pyroclastic welded tuffs with interbedded chert (gravel to pebble-size) and weathered feldspars. Reddish-brown fine-grained sedimentary unit consists of grey slightly-metamorphosed sandstone, local red/brown veins, heavily weathered. Locally interbedded with conglomerate with subrounded chert and volcanic clasts, pebble-sized. Clasts up to cobble size of TR are inbedded within the conglomerate, giving age relationships between the two units. Slight foliation visible. Cut by calcite and silica veins. This unit might be similar to the gradational stratigraphy contact between the Boulder Creek unit and Happy Creek Volcanic complex previously mapped ~1 km north in the Jackson Mountains (e.g. Quinn et al, 1997), which is dated as Upper Triassic to upper Middle Jurassic.

TR –Late Paleozoic to Mesozoic limestone. Grey limestone, heavily fractured with extensive calcite veins and local malachite. Extensive spitzkarren weathering. Local karst breccias with angular to sub-angular pebble to cobble size clasts; the breccias have local greenish-blue malacite and deep red to brown hemitite mineralization in the matrix. No observed fossils.

METHODS:

Magnetics: (Data from the survey are provided in Table 1.1.)

A magnetic survey was used to supplement Quaternary mapping and help locate faults. A magnetic survey was chosen in this case based on the fact that fault zones can sometimes show a magnetic anomaly based on certain mineral alterations. Basalt typically contains magnetite and has a high magnetic susceptibility. Previous work shows that magnetite can alter to hematite under certain conditions associated with a hydrothermal system. The transformation is typically a redox reaction shown here: $2Fe_3O_4(mt) + 1/2O_2(g) \rightarrow 3Fe_2O_3(hm)$ (e.g. Ohmoto, 2003). This can happen in a geothermal system when upward-moving hydrothermal fluids mix with O2-rich groundwater. While magnetite has a high magnetic susceptibility, hematite has a low susceptibility, which would produce a magnetic low in a ground survey. There are difficulties interpreting magnetic data; these include lateral flow patterns (heterogeneities and discrete fractures may allow for fluid flow outside of the fault zone), and differences in availability of hydrothermal fluids and ground water within the fault system.

GEM Systems GSM-19 v4.0 magnetometers from University of Nevada, Reno, were used to conduct the magnetic survey. The survey was completed using procedures from the *GEM Systems Magnetism Survey Tutorial,* compiled by University of Nevada, Reno student Colton Dudley. The survey requires two magnetometers – one as a base station that continuously takes magnetic readings, and the other as a mobile station. The base station is necessary to determine whether magnetic anomalies recorded by the mobile unit are a result of magnetic storms, or if they are actually related to subsurface

magnetic susceptibilities. If there is great variation in the magnetic base data, then the mobile data are difficult to interpret.

First, the base station was set up in a sheltered drainage just north of the active travertine fissure ridge. The sensor was set up on a tripod, facing north to align with the earth's magnetic field. The time on the base station computer and the mobile computer were synced with a GPS, in order to correctly compare readings. The mobile computer is strapped to a person and connected to a staff with the sensor on top. When collecting data, it is important to remove all metals from clothing/backpacks, etc, and always point the sensor north when taking a reading.

After the data were collected, they were modeled using Oasis Montage. The raw data were corrected for base station data and then reduced to the pole for easier interpretation. Although the data were corrected for the base station, the nT variation in the base station data were not more than 40 nT. By reducing the data to the pole, dipole anomalies are removed and a single anomaly over the magnetic body is shown.

Magnetic Data:

Raw Magnetic Data (UTM data is taken in NAD83, the magnetometer used was the Gem Systems GSM-19 v4.0). Survey was done on 6/27/2013.

STATION	nT	TIME	UTM_X	UTM_Y	NOTES
143	51300.48	10:05:00	355517	4545957	starting at travertine, walking into playa
144	51388.44	10:13:00	355156	4545870	
145	51373.58	10:19:17	354985	4545751	
146	51305.21	10:35:05	354355	4545519	
147	51295.09	10:38:47	354307	4545605	
148	51295.56	10:42:21	354284	4545644	on scarp
149	51300.09	10:45:09	354269	4545660	
149.5	51290.2	10:49:19	354213	4545719	lineament in aerial photo, possible scarp
150	51332.66	10:53:09	354172	4545751	
151	51324.71	10:57:39	354081	4545801	
152	51311.66	11:19:23	353901	4546001	start of SW traverse across fault, 100 m spacing
153	51342.56	11:25:35	353990	4545959	
154	51355.12	11:28:35	354080	4545921	
155	51373.26	11:32:56	354173	4545883	
156	51363.59	11:35:56	354196	4545871	25 m spacing from last station
157	51344.31	11:38:14	354214	4545859	
158	51338.73	11:39:59	354237	4545848	
159	51366.39	11:42:20	354258	4545837	
160	51328.2	11:44:59	354279	4545827	
161	51320.09	11:47:11	354300	4545876	
162	51329.78	11:49:47	354323	4545805	
163	51320.48	11:52:14	354344	4545792	
164	51331.81	11:54:08	354366	4545783	
165	51350.02	11:56:11	354396	4545770	on scarp
166	51355.85	12:09:05	354419	4545760	
167	51368.4	12:11:02	354441	4545749	
168	51379.65	12:12:35	354464	4545733	
169	513188.4	12:14:17	354487	4545726	
170	51399.8	12:16:44	354510	4545716	
171	51411.63	12:18:14	354533	4545707	
172	51416.7	12:20:08	354556	4545699	
173	51424.39	12:21:38	354577	4545686	
174	51428.72	12:23:17	354600	4545677	
175	51432.45	12:25:20	354621	4545665	
176	51403.84	12:28:59	354710	4545620	100 m from last point
177	51369.39	12:32:14	354797	4545572	
178	51351.77	12:35:50	354831	4545519	
179	5129.24	12:39:47	354970	4545473	end of traverse
180	51291.72	14:08:11	356443	4547516	start of second traverse

181	51260.22	14:18:44	356543	4547510	
182	51268.94	14:21:41	356594	4547507	
183	51272.48	14:24:09	356644	4547503	
184	51276.25	14:27:11	356692	4547506	
185	51277.57	14:30:41	356716	4547499	
186	51268.49	14:33:41	356740	4547495	
187	51257.27	14:34:59	356766	4547491	
188	51210.04	14:36:56	356790	4547488	
189	51157.46	14:38:56	356815	4547487	
190	51043.82	14:42:26	356841	4547483	
191	50949.79	14:45:20	356865	4547484	
192	50791.61	14:46:47	356889	4547473	on big scarp
193	50652.56	14:49:33	356910	4547464	
194	50608.08	14:51:35	356930	4547443	
195	50465.21	14:58:56	356955	4547445	
196	50319.58	15:00:32	356981	4547447	
197	50219.62	15:02:08	357006	4547439	
198	50157.74	15:04:02	357030	4547434	
199	50190.14	15:05:29	357054	4547431	
200	50193.5	15:08:05	357079	4547421	
201	50216.17	15:09:38	357102	4547423	
202	50316.6	15:11:50	357152	4547418	
203	50487.82	15:15:26	357202	4547414	
204	50984.79	15:17:50	357251	4547401	
205	51257.27	15:20:44	357300	4547398	
206	51253.79	15:25:26	357398	4547381	end of desert pavement plateau
207	51292.75	15:54:35	357323	4546968	
208	51446.72	15:59:05	357243	4547029	
209	51060.4	16:03:20	357214	4547070	
210	49997	16:05:35	357164	4547075	
211	49957.77	16:07:56	357117	4547092	
212	51258.75	16:10:35	357068	4547099	
213	50247.89	16:15:08	357021	4547114	
214	50764.44	16:17:44	356972	4547115	
215	51004.81	16:20:05	356924	4547134	
216	51230.32	16:22:17	356872	4547141	
217	51298.7	16:24:38	356822	4547146	
218	51320.91	16:26:38	356772	4547155	
219	51302.47	16:30:17	356676	4547172	
220	51309.6	16:33:11	356577	4547180	
221	51305.9	16:36:53	356477	4547198	
222	51294.27	16:39:41	356379	4547246	
223	51309.95	16:41:29	356324	4547225	
226	51246.18	19:06:29	355351	4545334	
227	51289.27	19:10:38	355449	4545317	

228	51322.37	19:13:59	355551	4545293	
229	51411.37	19:17:47	355649	4545281	
230	51473.49	19:19:56	355697	4545269	
231	51513.99	19:22:26	355746	4545258	
232	51605.68	19:27:29	355796	4545249	
233	51718.69	19:30:02	355820	4545239	
234	51786.85	19:31:56	355845	4545236	
235	51881.1	19:34:23	355869	4545231	
236	51995.12	19:35:50	355894	4545232	
237	52107.81	19:37:23	355932	4545224	
238	52175.23	19:39:17	355948	4545215	
239	52237.88	19:40:47	355972	4545209	
240	52223.77	19:42:11	355996	4545205	
241	52166.59	19:43:59	356020	4545193	
242	52136.19	19:45:29	356043	4545194	
243	52119.53	19:46:50	356068	4545192	
244	52105.53	19:48:50	356092	4545185	
245	52044.23	19:50:29	356116	4545181	
246	51856.28	19:51:53	356140	4545175	
247	51798.93	19:53:29	356161	4545161	
248	51888.51	19:55:44	356186	4545154	
249	51735.57	19:57:29	356210	4545145	
250	52487.93	20:02:20	356233	4545133	basalt/Q contact
251	49572.64	20:04:14	356239	4545123	in basalt
252	50734.32	20:06:44	356250	4545121	basalt

Shallow Temperature Surveys:

A series of shallow temperature surveys was conducted in order to test locations of shallow fluid flow related to faults or other permeable units and in order to discover areas of high temperature that might have been overlooked in previous work. The following summarizes the methods and results from these surveys.

Two-meter temperature surveys can be completed with relative ease using an ATV, temperature measuring device and two-meter metal probes. The equipment used in this survey was provided by the Great Basin Center for Geothermal Energy at University

of Nevada, Reno. The actual survey involves pounding the metal probes into the ground using a power drill and letting the temperature equilibrate for at least one hour. A base station is measured at various points throughout the day to make sure equipment is consistent. The temperatures are measured at a .5 m, 1 m and 2 m depth so that a temperature gradient can be calculated.

One-meter temperature surveys can also be completed with ease, and do not require the use of an ATV or power drill, so are ideal in Designated Wilderness Areas, or areas with terrain too rugged for an ATV. The survey involves walking to the survey location, pounding a 1 m probe into the ground, letting the temperature stabilize, measuring the temperature and then removing the probe. It is important to note that 1 m surveys only pick up larger temperature anomalies.

A one-meter temperature survey was also completed in areas that are designated Black Rock Desert Wilderness Area (no motorized vehicles allowed) and that are too rugged for an ATV. This method was chosen based on the correlation of high 1 m temperatures to 2 m temperatures in the previous two-meter survey. The hottest two-meter temperatures (>19.1 degrees) were picked up as a significant anomaly in the 1 m data, so a 1 m survey might pick up other high temperatures (see data table).

Once the temperature data are recorded, they can be put into Excel and corrected for the RTD (resistance temperature device) using a linear regression developed by Chris Sladek. There are also corrections that can be made based on albedo and slope (Sladek et al, 2009). To see if an albedo correction was necessary, I measured a couple of data points in close proximity to each other in areas with contrasting albedo. There was no

temperature difference, so no corrections were made. All of the data points were taken in relatively flat areas, so slope corrections were not necessary.

Shallow Temperature Data:

Shallow Temperature Data. UTMs are in NAD83, zone 11. This table shows both two-meter and one-meter surveys done at MacFarlane Hot Springs. Corr means RTD corrections and Grad means temperature gradient.

Station	UTM_X	UTM_Y	Date	1m	1.5m	2m	1m Corr	1.5m Corr	2m Corr	1.5-2m Grad
1 (base)	355610	4546121	11/15/2012	16.7	18.9	19.9	16.9	19.1	19.7	1.25
2	356154	4546593	11/15/2012	16.4	18.6	19.5	16.4	18.7	19.6	1.83
3	356420	4547191	11/15/2012	15.9	18.4	19.6	15.9	18.5	19.7	2.33
4	356772	4547004	11/15/2012	16.0	18.2	19.2	15.4	18.3	19.3	2.00
5	356839	4547396	11/15/2012	16.0	18.0	19	16.0	18.1	19.1	1.83
6	356506	4547447	11/15/2012	12.8	16.9	18.5	12.8	16.9	18.5	3.20
7	356949	4547959	11/15/2012	15.5	17.8	19.3	15.6	17.9	19.3	2.85
8	357377	4548330	11/15/2012	16.6	18.6	19.6	16.6	18.7	19.7	1.97
9	357366	4548293	11/15/2012	16.5	18.3	19	16.5	18.4	19.1	1.46
10	355764	4545820	11/15/2012	19.6	22.7	24.5	19.8	22.9	24.3	2.76
11	355870	4545832	11/15/2012	19.1	22.1	23.7	19.1	22.2	23.9	3.27
12	355864	4545793	11/15/2012	16.4	19.3	20.9	16.4	19.4	21.0	3.13
13	355920	4545720	11/15/2012	15.5	17.9	19.6	15.5	17.9	19.6	3.35
14	356033	4545786	11/15/2012	15.6	18.0	19.1	15.7	18.2	19.1	1.85
15	356000	4545739	11/15/2012	16.7	18.6	19.8	16.9	18.8	20.0	2.57
16	355997	4545648	11/15/2012	15.7	17.9	19.6	15.7	18.0	19.6	3.31
17	356361	4543533	11/15/2012	15.7	17.7	19.1	15.9	17.9	18.9	2.06
18	356446	4543373	11/15/2012	15.5	17.2	18.1	15.5	17.3	18.2	1.82
19	356410	4543427	11/15/2012	17.1	18.9	19.7	17.1	19.0	19.8	1.52
20	356216	4543663	11/15/2012	16.3	18.3	19.5	15.7	18.4	19.6	2.40
21	356212	4543494	11/15/2012	16.6	18.5	19.6	16.6	18.6	19.7	2.03
22 (base)	355611	4546128	5/22/2013	18.0			18.2			
23 (base)	355611	4546128	5/22/2013	17.3	15.9	15.3	17.3			-1.15
24	360905	4545921	5/22/2013	18.7			18.8			

25	355887	4545921	5/22/2013	17.9			17.3			
26	355999	4546011	5/22/2013	17.0			17.0			
27	356106	4546055	5/22/2013	17.0			17.0			
28	356191	4546120	5/22/2013	17.9			18.0			
29	356311	4546253	5/22/2013	17.0			17.0			
30 (base)	355611	4546128	5/22/2013	17.3	15.9	15.3	17.3			-1.9
31	355400	4545937	5/22/2013	21.3			21.3			
32	355368	4545831	5/22/2013	22.5			22.5			
33	355618	4545999	6/28/2013	20.9	19.6	18.9	21.1	19.8	18.7	-2.13
34	355575	4545906	6/28/2013	22.6	22.3	21.7	22.6	22.4	21.8	-1.16
35	355458	4545706	6/28/2013	21.6	20.1	18.6	21.7	20.2	18.7	-3.09
36	355306	4545494	6/28/2013	22.0	20.3	18	21.4	20.4	18.1	-4.67
37	355208	4545041	6/28/2013	21.7	20.1	18.6	21.7	20.3	18.7	-3.19
38 (base)	355611	4546128	6/28/2013	20.7	19.5	18.4	20.7	19.5	18.4	-2.20

REFERENCES

Adams, K., Wesnousky, S., 1998, Shoreline processes and the age of the Lake Lahontan highstand in the Jessup embayment, Nevada, Geological Society of America Bulletin, v. 110, no. 10, p. 1318-1332.

Adams, K.D., Wesnousky, S.G., 1999, The Lake Lahontan highstand: age, surficial characteristics, soil development, and regional shoreline correlation, Geomorphology, v. 30, pgs. 357-392.

Anderson, R.B., Faulds, J.E., Dering, G.M., 2013, Preliminary geologic map of the central Lakes Range, southern Fox Range, and northern Terraced Hill, Emerson Pass geothermal area, Washoe County, Nevada, Nevada Bureau of Mines and Geology Open-File Report 13-10, scale 1:24,000, 9 p.

Arehart, G.B., Coolbaugh, M.F., Poulson, S.R., 2003, Evidence for a magmatic source of heat for the Steamboat Springs geothermal system using trace elements and gas geochemistry, GRC Transactions, v. 27, pgs. 269-274.

Barton, C.A., Zoback, M.D., Moos, D., 1995, Fluid flow along potentially active faults in crystalline rocks, Geology, v. 23, no. 8, pgs. 683-686.

Bell, J.W., Caskey, J.S., House, K.P. House, 2009, Geologic Map of the Lahontan Mountains Quadrangle, Churchill County, Nevada, Nevada Bureau of Mines and Geology Map 168.

Bell, J.W., Katzer, T., 1990, Timing of late Quaternary faulting in the 1954 Dixie Valley earthquake area, central Nevada, Geology, v. 18, pgs. 622-625.

Bell, J.W. and Ramelli, A.R., 2007, Active faults and neotectonics at geothermal sites in the western Basin and Range: preliminary results, GRC Transactions, v. 31, pgs. 375-378.

Benoit, W.R., Hiner, J.E., and Forest, R.T., 1982, Discovery and Geology of the Desert Peak Geothermal Field; A Case History: Nevada Bureau of Mines and Geology Bulletin 97, 82 p.

Blank, R.R., Young, J.A., Allen, F.L., 1999, Aeolian dust in a saline playa environment, Nevada, USA, Journal of Arid Environments, v. 41, pgs. 365-381.

Blackwell D.D., Negraru, P.T., Richards, M.C., 2006, Assessment of the Enhanced Geothermal System Resource Base of the United States, Natural Resources Research, v. 15, pgs. 283-308.

Blissenbach, Erich, 1954, Geology of alluvial fans in semiarid regions, GSA Bulletin, v. 65, n. 2, pgs. 175-190.

Brogi A., Cepezzuoli, E., 2009, Travertine deposition and faulting: the fault-related travertine fissure-ridge at Terme S. Giovanni, Rapolano Terme (Italy), International Journal of Earth Science, v. 98, pgs. 931-947.

Brogi, A., Capezzuoli, E., Aque, R., Branca, M., Voltaggio, M., 2010, Studying travertines for neotectonic investigations: Middle-Late Pleistocene syn-tectonic travertine deposition at Serre di Rapolano (Northern Apennines, Italy), International Journal of Earth Science, v. 99, pgs. 1383-1398.

Brogi A., Capezzuoli, E., Buracchi, E., Branca, M., 2012, Tectonic control on travertine and calcareous tufa deposition in a low-temperature geothermal system (Sarteano, Central Italy), Journal of the Geological Society, v. 169, pgs. 461-476.

Cakir, Z., 1999, Along-strike discontinuity of active normal faults and its influence on Quaternary travertine deposition; examples from western Turkey, Journal of Earth Science, v. 8, pgs. 67-80.

Camp, V.E., Ross, M.E., Hanson, W.E., 2003, Genesis of flood basalts and Basin and Range volcanic rocks from the Steens Mountain to the Malheur River Gorge, Oregon, Geological Society of America Bulletin, v. 115, pgs. 105-128.

Cashman, P.H., Faulds, J.E., and Hinz, N.H., 2012, Regional Variations in Structural Controls on Geothermal Systems in the Great Basin, GRC Transactions, v. 36, pgs. 25-30.

Cashman, P.H., Trexler, J., Widmer, M., Queen, S., 2012, Post 2.6 Ma tectonic and topographic evolution of the northeastern Sierra Nevada: The record in the Reno and Verdi basins, Geosphere, v. 8, pgs. 972-990.

Chafetz H.S., Folk, R.L., 1984, Travertines: depositional morphology and the bacterially constructed constituents, Journal of Sedimentary Petrology, v. 54, pgs. 289-316.

Ciftci, N.B., Bozkurt, E., 2007, Anomalous stress field and active breaching at relay ramps: a field example from Gediz Graben, SW Turkey, Geology Magazine, v. 144 (4), pgs. 687-699.

Colgan, J.P., Dumitru, T.A., Reiners, P.W., Wooden, J.L., Miller, E.I., 2006, Cenozoic tectonic evolution of the Basin and Range province in northwestern Nevada, American Journal of Science, v. 306, pgs. 616-654.

Coolbaugh, M.F., Raines, G.L., Zehner, R.E., Shevenell, L., Williams, C.F., 2006, Predication and discovery of new geothermal resources in the Great Basin: multiple evidence of a large undiscovered resource base, GRC Transactions, v. 30, pgs. 867-873.

Coolbaugh, M., Lechler, P., Sladek, C., and Kratt, C., 2009, Carbonate tufa columns as exploration guides for geothermal systems in the Great Basin: Geothermal Resources Council Transactions, v. 33, pgs. 461-466.

Coolbaugh, M., Lechler, P., Sladek, C., Kratt, C., 2010, Lithium in tufas of the Great Basin: Exploration implications for geothermal energy and lithium resources, Geothermal Resources Council Transactions, v. 34, pgs. 521-526.

Cowie, P.A., Scholz, C.H., 1992, Physical explanation for the displacement-length relationship of faults using a post-yield fracture mechanics model, Journal of Structural Geology, v. 14, pgs. 1133-1148.

Curewitz, D., Karson, J.A., 1997, Structural settings of hydrothermal outflow: Fracture permeability maintained by fault propagation and interaction, Journal of Volcanology and Geothermal Research, v. 79, pgs. 149-168.

Crider, J.G., Peacock, D.C.P., 2004, Initiation of brittle faults in the upper crust: a review of field observations, Journal of Structural Geology, v. 26, pgs. 691-707.

dePolo, C.M., Ramelli, A.R., Bell, J.W., 1999, Preliminary Geologic Map of the Pahrump Quadrangle, Nye County, Nevada, Nevada Bureau of Mines and Geology Open File Report 99-14.

Dering, G., and Faulds, J., 2012, Structural controls of the Tuscarora geothermal field, Elko County, Nevada, GRC Transactions, v. 36, pgs. 41-46.

Faulds, J.E., Geissman, J.W., Shafiqullah, M., 1992, Implications of paleomagnetic data on Miocene extension near a major accommodation zone in the Basin and Range province, northwestern Arizona and southern Nevada, Tectonics, v. 11, pgs. 204-227.

Faulds, J., Coolbaugh, M., Blewitt, G., and Henry, C.D., 2004, Why is Nevada in hot water? Structural controls and tectonic model of geothermal systems in the northwestern Great Basin, GRC Transactions, v. 28, pgs. 649-654.

Faulds, J., Coolbaugh, M., Vice, G., Edwards, M., 2006, Characterizing structural controls of geothermal fields in the northwestern Great Basin: a progress report, GRC Transactions, v. 30, pgs. 69-76.

Faulds, J.E., and Henry, C.D., 2008, Tectonic influences on the spatial and temporal evolution of the Walker Lane: An incipient transform fault along the evolving Pacific-North American plate boundary, Arizona Geological Society Digest, v. 22, pgs. 437-470.

Faulds, J.E., Hinz, N.H., Dering, G.M., Siler, D.L., 2013, The hybrid model – the most accommodating structural setting for geothermal power generation in the Great Basin, Western USA, GRC Transaction, v. 37, pgs. 3-10.

Faulds, J.E., Hinz, N., Kreemer, C., and Coolbaugh, M., 2012, Regional Patterns of Geothermal Activity in the Great Basin Region, Western USA: Correlation With Strain Rates, GRC Transactions, v. 36, pgs. 892-902.

Faulkner, D.R., Jackson, C.A.L., Lunn, R.J., Schlischa, R.W., Shipton, Z.K., Wibberley, C.A.J., and Withjack, M.O., 2010, A review of recent developments concerning the structure, mechanics and fluid flow properties of fault zones, Journal of Structural Geology, v. 32, pgs. 1557-1575.

Ferrill, D.A., Winterle, J., Wittmeyer, G., Sims, D., Colton, S., Armstrong, A., 1999, Stressed Rock Strains Groundwater at Yucca Mountain, Nevada, GSA Today, v. 9, n. 5, pgs. 2-7.

Ferrill, D.A., and Morris, A.P., 2000, Displacement gradient and deformation in normal fault systems, Journal of Structural Geology, v. 23, pgs. 619-638.

Ferrill, D.A. and Morris, A.P., 2003, Dilational normal faults, Journal of Structural Geology, v. 25, pgs. 183-196.

Ford, T.D., and Pedley, H.M., 1996, A review of tufa and travertine deposits of the world, Earth-Science Reviews, v. 41, pgs. 117-175.

Gartell, A., Zhang, Y., Lisk, M., Dewhurst, D., 2004, Fault intersections as critical hydrocarbon leakage zones: integrated field study and numerical modeling of an example from the Timor Sea, Australia, Marine and Petroleum Geology, v. 21, pgs. 1165-1179.

Gruszczynsky M., Kowalski, BJ., Soltysik, R., Hercamn, H., 2004, Tectonic origin of the unique Holocene travertine from the Holy Cross Mts.; microbially and abiologically

mediated calcium carbonate, and manganese oxide precipitation, Acta Geologica Polonica, v. 54, pgs. 61-76.

Hammond, W.C., Blewitt, G., Kreemer, C., 2011, Block modeling of crustal deformation of the northern Walker Lane and Basin and Range from GPS velocities, Journal of Geophysical Research, v. 166, B04402

Hammond, W.C. and Thatcher, W., 2005, Northwest Basin and Range tectonic deformation observed with the Global Positioning System, 1999–2003, Journal of Geophysical Research, v. 100, no. B10, B10104

Hancock, P.L., Altunel, E., 1993, Morphology and structural setting of Quaternary travertines at Pamukkale, Turkey, Geological Journal, v. 28, pgs. 335-346.

Hancock, P.L., Chalmers, R.M.L., Altunel, E., Cakir, Z., 1999, Travitonics: using travertines in active fault studies, Journal of Structural Geology, v. 21, pgs. 903-916.

Hose, R.K., Taylor, B.E., 1974, Geothermal Systems of Northern Nevada, Geological Survey Technical Report, Reston, Va.

Jewell, P.W., Nicoll, K., 2011, Wind regimes and aeolian transport in the Great Basin, USA, Geomorphology, v. 129, pgs. 1-13.

Kratt, C., Coolbaugh, M., Peppin, B., Sladek, C., 2009, Identification of a new blind geothermal system with hyperspectral remote sensing and shallow temperature measurements at Columbus Salt Marsh, Esmeralda County, Nevada.

LaBrecque, J.L., Kent, D.V., Cande, S.C., 1977, Revised magnetic polarity time scale for Late Cretaceous and Cenezoic time, Geology, v. 5, pgs. 330-335.

Larsen, P.H., 1988, Relay structures in Lower Permian basement-involved extension system, East Greenland, Journal of Structural Geology, v. 10, no. 1, pgs. 3-8.

Lerch, D.W., Klemperer, S.L., Glen, J.M.G., Ponce, D.A., Miller, E.L., Colgan, J.P., 2007, Crustal structure of the northwestern Basin and Range province and its transition to unextended volcanic plateaus, Geochemistry Geophysics Geosystems, v. 8, n. 2.

Lerch, D. W., Miller, E., McWilliams, M. and Colgan, J., 2008, Tectonic and magmatic evolution of the northwestern Basin and Range and its transition to unextended volcanic plateaus: Black Rock Range, Nevada, Bulletin of the Geological Society of America, v. 120, n. 3, pgs. 300-311.

Louie J., Shields, G., Ichinose, G., Hasting, M., Plank, G., Bowman, S., 1998, Shallow geophysical constraints on displacement and segmentation of the Pahrump Valley fault zone, California-Nevada border: in W. R. Lund, Ed., Proceedings of the May 13-15 Basin and Range Seismic Hazards Summit, Utah Geological Survey Misc. Pub. 98-2, Cedar City, Utah.

Maher, K.A., 1989, Geology of the Jackson Mountains, Northwest Nevada, Ph.D. thesis at California Institute of Technology.

Mass, K.B., Cashman, P.C., Trexler, J.H., 2009, Stratigraphy and structure of the Neogene Boca basin, northeastern California: Implications for late Cenezoic tectonic evolution of the northern Sierra Nevada, GSA Special Paper, v. 447, pgs. 147-170.

Ohmoto, H., Nonredox transformations of magnetite-hematite in hydrothermal systems, 2003, Economic Geology, v. 98, pgs. 157-161.

Oldow, J.S., 1984, Evolution of a Late Mesozoic back-arc fold and thrust belt, Northwestern Great Basin, U.S.A, Tectonophysics, v. 102, pgs. 245-274.

Oldow, J.S., 1983, Tectonic implications of a late Mesozoic fold and thrust belt in northwestern Nevada, 1983, Geology, v. 11, no. 9, pgs. 542-546.

Peacock, D.C.P., Sanderson, D.J., 1991, Displacements, segment linkage and relay ramps in normal fault zones, Journal of Structural Geology, v. 13, n. 6, pgs. 721-733.

Peacock, D.C.P., Sanderson, D.J., 1994, Geometry and Development of Relay Ramps in Normal Fault Systems, American Association of Petroleum Geologists, v. 78, no. 2, pgs. 147-165.

Peterson, F.F., 1981, Landforms of the Basin and Range Province Defined for Soil Survey, Nevada Agricultural Experiment Station, Technical Bulletin 28.

Richards, M. and Blackwell, D., 2002, A difficult search; why Basin and Range systems are hard to find, Geothermal Resources Council Bulletin, pgs. 143-146.

Russell, B.J., 1984, Mesozoic geology of the Jackson Mountains, northwestern Nevada, GSA Bulletin, v. 95, no. 3, pgs. 313-323.

Shields, G., Allander, K., Brigham, R., Crosbie, R., Trimble, L., Sleeman, M., Tucker, R., Zhan H., Louie, J.N., 1998, Geophysical surveys of an active fault: results from Pahrump Valley, California-Nevada border, Bull. Seismol. Soc. Amer., v. 88, pgs. 270-275.

Sibbett, B.S., Zeisloft, J., Bowers, R.L., 1982, Geology of MacFarlane's spring thermal area, Geothermal Resources Council, Transactions, v. 6, pgs. 47-50.

Skord, J., Cashman, P.H., Coolbaugh, M.,amd Hinz, N., 2011, Mapping Hydrothermal Upwelling and Outlfow Zones: Perliminary Results from Two-Meter Temperature Data and Geologic Analysis at Lee Allen Springs and Salt Wells Basin, GRC Transactions, v. 35, pgs. 1017-1021.

Sladek, C., Coolbaugh, M.F., Kratt, C., 2009, Improvements in Shallow (Two-Meter) Temperature Measurements and Data Interpretation, GRC Transactions, v. 33, pgs. 535-541.

Swanberg, C.A., Bowers, R.L., 1982, Downward continuation of thermal temperature gradients at Macfarlane's hot spring, northern Nevada. GRC Transactions, v. 6, pgs. 177-180.

Trudgill, B. and Certwright, J., 1994, Relay-ramp forms and normal-fault linkages, Canyonlands National Park, Utah, GSA Bulletin, v. 106, pgs. 1143-1157.

Quinn, M.J., Wright, J.E., Wyld, S.J., 1997, Happy Creek igneous complex and tectonic evolution of the early Mesozoic arc in the Jackson Mountains, northwest Nevada, GSA Bulletin, v. 109, pgs. 461-482.

U.S. Geological Survey, 2006, Quaternary fault and fold database for the United States, accessed 12/2013, from USGS web site: http//earthquakes.usgs.gov/regional/qfaults/.

Wallace, R.E., 1977, Profiles and ages of young fault scarps, north-central Nevada, GSA Bulletin v. 88, no. 9, pgs. 1267-1281

Willden, R., 1964, Geological and Mineral Deposits of Humboldt County, Nevada, Nevada Bureau of Mines and Geology, Bulletin 59.

Wright, Phillip M, 1991, Geochemistry, Technical Report. Geothermal direct use engineering and design guidebook, Oregon Institute of Technology, Klamath Falls, Oregon, Lienau, P.J., Lunis, B.C.,1991.

PLATE 1

Kraushaar, Sabina, 2014, Structural controls of the MacFarlane geothermal system, Humboldt County, NV: new insights based on detailed geologic mapping, shallow temperature surveys and magnetic data, MS thesis, 130 p.

GEOLOGIC MAP OF MACFARLANE GEOTHERMAL AREA, HUMBOLDT COUNTY, NEVADA

Sabina M. Kraushaar
Mackay School of Earth Sciences and Engineering

2014

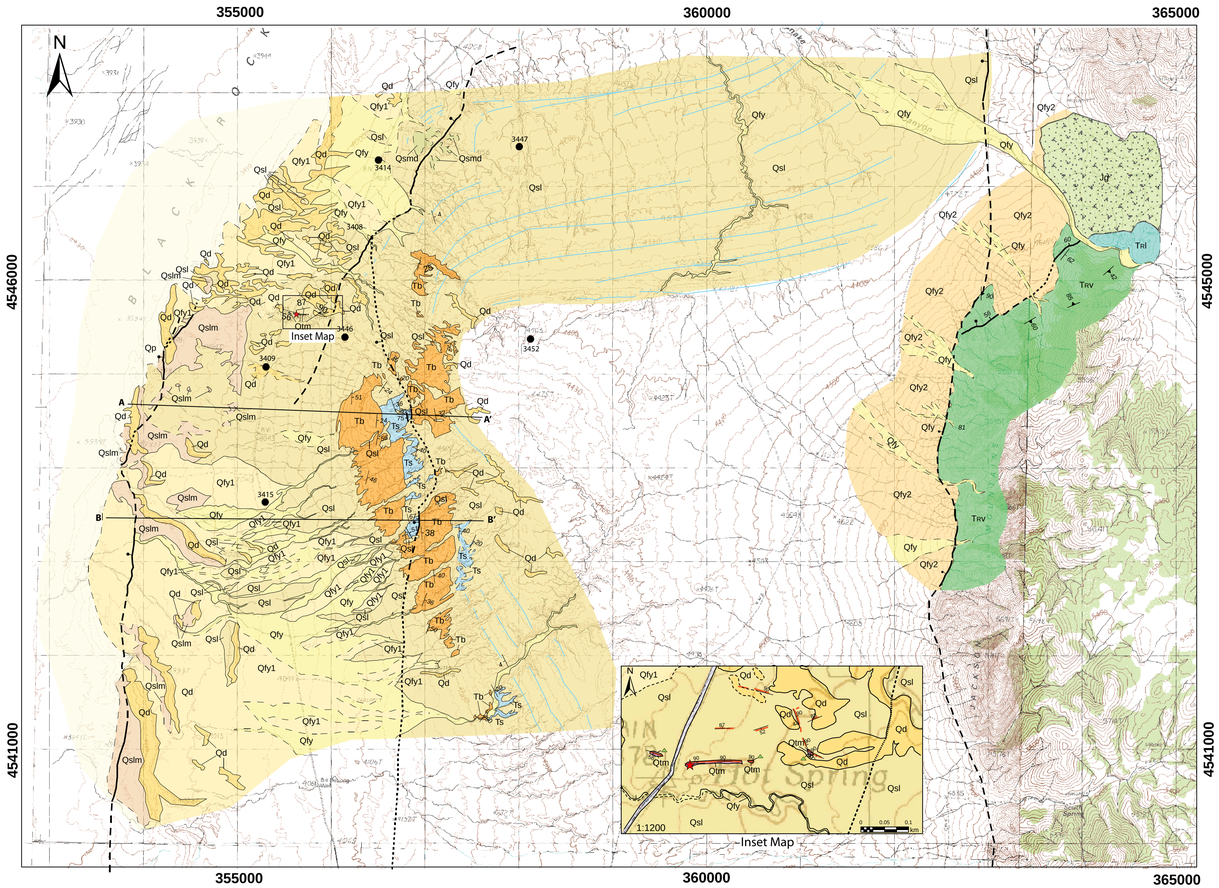

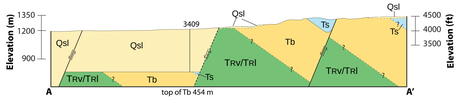

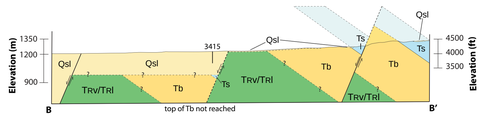

Scale 1:24,000

0 0.5 1 kilometer

0 0.5 1 mile

0 1000 3000 5000 feet

CONTOUR INTERVAL 20–40 FEET

Projection: Universal Transverse Mercator, Zone 11, North American Datum 1983 (m)

Base map: U.S. Geological Survey Salt Water Spring 7.5' quadrangle (1983)
Base map: U.S. Geological Survey Red Butte 7.5' quadrangle (1983)

References:

Maher, K.A., 1989, Geology of the Jackson Mountains, Northwest Nevada, Ph.D. thesis at California Institute of Technology.

Quinn, M.J., Wright, J.E., Wyld, S.J., 1997, Happy Creek ingenous complex and tectonic evolution of the early Mesozoic arc in the Jackson Mountains, northwest Nevada, GSA Bulletin, v. 109, pgs. 461-482.

Sibbett, B.S., Zeisloft, J., Bowers, R.L., 1982, Geology of MacFarlane's spring thermal area, Geothermal Resources Council, Transactions, v. 6, pgs. 47-50.

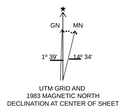

UTM GRID AND
1983 MAGNETIC NORTH
DECLINATION AT CENTER OF SHEET

Drill Hole Data (Sibbett et al., 1982)

Drill Hole #	Total Depth (m)	Depth to Top of Tb (m)
3408	152	(not reached)
3409	610	454
3414	610	(not reached)
3415	122	(not reached)
3446	150	15
3447	150	85
3452	585	38

Quaternary Units

Road (human disturbance)

Eolian Deposits

Qd — Dune deposits

Playa Deposits

Qp — Playa deposits

Alluvial Deposits

Qfy — Active stream channels and channel deposits

Qfy1 — Inactive alluvial fan deposits

Qfy2 — Inactive alluvial fan deposits near range front

Lacustrine Deposits Associated with Lake Lahontan

Qsl — Recessional beach and bar deposits

Qsmd — Algal tufa mats

Qslm — Deep water sediments

Hydrothermal and Spring Related Deposits

Qtm — Travertine fissure ridges and associated mounds

Tertiary Units

Ts — Diatomite and tuffaceous sandstone

Tb — Tertiary basalt

Late Paleozoic to Mesozoic Units

Jg — Granodiorite pluton

Trv — Volcanic strata related to the Happy Creek Complex, previously mapped in the Jackson Mountains by Maher (1989) and Quinn et al., (1997)

Trl — Limestone related to the Bliss Canyon Fm, previously mapped in the Jackson Mountains by Maher (1989)

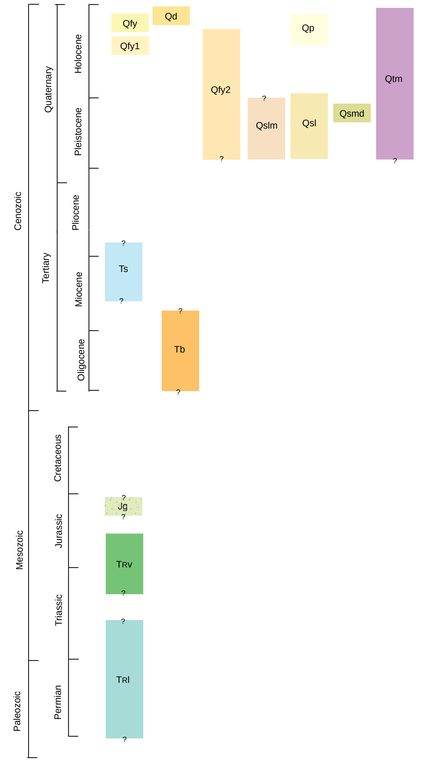

Symbology

Contact Solid where certain and location accurate, long-dashed where approximate, short-dashed where inferred, dotted where concealed.

Normal fault Showing dip of fault; ball on downthrown side; solid where certain and location accurate, dashed where approximate, dotted where concealed

Lake Lahontan shorelines

travertine fissure ridge

weathered travertine deposit

Strike and dip of bedding in sedimentary rock and layering in volcanic rocks

41 Inclined

Strike and dip of foliation in metamorphic rock

47 Inclined

MacFarlane hot springs

3452 Drill hole (Sibbett et al., 1982)

Map location

Adjoining 7.5' quadrangle names

1 Crowbar Spring
2 King Lear Peak NW
3 King Lear Peak
4 Schoolhouse Butte
5 Pidgeon Spring SE
6 Salt Water Spring
7 Red Butte
8 Donna Schee Spring
9 Rabbithole NE
10 Floka
11 Sugerloaf Knob
12 Jungo
13 Rabbithole
14 Sulphur
15 Sawtooth Knob
16 Long Canyon